A Cloud Chamber Investigation of the Single Nuclear Scattering in Argon of High Energy Electrons and Positrons.

by

Allan F. Howatson, M.A.

A Thesis presented to the University of Glasgow for the Degree of Doctor of Philosophy.

ProQuest LLC.
789 East Eisenhower Parkway
P.O. Box 1346
Ann Arbor, MI 48106 – 1346

PREFACE

The thesis is an account of an experimental investigation of the scattering of electrons and positrons by argon nuclei using the expansion chamber technique. The apparatus was designed and constructed in the Glasgow University Natural Philosophy Department in collaboration with Mr. J. R. Atkinson with the technical assistance of Mr. P. R. Price. The author was personally responsible for most of the track photography. The analysis of the tracks, the collection of the statistical data and the conclusions derived therefrom are entirely his responsibility. The experiments described are believed to be the first in which statistics have been obtained on the single nuclear scattering of positrons.

The thesis is divided into six chapters with an introduction and two appendices. Chapter I consists of a review of previous experimental work on electron and positron scattering. In Chapter II is presented an outline of relevant theories of scattering together with a discussion of the method of projected angles. In Chapter III the technique of cloud-chamber operation and photography is discussed. A detailed description of the apparatus designed for the investigation follows in Chapter IV; some new features and improvements incorporated in the apparatus are mentioned. Chapter V is concerned with the method used in analysing the cloud-chamber tracks, and with errors of measurement. In Chapter VI the experimental results are presented and compared with theoretical predictions, and the conclusions derived therefrom are discussed.

A shorter account of the investigation has been published in the Philosophical Magazine (Series 7 Vol. xlii, p.1136). Additional

published papers by the writer, and by the writer in collaboration with Dr. R. A. Houston, on topics unconnected with the main thesis, are enclosed.

The author is glad to acknowledge the encouragement and direction given by Professor P. I. Dee, F.R.S., during the course of the research. In particular, the design of the cloud-chamber and auxiliary equipment owes much to his advice. He is also indebted to Mr. J. M. Reid for preparing the copper 62 positron sources in the Glasgow University synchrotron and to Mr. P. R. Price for much help in the preparation of diagrams and photographs.

CONTENTS.

		Page
Introduction	.....	1
Chapter I :-	Review of Previous Experimental Work	3
Chapter II :-	Outline of Scattering Theory and Projection of Scattering Formulae	27
Chapter III :-	Cloud Chamber and Photographic Technique.	42
Chapter IV :-	Apparatus and Materials	60
Chapter V :-	Analysis of Tracks and Errors of Measurement	100
Chapter VI :-	Results and Conclusions	115
Appendix I :-	.....	132
Appendix II :-	.....	137
References :-	.....	140

INTRODUCTION

The importance in physics of the study of the behaviour of charged particles in their passage through matter can scarcely be overestimated. Observations on the scattering of such particles have yielded information of the highest value not only about the charged particles themselves but also about the structure of the atoms through which they pass. The classical experiments of Rutherford on the scattering of α-particles in thin metal foils were forerunner of innumerable investigations of essentially the same nature in which particles of many different types and energies have been used.

The most precise and useful information is obtained in experiments in which 'single scattering' occurs i.e. under conditions such that the bombarding particle in its passage through the scattering material collides with only one other particle. It is the peculiar advantage of the cloud-chamber (now shared to some extent by special photographic emulsions) that it effectively renders visible individual scattering events, and is therefore pre-eminently suitable for the study of single scattering.

The present investigation is concerned with the scattering by atomic nuclei of high energy electrons and positrons. Numerous experiments have previously been carried out with the purpose of testing the theory of electron scattering, but largely owing to the difficulty of obtaining suitable sources, little or no work has been done on positron scattering. It is shown, however, in Chapter II, that for scattering elements of low or moderate atomic number, positron scattering

statistics are a more sensitive test of theory than electron scattering data. The investigation of electron scattering was carried out partly for comparison with the results obtained by previous investigators and partly to aid the assessment of experimental errors in evaluating the results for positrons.

CHAPTER I

REVIEW OF PREVIOUS EXPERIMENTAL WORK.

The experiments fall in general into two classes: in the first the scattering material is in the form of a thin foil and the scattered electrons are detected by ionisation chambers or counters, and in the second the electrons are scattered in the gas of a Wilson cloud-chamber, the tracks being photographically recorded. The earliest investigations were of the first type.

The first experiment in which single scattering conditions predominated was that of Chadwick and Mercier (C 1), who in 1925 measured the scattering of electrons from RaE (mean energy 0·3 Mev) in foils of aluminium, copper, silver and gold, by the annular ring method which had previously been used to study the scattering of α-particles. The foils were thin enough to ensure substantially single nuclear scattering. Good agreement with the classical Rutherford theory was obtained for the variation of scattering cross-section with atomic number except for the case of gold. The experimental uncertainties were too great to allow the calculation of accurate values for the absolute scattering cross-sections.

In subsequent investigations of this type until 1941 comparatively low energy electrons, artificially accelerated, were employed. Schonland (S 1) in 1926 studied the scattering of electrons of energy 77 Kev in aluminium, copper and silver, and obtained results in agreement with Darwin's (D 1) classical relativistic theory in which account was taken of the change in mass of the electron as it passed the nucleus. The anomalous results for gold persisted, but, contrary to the findings of Chadwick and Mercier, the experimental cross-section was higher than the

theoretical value. However, the validity of the particle concept of the electron was by this time in question.

The theoretical basis was put on a firmer foundation in 1929 when Mott (M 1) derived a scattering formula based on Dirac's relativistic electron theory. The expression is in the form of a conditionally convergent infinite series. The first approximation yields the "Mott formula" which is accurate only for scattering elements of low atomic number. Mott (M 2) calculated the exact value of the cross-section for scattering in gold at the particular scattering angle of 90^{o}, but an accurate summation of the series for heavy elements over the whole angular range was not made till 1940 by Bartlett and Watson (B 1). At large scattering angles Mott's theory predicts considerable variations from the classical cross-sections, especially for elements of high atomic number.

In 1931 Neher (N 1) repeated Schonland's experiment with electrons in the energy range 50 - 145 Kev. He paid particular attention to the suppression of extraneous electrons which are a source of inaccuracy in this type of experiment. Neher's results for scattering in aluminium are reproduced in Table 1.

TABLE 1

Aluminum.

$nt = 3.68 \times 10^{18}$		$\theta_1 = 95°10'$		$\theta_2 = 172°5'$	
β	V	Relative values of ρ			
		Exp	Mott	Darwin	k/V^2
0.436	56.1 kv	0.00340	0.00340	0.00340	0.00340
0.474	68.9	0.00231	0.00229	0.00241	0.00226
0.511	82.0	0.00157	0.00157	0.00178	0.00160
0.543	96.9	0.00110	0.00114	0.00134	0.00115
0.574	112.2	0.00082	0.00084	0.00104	0.00085
0.603	128.4	0.00061	0.00064	0.00088	0.00065
0.630	145.1	0.000485	0.000495	0.00077	0.000505
β	V	Absolute values of ρ			
		Exp	Mott	Darwin	Rutherford ($\alpha 1/V^2$)
0.436	56.1 kv	0.00340	0.00257	0.00460	0.00264
0.474	68.9	0.00231	0.00174	0.00326	0.00176
0.511	82.0	0.00157	0.00118	0.00242	0.00124
0.543	96.9	0.00110	0.00086	0.00182	0.00089
0.574	112.2	0.00082	0.00063	0.00141	0.00066
0.603	128.4	0.00061	0.00049	0.00119	0.00051
0.630	145.1	0.000485	0.000375	0.00104	0.00039

He found good agreement with either Rutherford's or Mott's equation for dependence of scattering cross-section on angle and energy. The absolute value of the cross-section was, however, 1·32 times the value given by Mott's theory. The variation of scattering cross-section with the atomic number of the scattering element agreed better with relativistic than with classical theory. The experimental results did not support the modifications introduced into the classical theory by Darwin.

In a similar type of experiment Chase and Cox (C 2) in 1940 measured

the scattering of 50 Kev electrons in thin aluminium foils. The angular distribution and the ratio of experimental to theoretical cross-sections (Mott theory) were found to be within the experimental uncertainties which were $\pm$ 20%.

In 1941 Pataklov and Vyshinski (P 1) measured the scattering coefficient of aluminium and gold over the restricted angular range 119°-122° for energies of 40 - 120 Kev. A magnetic selector was used to eliminate secondary electrons. The scattering cross-section between 119° and 122° was found to agree with the value obtained from Mott's formula, within the limits of experimental error, for aluminium but not for gold.

About this time a return was made to the investigation of high energy electron scattering by groups of workers in Russia and America. Alichanow et al (A 1,2,3) used two Geiger counters in coincidence to count the electrons scattered through the angular range 82° - 90° by thin foils of celluloid, aluminium, copper and gold. The source was a radon tube emitting electrons in the energy range 600 - 2,000 Kev, the energies being selected by a semi-circular focussing spectrograph. The authors studied the Wantzel criterion (W 1) for single scattering in thin foils, and, in common with previous workers, found it to be quite inadequate. They used a factor of the form $t+\frac{kt^2}{E}$ (t is the thickness of the foil) to correct for multiple scattering. The dependence of the scattering cross-section (σ) on energy and atomic number was studied. Good agreement with the Mott theory for all four substances for variation of σ with energy over the range 600 - 2,000 Kev was claimed.

Table 2 shows the dependence of σ on Z, the cross-section of aluminium at 1,000 Kev being taken as unity. The two values shown for σ_{th} for gold are the results obtained from Mott's exact calculation for

gold at 90° (178) and from the expansion up to the first power of Z (67). The large difference shows the error involved in using the approximate formula for elements of high Z. According to these authors $\sigma_{exp.}$ increases faster than Z^2 but not so fast as predicted by Mott. The absolute value obtained for the scattering cross-section in aluminium for 1 Mev electrons was 20% lower than the corresponding theoretical value.

TABLE 2

SUBSTANCE	Z	$\sigma_{exp.}$	$\sigma_{th.}$
Celluloid	7·1	0·31	0·29
Aluminium	13	1	1
Copper	29	5·6	6
Gold	79	78	178 (67)

In a similar type of experiment Saunderson and Duffendach (S 3) measured the scattering of electrons from RaE of energy greater than 0·2 Mev over the angular range 20° - 45°. They concluded that such deviations from the Mott formula as exceeded experimental error were due to the effects of multiple scattering and the inadequacy of the Wentzel criterion for elements of small Z.

In 1946 Van de Graaff et al (G 1) described an investigation carried out in 1943 which incorporated a number of improvements in technique. By using a high voltage electrostatic generator they were able to accelerate electrons to β-ray energies (1·27 - 2·27 Mev) and maintain the voltage constant to ± 1%. This avoided the decay and energy spread associated with radioactive sources. They used as the electron detector an ionisation chamber specially designed to minimise errors due to X-ray background.

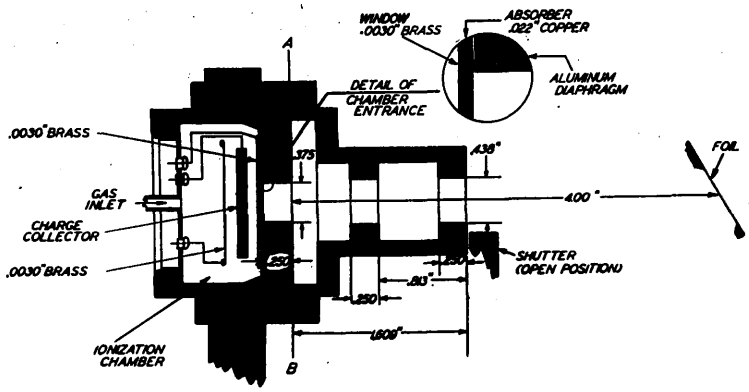

Details of ionization chamber.

FIGURE 1

A section of the ionisation chamber used is shown in Figure 1. The charge collector was a brass disc, 2mm thick, at zero potential, sandwiched between two thin brass discs, one at +1,000 volts and the other at -1,000 volts. Ionisation due to X-ray background was balanced out by adjusting the potentials of the thin plates so that the collector current was zero when no electrons were entering the chamber. Scattered electrons entering the chamber produced full net ionisation current since they only passed through the half of the chamber nearer the foil. The background of electrons which had lost energy by inelastic nuclear scattering or electron-electron scattering was removed by placing an absorber of thickness slightly less than the range in the material of electrons of the accelerating voltage used. The ratio of the ion current observed to the current actually carried into the chamber by elastically scattered electrons was obtained by rotating the collector into the main beam (suitably reduced in intensity) and determining the ratio of the ion current to the primary

beam current as measured by a Faraday cage. A Schematic diagram of the apparatus is shown in Figure 2.

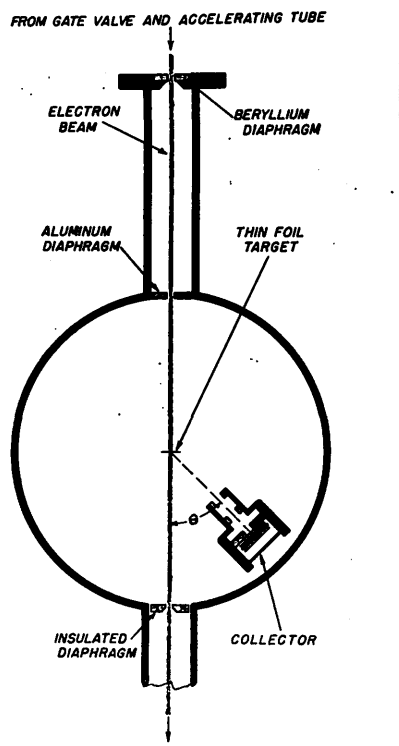

Schematic diagram of scattering chamber.

FIGURE 2

An angular range of scattering of 20° - 50° was investigated, readings being taken on both sides to avoid errors due to asymmetry in the beam. Correctins were made for multiple scattering: many points required no correction but some as much as 20%. The experimental observations were compared with the predictionsof the Mott formula (first order expansion) for the scattering elements aluminium, copper and silver. In the case of gold and platinum Bartlett and Watson's calculation for heavy elements was used.

TABLE 3

Ratios of the experimental results to the theoretical predictions. Only those points have been included for which observations were made on both sides of the beam and for which the multiple scattering correction did not exceed 20 percent.

Energy (Mev)	20°	30°	40°	50°
		Nucleus: aluminum		
1.49		1.01	0.97	1.04
1.81		1.02	0.96	0.97
2.00		0.95	0.97	1.02
2.27	1.11	1.26	1.52	1.64
		Nucleus: copper		
1.49		0.97	0.88	1.12
1.81		0.96	1.09	1.07
2.00		1.05	0.96	0.96
2.27		1.15	1.06	
		Nucleus: silver		
1.27			0.93	
1.49		0.97	1.03	1.02
1.81		0.97	1.02	1.03
2.00		1.01	1.06	1.07
		Nucleus: gold and platinum		
1.49				1.08
1.81				1.09
2.00			1.10	1.00

The results were in very good agreement with relativistic theory except for one particular case - the scattering of 2·27 Mev electrons in aluminium. This is shown in Table 3 which gives the ratios of the experimental results to the theoretical predictions for various scattering angles.

The apparatus was reassembled after the War by Buechner, Van de Graaff et al (B 2) to investigate this anomaly but it was found that the discrepancy no longer existed. The reason for the previous discrepancy was unknown. The range of scattering elements investigated was extended by the inclusion of beryllium.

The agreement with the Mott Relativistic scattering formula, extended by the calculations of McKinley and Feshbach (M 3) to cover all elements, is shown in Figure 3. The ordinate represents the ratio of the relativistic scattering cross-section to the Rutherford value, the solid line being obtained from Mott's theory. Experimental values for aluminium

copper, silver and gold agree well with the Mott theory but not with the classical Rutherford formula.

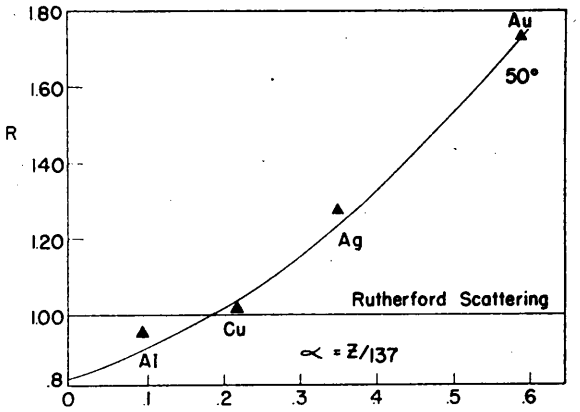

Comparison of theory and experiment at electron energy of 2 Mev. The solid line is given by the theory. The triangles give the experimental points as obtained by Van de Graaff, Buechner *et al.*

FIGURE 3

In view of these results it must be assumed that the discrepancies obtained by earlier investigators, especially in the case of gold, were due to faulty technique, to incorrect allowance for multiple scattering, or to lack of appreciation of the limitations of the Mott formula in its approximate form.

The description of the apparatus used in this investigation emphasises the elaborate precautions which must be taken if inaccuracies are to be avoided in scattering experiments of this type. The number of electrons scattered through large angles is a minute fraction of the total number of incident electrons. Consequently extreme precautions have to be taken to avoid recording as electrons scattered by the foil, those which arise from the X-rays which are unavoidably present or by

scattering from the walls of the containing vessel. Unless the foils are extremely thin, and therefore inefficient scattering agents, a certain amount of plural and multiple scattering takes place. This must be allowed for in calculating scattering cross-sections. It has been shown by a number of workers that the Wentzel criterion for single scattering cannot be relied on as it is insufficiently rigorous. In the case of light elements a further small correction for electron-electron scattering is required.

Cloud-Chamber Investigations

With the cloud-chamber method, since individual scattering events are observed, difficulties of the above nature do not arise. Every deflection can be assumed to be single, and electron-nuclear can easily be distinguished from electron-electron collisions. Moreover, by applying a uniform magnetic field, the energy of each electron before and after collision can be determined, and any large energy loss detected.

To offset these advantages the cloud-chamber method is handicapped by the difficulty of securing enough data to provide results of statistical reliability. Moreover, since fast electrons produce tracks of low specific ionisation, a high standard of cloud chamber and photographic technique is required to obtain accurate information. Such considerations delayed the application of the Wilson cloud-chamber to the problem, and it was not till 1936 that the first measurements were published. Since that date a large number of investigations has been made, covering a wide range of electron energy and a variety of scattering substances. The principal object of these investigations was to check the Mott scattering formula with regard to absolute scattering intensity, and the variation of

intensity with scattering angle and with the atomic number of the scattering material. In addition attempts were sometimes made to assess the number of collisions involving large energy loss (radiative collisions) and the probability of pair formation by fast electrons.

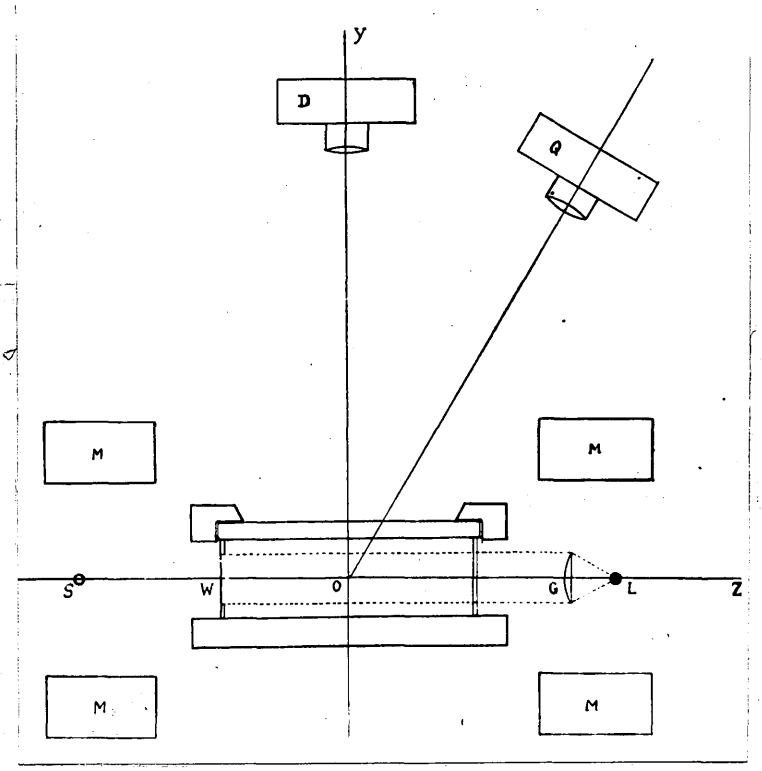

FIGURE 4

A typical experimental arrangement is shown in Figure 4. The cloud-chamber is situated in a uniform magnetic field produced by a pair of Helmholtz coils denoted by M, and the scattering substance is introduced in gaseous form along with the condensing vapour. The electrons from a source S enter the chamber through a thin window in the side, and the tracks of those which cross the chamber during the sensitive period are illuminated by a collimated beam from a flash-lamp L, and photographed

by a stereoscopic pair of cameras D and Q. The tracks are analysed either by making measurements directly on the plates or films, or by returning the developed film to the cameras and projecting an image of the tracks on to a suitable screen.

During the early 1930's Champion (C 3) using a slightly modified form of the experimental equipment developed by Blackett (B 3, 4) and others for the photography of α-ray tracks, recorded a large number of tracks of electrons from a RaE source. The cloud-chamber used was cylindrical, about 16cm in diameter and 6cm deep, but the useful area was restricted to a diameter of 12cm by the necessity of screening the peripheral parts of the chamber from the illuminating beam which was inclined at 15° to the horizontal. The tracks were photographed by two cameras with their image planes mutually at right angles (see Figure 16(b)). The chamber was placed in a uniform magnetic field of several hundred gauss. The measurements of curvature and scattering angles were made directly on the photographic plates. Only collisions in which the electron was deflected in a direction opposite to the original direction of curvature of the particle were recorded. Such collisions are more easily observed as they are indicated by a cusp in an otherwise smooth curve.

In 1936 Champion (C 4) published the electron-nuclear scattering data obtained from the analysis of 875 metres of track in nitrogen. A comparison of the experimental observations with predictions based on various theories is shown in Table 4. The best agreement is with the Mott theory which gives over the angular range 20° - 180° a ratio of experiment to theory of 0·85. Almost as good agreement is obtained,

however, by inserting the relativistic expression $m_0/(1-\beta^2)^{\frac{1}{2}}$ for the electron mass in the classical Rutherford expression. (Column 5).

TABLE 4

Ang. Int.	Obs.	Mott	Darwin	Classical	$c(1-\beta^2)$
20^o - 30^o	111	142	146	579	145
30^o - 60^o	73	80	108	347	86
60^o -180^o	17	16	50	95	26
20^o -180^o	201	238	304	1021	257

About the same time Skobeltzyn and Stepanova (S 4) and Stepanova (S 5, 6) reported results of measurements on electron scattering in nitrogen whichwere greatly at variance with the above, and with the theoretical predictions. For the energy range 0·2 - 1·1 Mev they found a ratio expt. : theory of about 1·5, and for the range 1·5-3.0 Mev a ratio of 10 to 30. Bosshard and Scherrer (B 5), somewhat later, also observed excessive scattering in nitrogen at large scattering angles.

On the other hand Klarmann and Bothe (K 1) found the scattering cross-sections in krypton and xenon for electrons in the energy range 0·5 - 2·6 Mev to be much smaller than the theoretical values, the ratio expt. : theory being 0·16 and 0·2 respectively.

Further work on nitrogen by Borisov et al (B 6), Bleuler (B 7) and Bleuler, Scherrer and Zunti (B 8) failed to confirm the large discrepancies reported by Skobeltzyn and Stepanova, though the agreement with theory and the internal consistency was not good.

Bleuler et al also measured the scattering coefficient in fluorine and in argon, and obtained results in approximate agreement with theory

the ratio expt. : theory being 1·2 and 1·3 respectively. Results for argon reported by Stepanova (S 6) gave good agreement over the energy range 0·2 - 1·1 Mev but 2·5 times the theoretical value in the range 1·5 - 3·0 Mev.

Further work with heavy scattering elements gave very inconsistent results. The low value observed by Klarmann and Bothe for scattering in xenon was not confirmed by Sen Gupta (G 3) who obtained a ratio expt. : theory of 0·85. On the other hand Champion and Barber (C 5), (B 12) obtained very low cross-sections for scattering in iodine and in mercury, the ratios being 0·4 and 0·15 respectively. In 1943 Segrist (S 7) obtained close agreement with theory for electron scattering in iodine. The source of electrons in all these experiments was one of the natural β-emitting radioactive elements, usually RaC or RaE.

It is difficult to draw any conclusions about the validity of the relativistic theory of scattering from results of such wide diversity, though it is noticeable that the general tendency in the later results is towards better agreement with theory. It is unfortunate that many authors do not describe in detail the experimental techniques and methods of analysis which they employed. In a later section it is pointed out that unless the quality of the tracks and of the track photography is of a high standard, serious errors in interpretation are likely to occur. The standard appropriate to this type of work is such that individual background drops should be clearly distinguishable over the whole of the illuminated part of the cloud chamber. Since it is only within recent years that rare gas discharge lamps have been developed of sufficient output to allow the vertical photography of individual drops and thinly

ionising tracks over a large cloud-chamber volume, it seems probable that the large discrepancies observed by some earlier workers are attributable to experimental difficulties in the photography and consequent inaccuracies in the analysis of the tracks.

One recent investigation which appears to be largely free from the above objections is that of Randels, Chao and Crane (R 1). These authors described an extensive investigation covering a wide energy range and involving measurement on 2173 metres of electron track in air, argon, krypton and xenon. For lower energies (up to 1·5 Mev) the source was radioactive phosphorus, P32: for moderate energies (1·5 - 2·5 Mev), a capsule containing 0·5mg. of radium. The energy range was extended up to 12 Mev by using the electrons produced by the bombardment of Li8 by deuterons. The cloud-chamber used was small (15cm in diameter) but was fully automatic. The tracks were photographed by 35mm cameras, one with its axis vertical, the other with its axis at 20° to the vertical. The number of tracks was restricted to an average of three per photograph in order to avoid confusion. These authors were among the first to use the method of projected angles for the measurement of curvature and scattering angles, the results being compared with a projected form of the Mott scattering formula. No large discrepancy with theory was observed for any of the gases in any of the energy ranges.

The results, summed over all energies and all scattering elements are shown in Table 5.

TABLE 5

Ang. Range	15°-25°	25°-35°	35°-45°	45°-55°	55°-65°	65° -75°	75°-85°	85°-90°
Theory	569·5	126·7	45·3	21·6	11·5	6·5	3·9	2·5
Expt.	529·5	152·5	64·0	27·0	13·5	9·0	3·0	3·0

There is a measured excess of scattering over the calculated values in the intervals 25°-35°, 35°-45°, and 45°-55° of 20%, 45% and 25% respectively. The authors regard the evidence for a significant excess over theory as strong, though not conclusive. The authors used the approximate Mott formula in calculating theoretical values. Expansion of the Mott formula beyond the first term gives appreciably larger scattering cross-sections for elements of medium and high atomic number but an approximate calculation by the writer shows that the increase is not sufficient to account for the discrepancy.

The number of cases of large energy loss during collision was too small to permit statistical study, only two collisions in which the energy loss was more than 50% being observed in the xenon series. The number predicted by theory was eight.

The general conclusion drawn from the investigation was that the highly anomalous results obtained by some earlier workers were not substantiated. The measurements, however, were not sufficiently exact to test the Mott formula in detail. In connection with a comparison between the full Mott formula and the first term only (which is equivalent to the Rutherford formula with relativistic mass) the authors state -

"It is our opinion that the combination of the inaccuracies in the

cloud-chamber measurements made to date and the uncertainties due to the approximation in the theory place such a decision just outside the range of possibility."

The theoretical position has since been improved by the work of Bartlett and Watson (B 1, 2) and McKinley and Feshbach (M 3) whose calculations enable the scattering cross-section to be found for all elements. The difficulty remains, however, of securing sufficient experimental data to distinguish unambiguously between the relativistic and the semi-classical theory, the results from which, except for heavy elements, do not differ greatly.

The only post-war measurement on electron scattering in gases by the cloud-chamber method was recorded by Champion and Ray (C 6) in 1948. Three Geiger counters were placed inside a chamber containing nitrogen, in such a position that they were traversed only by electrons scattered through a large angle. Expansions were made at one minute intervals with the photographic plate permanently exposed. Illumination was arranged to occur, and a record obtained, when a counter was discharged by an electron scattered through an angle between 80° and 130°. 1500 expansions were made for every photograph obtained. A correction was applied for particles missed by the counters, and only those scattered within a limited area of the chamber were included in the statistics.

The results obtained are shown in Table 6.

TABLE 6

Ang. Interval	Observed	Observed (corrected)	Theory (Mott)
85° - 100°	74	88	55
100° - 120°	34	34	37
120° - 180°	23	23	26
85° - 180°	131	145	118

This gives, over the angular range 80°-180°, a ratio expt.: theory of 1·2. Thus the anomalous excessive scattering at large angles in nitrogen, observed by Skobeltzyn and Stepanova and by Bosshard and Scherrer, was not confirmed. The conclusion was that in nitrogen the Mott formula is in good agreement with experiment at all angles of scattering.

A summary of the results of all the experiments on the nuclear scattering of electrons in gases by the cloud-chamber method, so far as the author has been able to collect them, is presented in Table 7. Information on the principal non-cloud-chamber experiments has also been collected in Table 8.

Scattering of Positrons

As previously mentioned the source of electrons in nearly all the experiments described was one of the naturally occurring radioactive elements - usually radium or one of its products. The lack of any corresponding work on the equally important problem of the scattering of positrons can be attributed to the difficulty of obtaining a suitable positron source. Only two experiments have been reported on the nuclear scattering of positrons and in both of these the scattering was mainly

plural or multiple.

In 1938 Fowler and Oppenheimer (F 1) used a series of cloud-chamber photographs taken to determine the energy spectrum of the γ-radiation emitted by the bombardment of lithium with protons, in order to obtain data on the scattering and loss of energy of fast electrons and positrons in traversing a thin sheet of lead. The tracks of 234 electrons and 128 positrons of energy between 7·5 and 14·5 Mev. were analysed. 21 electrons and 8 positrons had emergent tracks too short for measurement. The results obtained are shown in Table 9.

TABLE 9

Comparison of electron and positron scattering.

		Number Scattered		Ratio Electron/ Positron Scattering			
	N_0	8.5° to 14.5°	>14.5°	8.5° to 14.5°		>14.5°	
				Obs.	Theor.	Obs.	Theor.
Electrons	255	36	27	1.2±0.3	1.3	1.6±0.4	>1.5
Positrons	136	16	9				

According to the Wentzel criterion the scattering was single beyond 13°. The conclusion of the authors was that some evidence had been found for an excess scattering at large angles of electrons over positrons (as predicted by relativistic theory). The preponderance of multiple scattering, however, introduces uncertainties and the observations are too few in number to have great significance.

In 1948 Lasich (L 1) studied the angular distribution of positrons

and electrons scattered in a thin gold foil stretched across a cloud-chamber. The angular distribution was regarded as compounded of a multiple scattering distribution merging into a single scattering 'tail' at large angles. The source of positrons was an impure specimen of Co 56 with a maximum particle energy of 1·2 Mev. The electron source for the upper part of the energy range was radio phosphorus, P 32, and for lower energies Ra(D + E) lead.

TABLE 10

PROJECTED SINGLE SCATTERING IN GOLD FOIL

	Radius of Curvature (cm.)	Mean Energy (Mev.)	Angular Range (φ_1, φ_2)	Total No. of Particles	No. of Scattered Particles	Scattering Probability N' (φ_1, φ_2) Expt.	Theory (in units of 10^{-5})
Positrons	5 and 6	0·45	27°–54°	301	12	4·0	3·9
	7 and 8	0·68	21°–43°	376	13	3·5	3·5
	9, 10, and 11	0·95	17°–33°	189	5	2·6	2·8
Electrons	5 and 6	0·45	27°–54°	338	22	6·5	8·8
	7 and 8	0·68	21°–43°	318	18	5·7	6·4
	9, 10, 11, and 12	0·99	17°–33°	304	13	4·3	4·7

The small-angle scattering was found to be in reasonable agreement with multiple scattering theory. A comparison between positron and electron scattering was made at larger scattering angles "where the single scattering effect was not greatly diluted by the multiple scattering process". The data obtained are shown in tables 10 and 11.

TABLE 11

RATIO OF ELECTRON TO POSITRON SCATTERING AT LARGE ANGLES

Mean Energy (Mev.)	Angular Range (φ_1, φ_2)	Ratio of Scattering Probability	
		Expt.	Theory
0·45	27°–54°	1·6	2·3
0·68	21°–43°	1·6	1·8
0·97	17°–33°	1·6	1·7

The results again indicate a greater cross-section for electron than for positron scattering, but as in the previous experiment the statistical basis is poor, and the uncertainties due to a proportion of multiple scattering remain.

Before concluding this chapter it may be useful to summarise the present state of agreement between experiment and theory as it appears from this review.

1) The scattering of electrons as measured by the ionisation chamber method agrees well with relativistic theory with regard to energy dependence (in the range 1·27 - 2·27 Mev), absolute intensity, and variation with the atomic number of the scatterer. It does not agree with the Rutherford semi-classical theory.

2) With the cloud-chamber method the large discrepancies observed by some earlier investigators have not been confirmed by recent work. Fairly good agreement with theory is now general for scattering in

elements of low atomic number, but several large discrepancies still remain unexplained in the case of heavier elements.

3) No statistics have been obtained on the single nuclear scattering of positrons but some evidence has been produced in experiments where multiple scattering predominated, of an excess of electron over positron scattering in foils of heavy elements. This is in agreement with predictions of relativistic theory.

TABLE 7

SINGLE NUCLEAR SCATTERING OF ELECTRONS IN GASES. CLOUD CHAMBER DATA.

ELEMENT Symbol	Z	ENERGY Mev.	ANGLE Deg.	TRACK LENGTH Meters	No. of Deflections	Ratio Expt./Theory	Author	Reference and date
H	1	0·5 - 1·1	20 - 180	124	2	1 predicted	Ray & Champion	R3 1944
N	7	0·4 - 1·1	20 - 180	875	201	0·85	Champion	C4 1934
		1·5 - 3·0	20 - 180	180	212	10 to 100	Skobeltzyn & Stepnanova	S4 1936
		0·2 - 1·1	20 - 180	82	113	1·7	Stepanova	S5 1937
		0·3 - 2·5	20 - 180	294	47	0·7	Borisov et al	B7 1940
		0·074-3·2	20 - 30			0·49	Bosshard & Scherrer	B6 1941
			30 - 60			2·08		
			60 - 180			8·59		
		0·2 - 3·1	15 - 180	367	41	1·5	Bleuler	B8 1942
		0·2 - 3·0	15 - 180	515	42	1·3	Bleuler, Scherrer et al	B9 1942
		0·5 - 1·0	85 - 180	145		1·23	Champion & Ray	C6 1948
Air		1·0 - 4·5	not specified	800	-	1·5	Randels et al	R1 1940
		0·9 - 4·5	15 - 25	-	182	0·87	R.C.& Crane	R1 1945
			25 - 90	-	99	1·4		
F	9	0·2 - 3·0	15 - 180	910	113	1·2	Bleuler et al	B9 1942
A	18	1·7 - 2·4	30 - 60	-	-	0·7	Zuber	Z1 1938
			60 - 180			1·0		
		0·2 - 1·1	20 - 150	103	308	1·0	Stepanova	S6 1939
		1·5 - 3·0	20 - 150	130	84	2·5	"	S6 1939
		1·0 - 9·5	-	508	-	1·5	Randels et al	R1 1940
		0·2 - 3·0	15 - 180	708	153	1·3	Bleuler et al	B8 1942
		0·8 - 9·3	15 - 25	-	82	1·3	Randels et al	R1 1945
		0·8 - 9·3	25 - 90	-	40	1·6	"	R1 1945

TABLE 7 (contd.)

ELEMENT Symbol	Z	ENERGY Mev.	ANGLE Deg.	TRACK LENGTH Meters	No. of Deflections	Ratio Expt. / Theory	Author	Reference and date
Kr	36	0·5 - 2·6	40 - 180	140	10	0·16	Klarmann & Bothe.	K1 1936
		1·9 - 9·5	-	112	-	1·5	Randels et al	R1 1940
		1·5 - 2·9	15 - 25	-	43	1·3	"	R1 1945
		1·5 - 2·9	25 - 90	-	12	0·9	"	R1 1945
I	53	0·7 - 1·2	20 - 180	360	114	0·4	Champion & Barber	C5 1939
		0·8 - 3·2	15 - 180	459	249	1·0	Segrist	S7 1943
Xe	54	0·5 - 2·6	40 - 180	240	51	0·2	Klarmann & Bothe	K1 1936
		2·1	40 - 180	172	101	0·85	Sen Gupta	G3 1939
		2·1	20 - 180	64	161	0·85	"	G3 1939
		1·5 - 11·5	not specified	804	-	1·5	Randels et al	R1 1940
		2·9 - 12·0	15 - 25	-	149	0·8	"	R1 1945
		2·9 - 12·0	25 - 90	-	88	1·3	"	R1 1945
Hg	80	0·5 - 1·1	20 - 180	350	152	0·15	Barker & Champion	B12 1938

TABLE 8

NON CLOUD CHAMBER DATA

METHOD	ELEMENT	ENERGY MEV.	ANGLE DEG.	EXPT. / THEORY	AUTHOR	REF.	DATE
RaE β-rays Annular ring	Al, Cu Ag, Au	0·3	24°-40°	1·25 (Darwin theory)	Chadwick & Mercier	C1	1925
Cathode rays: Current balance	Al, Cu Ag, Au	0·077	90°-161°	0·98(Al) (Darwin theory)	Schonland	S1,2	1927
Cathode rays: ion chamber	Al, Ag Au	0·056-0·145	95°-173°	1·32(Al)	Neher	N1	1931
Radon tube: coincidence counters	Celluloid Al, Cu Au	0·6-2·0	82°-90°	0·8 for Al Discrepancy for Au.	Alichanow et al	A1,2,3	1941
RaE β-rays Geiger counters	Al, Cu Ag, Au	0·1-1·1	20°-45°	No definite discrepancy	Saunderson & Duffendach	S3	1941
Electrostatic Generator: Ion chamber	Al, Cu Ag, Au	1·27-2·27	20°-50°	1·0 except for Al at 2·27 Mev for which ratio = 1·5	Van de Graaff et al	G1	1946
As above	Be, C Al	2·1-2·3	up to 60°	0·99. Al anomely resolved	Buechner, Van de Graaff et al	B3	1947

CHAPTER II

OUTLINE OF SCATTERING THEORY AND PROJECTION OF SCATTERING FORMULAE

The basic scattering formula is that derived by Rutherford (R2,p.191) using classical Newtonian dynamics. For a beam of electrons of charge e, and mass m_0, moving with velocity v in the Coulomb field of a nucleus of charge Z the differential scattering cross-section, σ, is given by

$$\sigma = \left(\frac{Ze^2}{2m_0v^2}\right)^2 \operatorname{cosec}^4 \theta/2 \qquad \text{——————(II. 1)}$$

where θ is the angle between the incident beam and the direction of scattering.

Exactly the same formula may be deduced by wave mechanical theory. The solution is obtained most easily by using the Born approximation which is valid for electrons in the energy range here considered.

The non-relativistic wave equation for motion in a field of potential V is, in the usual notation,

$$\nabla^2\psi + \frac{2m_0}{\hbar^2}(E-V) = 0 ,$$

i.e.
$$(\nabla^2 + k^2)\psi = \frac{2m_0}{\hbar^2} V\psi \qquad \text{——————(II. 2)}$$

where $k^2 = 2m_0/\hbar^2$.

$\psi = \psi_0$, where ψ_0 is of the form e^{ikz}, representing a plane wave, is a solution of equation (II. 2) with the R.H.S. = 0, i.e. in a field-free space.

In equation (II.2) let $\psi = \psi_0 + \psi_1$ where ψ_1 represents the effect of the field

then
$$(\nabla^2 + k^2)\psi_1 = \frac{2m_0}{\hbar^2} V(\psi_0 + \psi_1)$$
$$= \frac{2m_0}{\hbar^2} V\psi_0 \quad \text{if } V\psi_1 \text{ be neglected (Born's approximation).}$$

The solution at points distant from the scattering centre (asymptotic form) is

$$\psi_1 = \frac{e^{ikr}}{r} f(\theta)$$

Hence $$\psi \rightarrow e^{ikz} + e^{ikr}/r \cdot f(\theta)$$

$f(\theta)$ is related to the scattering cross-section as shown below.

The number of particles per unit volume in the scattered wave at distance r is $|f(\theta)|^2/r^2$. If v is the velocity, the number incident per unit time on an element of area ds is

$$v \, ds \, |f(\theta)|^2/r^2$$

i.e. the number scattered per second into solid angle dw is

$$v \, |f(\theta)|^2 \, dw$$

But $\sigma(\theta)$, the differential scattering cross-section (or scattering probability) is the fraction of the incident particles scattered at angle θ per unit solid angle. Hence

$$\sigma(\theta) = |f(\theta)|^2$$

The problem is to find the form of $f(\theta)$. The solution obtained by Mott is as follows.

The wave function representing the incident and scattered wave is

$$\psi = \sum_{n=0}^{\infty} (2n+1) i^n e^{i\eta_n} L_n(r) P_n(\cos\theta),$$

and for the asymptotic form of the scattered wave

$$r^{-1} e^{ikr} f(\theta) \qquad \text{with}$$

$$f(\theta) = \frac{1}{2ik} \sum_{n=0}^{\infty} (2n+1)\left[e^{2i\eta_n} - 1\right] P_n(\cos\theta).$$

$f(\theta)$ is complex. The scattered intensity $\sigma(\theta) = |f(\theta)|^2$ is given by the square of the modulus i.e. by $A^2 + B^2$ where

$$A = \frac{1}{2k} \sum (2n+1)(\cos 2\eta_n - 1) P_n ,$$

$$B = \frac{1}{2k} \sum (2n+1) \sin 2\eta_n \cdot P_n .$$

These series are in general convergent, but there is only one case in which they can be summed in terms of known functions, namely the Coulomb field. For this, as previously mentioned, the scattering cross-section is the same as that given by classical theory (equation II.1). This is not so for any other field investigated.

The simple wave equation cannot be expected to give correct results for high-energy electrons. However, the formula obtained by substituting the relativistic expression for the mass, $m = m_0 / (1 - \beta^2)^{\frac{1}{2}}$, in the Rutherford formula, namely

$$\sigma = \left(\frac{Ze^2}{2m_0c^2}\right)^2 \frac{1-\beta^2}{\beta^4} \operatorname{cosec}^4 \theta/2 \qquad \text{——————} (II.3).$$

where $v = \beta c$ and m_0 = rest mass of electron, gives, within limits to be discussed later, good agreement with experiment. It is the formula against which more refined expressions are usually compared. The R.H.S. of equation (II.3) will be denoted by R.

The same problem can be solved using the relativistic form of the wave equation. This may be written

$$\nabla^2\psi + \frac{1}{\hbar^2c^2}\left\{(E - V)^2 - m^2c^4\right\}\psi = 0 ,$$

where $E = mc^2 = m_0\gamma c^2$, $\gamma = (1-\beta^2)^{\frac{1}{2}}$

i.e. $$\left(\nabla^2 + k^2\right)\psi = \left(\frac{2m_0\gamma}{\hbar^2} V - \frac{1}{\hbar^2c^2} V^2\right)\psi \qquad \text{——————} (II.4),$$

where the additional term on the R.H.S. arises from the variation of mass with velocity.

Neglecting the V^2 term, the scattering cross-section obtained is

$$\sigma(\theta) = \left(\frac{Ze^2}{2m_0c^2}\right)^2 \frac{1-\beta^2}{\beta^4} \cdot \operatorname{cosec}^4\theta/2 = R$$

that is, the Rutherford formula with relativistic mass.

If the V^2 term is retained in the relativistic equation, the solution obtained is

$$\sigma(\theta) = R\left\{1 + \pi Z\alpha\beta \sin\theta/2\,(1 + \text{terms of order } Z\alpha, (Z\alpha)^2, \text{etc})\right\},$$

where $\alpha = e^2/\hbar c = 1/137$.

The above relativistic equation takes no account of electron spin.

In 1929 Mott (M 1) considered the scattering problem from the standpoint of Dirac's relativistic electron theory. In the equation corresponding to (II.4) above there is an extra term representing the effect of spin.

The equation is (c.f. Williams, W 2)

$$\left(\nabla^2 + k^2\right)\psi = \left\{\frac{2m_0\gamma}{\hbar^2} V - \frac{1}{\hbar^2c^2} V^2 + i\,\frac{\partial V}{\partial \bar{r}}/\hbar c\bar{r} \cdot \rho(\bar{\sigma}.\bar{r})\right\}\psi \qquad \text{(II.5)}$$

For a Coulomb field the ratio of the V^2 term to the V term is

$$\frac{V}{2m_0\gamma c^2} = \frac{Ze^2}{r.\,2mc^2} = \beta\frac{Ze^2}{\hbar c}\cdot\frac{\hbar}{mvr} = \frac{\beta Z}{137}\cdot\frac{\lambda\!\!\!^{-}}{r}$$

where $\lambda = 2\pi\lambda\!\!\!^{-}$ is the electron wavelength. For all values of Z the ratio is small at distances from the nucleus large compared with the wavelength ($r \gg \lambda\!\!\!^{-}$). It can be shown that the ratio of the spin term to the V term is also small for $r \gg \lambda\!\!\!^{-}$.

Since scattering through an angle θ in the nuclear field is due to the field at $r \sim \lambda\!\!\!^{-}/\theta$, it follows that for small-angle scattering $r \gg \lambda\!\!\!^{-}$, and the second and third terms inside the bracket in equation (II.5) are small compared with the first. The scattering intensity consequently differs but little from the value deduced from classical theory or non-relativistic wave-mechanics (with the relativistic expression for the mass).

For scattering at large angles, and particularly by elements of high atomic number, the second and third terms are no longer small compared with the first, and the scattering distribution deduced from Mott's formula differs considerably from the classical one. This is clearly seen in Figure 5 which is referred to below.

Returning to equation (II.5) the solution obtained by Mott is in the form of a conditionally convergent infinite series. It may be expressed

$$\sigma(\theta) = R\left\{ 1 - \beta^2 \sin^2\theta/2 + \pi Z\alpha\beta \left(1 - \sin^2\theta/2 + \text{terms of order } Z\alpha, (Z\alpha)^2, \text{etc.} \right) \right\}$$

This formula is fairly accurate in the first approximation for all angles, provided Z is small, but for large Z it is necessary to evaluate the terms in $Z\alpha$, $(Z\alpha)^2$ etc. Mott (M 2), in 1932 evaluated the series accurately for the particular case of scattering in gold at 90°. The calculation of the solution for all scattering angles was undertaken by Bartlett and Watson for the case of mercury (Z = 80). In 1948 McKinley and Feshbach expanded the Mott series in the form of a power series in $Z\alpha$ and $\frac{Z\alpha}{\beta}$ ($\beta = {}^{v}/_{c}$), the series being accurate for the middle Z elements. By using the results of Bartlett and Watson they extended the calculation to obtain the cross-section for scattering of all elements to an accuracy of a few per cent. The results are given in terms of the ratio of the calculated scattering cross-section to the Rutherford cross-section at different scattering angles. Figure 5 shows the curve obtained for mercury from Bartlett and Watson's exact calculation together with that due to McKinley and Feshbach. The solution of the latter even without adjustment is shown to give a similar type of curve.

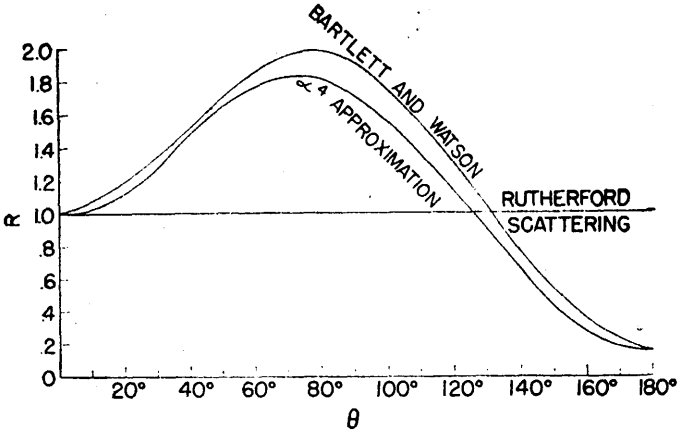

Comparison between α^4-approximation and exact calculation of Bartlett and Watson for Hg. The energy of the electron is 2 Mev. R is the ratio of the scattering cross section to Rutherford scattering.

FIGURE 5

McKinley and Feshbach also deduced from Mott's theory an approximate formula valid for $Z/137 < 0{\cdot}2$ which differs slightly from the Mott approximate formula, and is more accurate over the middle range of angles. McKinley and Feshbach's approximate formula which is

$$\sigma(\theta) = R\left\{1 - \beta^2 \sin^2\theta/2 + \pi Z\alpha\beta \sin\theta/2\,(1 - \sin\theta/2)\right\} \qquad \text{(II.6)}$$

may be compared with Mott's approximate formula

$$\sigma(\theta) = R\left\{1 - \beta^2 \sin^2\theta/2 + \pi Z\alpha\beta \sin\theta/2\,(1 - \sin^2\theta/2)\right\} \qquad \text{(II.7)}.$$

It is apparent from Figure 5 that for elements of high atomic number, the relativistic theory predicts cross-sections for electron scattering quite different from those expected on classical grounds. The ratio of relativistic to classical cross-section reaches a maximum of nearly 2 at a scattering angle of about 80° and then decreases rapidly, falling

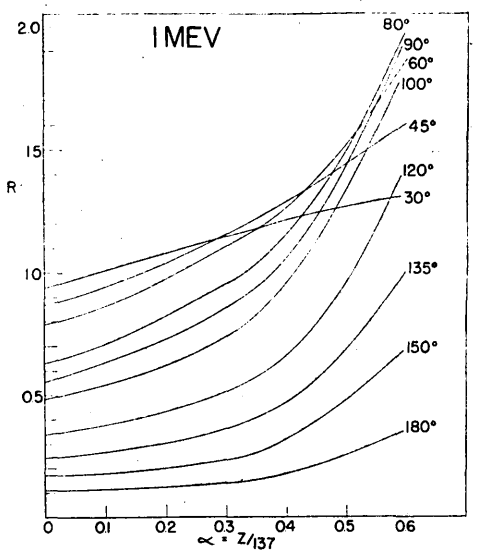

The ratio R of the scattering cross section to Rutherford scattering as a function of $Z/137$ for the various scattering angles labelling each curve. Electron energy 1 Mev.

(a)

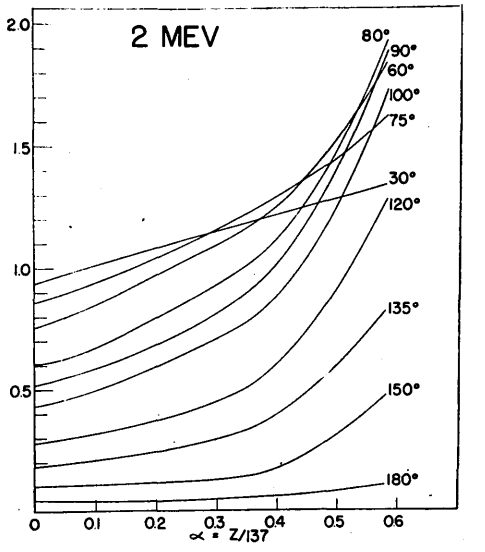

The ratio R of the scattering cross section to Rutherford scattering as a function of $Z/137$ for the various scattering angles labelling each curve. Electron energy 2 Mev.

(b)

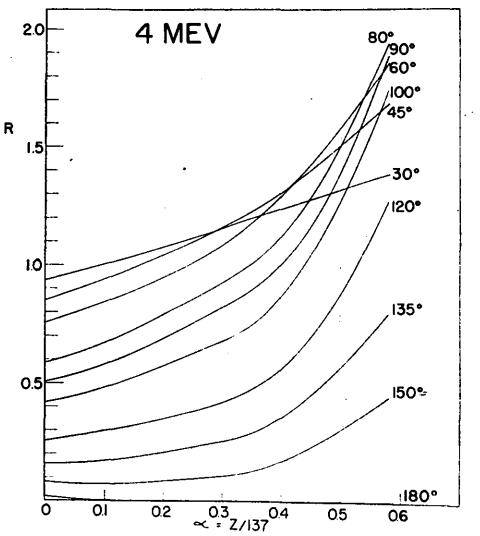

The ratio R of the scattering cross section to Rutherford scattering as a function of $Z/137$ for the various scattering angles labelling each curve. Electron energy 4 Mev. The energy dependence of the ratio R may be neglected within the accuracy of these calculations above 4 Mev.

(c)

FIGURE 6.

to very low values at angles greater than 150°.

Convenient graphs from which similar curves can be drawn for any element have been constructed by McKinley and Feshbach and are reproduced in Figure 6. They give the ratio of the scattering cross-section to Rutherford scattering as a function of αZ at various scattering angles for electron energies of 1, 2 and 4 Mev. A curve showing the theoretical scattering of 1 Mev electrons in argon, constructed in this way, is illustrated in Figure 6(d)

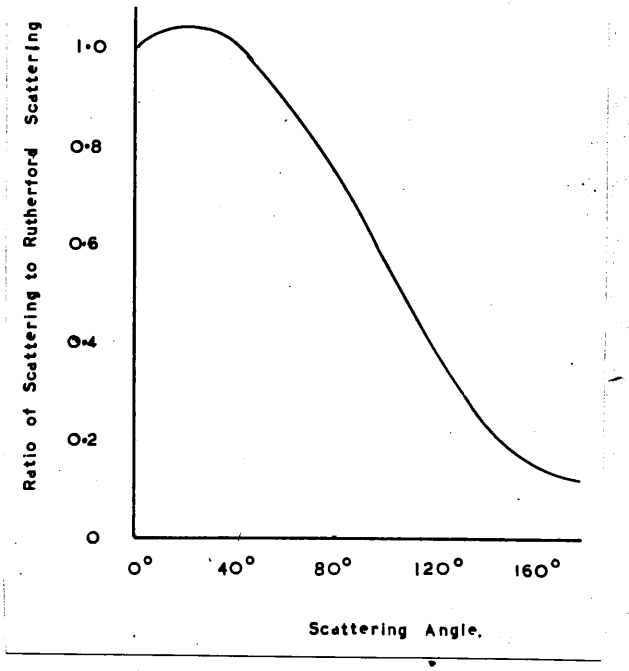

FIGURE 6(d)

Throughout the discussion on scattering the following have been neglected:-

1. The screening of the nucleus by extra-nuclear electrons.

2. Radiative collisions.

3. Electron-electron collisions.

The effect of these on the main scattering distribution can be shown to be negligible in the energy range investigated.

The scattering of an electron through angle θ in a nuclear field is due to the field at a distance $r \sim \lambda\!\!\!^{-}/\theta$. Substituting values corresponding to the lowest measured angles and electron energy gives $r \sim 10^{-10}$ cm, which is smaller than the radius of the innermost electron orbit, so that even in the most unfavourable case no shielding of the nucleus occurs.

It can be shown that the number of radiative collisions to be expected on theoretical grounds during the passage of electrons of the energy investigated (~ 1 Mev) through a medium of the atomic number of argon is extremely small.

Electron-electron scattering cross-sections are much smaller than electron-nuclear in all except the lightest elements. The two types of scattering can in any case be easily distinguished in the cloud chamber.

Positron Scattering.

On the basis of classical mechanics the scattering of positrons follows the same law as the scattering of electrons. If, however, the positron is regarded as a positively charged Dirac particle, the change in sign of the Coulomb force affects the spin-orbital coupling, and results in an appreciable difference in the scattering cross-section, particularly for elements of high atomic number. Massey (M 4) using tables drawn up by Bartlett and Welton for the electron case, calculated the theoretical

cross-section for the scattering of positrons in mercury. The results of his calculations for positrons of various energies are shown in graphical form in Figure 7.

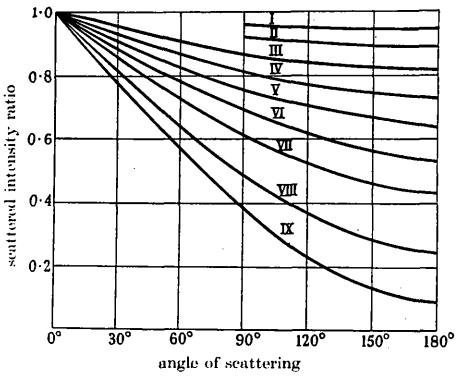

Angular distributions of positrons of various energies scattered by mercury nuclei. The scattered intensity is given as the ratio to that, $q^2 \operatorname{cosec}^4 \frac{1}{2}\theta/k^2$, given by the Rutherford formula. Curves I–IX respectively correspond to positrons of energies 0·046, 0·086, 0·145, 0·232, 0·314, 0·463, 0·666, 1·28 and 3·35 mc^2.

FIGURE 7.

The graph shows that, according to the relativistic theory, the scattering cross-section for positrons is always lower than the Rutherford value, reaching a small fraction of that value at large scattering angles in the case of high energy positrons. The large difference predicted between electron and positron scattering intensities in a heavy element is well illustrated in Figure 8.

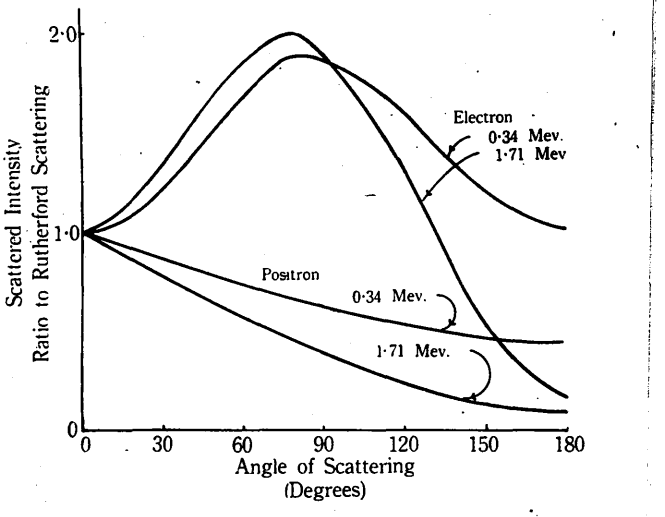

—Calculated scattering *v.* angle for positrons and electrons.

FIGURE 8.

For elements of low or moderate atomic number an approximate scattering formula similar to (II.6) or (II.7) can be used to calculate cross-sections. The only alteration is in the sign of the third term which for positrons is minus instead of plus. Figure 9 shows curves similar to those of Figure 8 for the light element argon (Z = 18), but calculated for projected angles (vide infra).

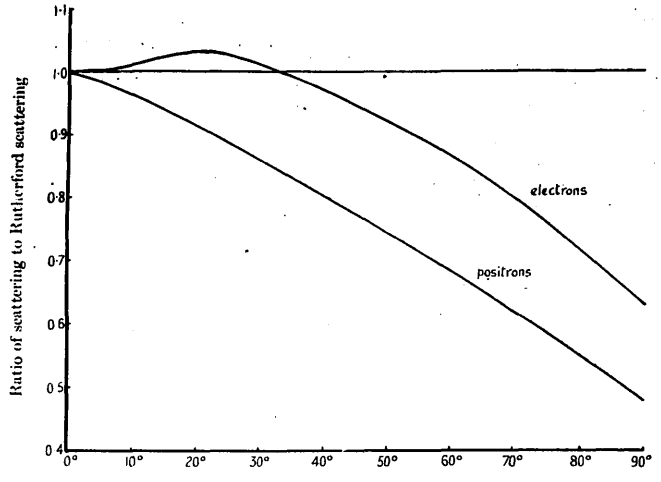

1 MeV. electrons and positrons: calculated ratio of scattering to Rutherford scattering (projected angles, $\rho=1$) in Argon.

FIGURE 9.

In cloud chamber experiments the region of interest lies in the angular range 20° - 60°. Scattering angles smaller than 20° are difficult to detect and measure accurately, and the number of events at angles greater than 60° is too small to be significant. Figure 9 shows that for the element argon the difference in scattering cross-section for 1 Mev electrons between the predictions of the relativistic and the semi-classical theory is very small in the significant angular range. The difference is too small to be detected by the cloud chamber method. Indeed it is doubtful if any cloud chamber experiment has been able to distinguish unambiguously between the Mott and Rutherford theories by measurements on electron scattering by any element. As Figure 9 shows,

however, the scattering of positrons offers a much more sensitive test of the theory. Even for an element of comparatively low atomic number such as argon, the predicted difference is of the order of 20% in the significant angular range. This difference should be experimentally demonstrable by the cloud-chamber method. It may be noted that the method used by Van de Graaff et al (G1, B3) which gave results in good agreement with relativistic theory (see Figure 3) is not applicable to the positron case, since it involved the use of an artificially accelerated beam of electrons.

The collection of data on positron scattering is thus of considerable value, not only to check the absolute scattering intensity and angular distribution but also to test the applicability of the Mott theory of scattering, involving as it does the concept of spin, to scattering problems.

Projection of Scattering Formulae.

It is convenient at this stage to consider the method of converting the various scattering formulae to a form suitable for comparison with measurements made in a single plane, this being the method of analysis adopted (Chapter V).

Randels et al (R 1) have derived the projected form of the Mott scattering formula for the particular case in which measurements are made on all tracks, whatever their length. It is shown in Chapter V that to obtain accurate measurements it is desirable to accept tracks with lengths greater than a certain minimum value. The projected form of the general scattering law, making allowance for such a mimimum length, has been derived by O'Ceallaigh and MacCarthaigh (O 1), whose notation will be followed.

The calculation of the scattering angle distribution in the projected system is based on the fact that the usual scattering formulae can be expressed in the form

$$P(\theta)\, d\theta = N f(Z,\beta)\, F(\theta).\, 2\pi \sin\theta\, d\theta$$

where $P(\theta)d\theta$ is the probability that a particle moving at speed βc through a medium containing N nuclei of atomic number Z per unit volume will be scattered once through an angle lying between θ and $\theta + d\theta$ in a path-length of 1 cm, and where $F(\theta)$ is of the form

$$\operatorname{cosec}^4\theta/2 + A\operatorname{cosec}^3\theta/2 + B\operatorname{cosec}^2\theta/2 + C\operatorname{cosec}\theta/2$$

e.g. in Mott's formula

$$F(\theta) = \operatorname{cosec}^4\theta/2 - \beta^2\operatorname{cosec}^2\theta/2 + \pi Z\alpha\beta\,(\operatorname{cosec}^3\theta/2 - \operatorname{cosec}\theta/2)$$

or, in the formula derived by McKinley and Feshbach :-

$$F(\theta) = \operatorname{cosec}^4\theta/2 - \beta^2\operatorname{cosec}^2\theta/2 + \pi Z\alpha\beta\,(\operatorname{cosec}^3\theta/2 - \operatorname{cosec}^2\theta/2).$$

The probability of scattering into the angular range ϕ to $\phi + d\phi$, where ϕ is the projection of θ in a plane perpendicular to the axis of the camera (y-axis, Figure 4) is shown to be

$$P(\phi)\, d\phi = \frac{2N f(Z,\beta)}{a} \sec^2\phi \int_{-a}^{a} dy \int_{\phi}^{\theta_M} \frac{F(\theta)\sin\theta}{(\sec^2\theta - \sec^2\phi)^{\frac{1}{2}}}\, d\theta\, d\phi\ ,$$

where

$$\cos\theta_M = \frac{\lambda_c \cos\phi}{\left\{\lambda_c^2 + (a \pm y)^2\right\}^{\frac{1}{2}}}$$

The boundaries of the illuminated region of the cloud-chamber are the planes $y = \pm a$. λ_c is the minimum projected length of the tracks which are to be included in the measurements. It is assumed that the incident particles travel normal to the y-axis in a parallel beam of uniform intensity covering the entire depth of the illuminated layer.

Barker (B 10) gives value of $P_n(\phi)/N f(Z, \beta)$ corresponding to $\phi = 10^\circ, 20^\circ, \ldots\ldots, 90^\circ$ for $F(\theta) = \operatorname{cosec}^n\theta/2$ where n = 1, 2, 3, and 4,

and for values of $\rho = 0,\ 0{\cdot}5,\ 1{\cdot}0$, and $2{\cdot}0$. From these figures, by graphical integration or otherwise, the integrated values over suitable angular ranges may be calculated. O'Ceallaigh (0 2) presents tables containing the integrated values calculated for the angular ranges $20^{\circ} - 30^{\circ}$, $30^{\circ} - 40^{\circ}$, etc. for a number of different values of ρ. $\left(\rho = \frac{\lambda_c}{2a}\right)$.

CHAPTER III

CLOUD CHAMBER AND PHOTOGRAPHIC TECHNIQUE

The discovery of the principle on which the cloud chamber operates followed directly from studies by Aitken (A 4) and Coulier (C 7), and especially C.T.R. Wilson (W 3) on the conditions for condensation or cloud-formation in moist air. These conditions were clearly demonstrated by C.T.R. Wilson in the investigations described in his classical papers of 1897 and 1899. Wilson found that in air initially saturated with water vapour from which all dust nuclei had been removed, three critical values of supersaturation could be distinguished :-

1) Fourfold supersaturation at which negative ions begin to act as condensation nuclei.

2) Sixfold supersaturation at which positive ions begin to act as condensation nuclei.

3) Eightfold supersaturation at which condensation takes place to an extent which increases very rapidly with further increase in supersaturation on uncharged nuclei consisting possibly of molecular aggregates.

In addition, following the formation and evaporation of a cloud, nuclei remain on which condensation takes place readily at low values of supersaturation.

During the period 1901-1912 Wilson perfected the first cloud-chamber (see p. 61 for description), in which supersaturation conditions corresponding to condensation on ions were momentarily produced by the adiabatic expansion of a closed volume of moist air. He showed that if 'old' ions were removed by means of an electric field, the tracks of charged particles which had traversed the chamber at or near the moment

of expansion were sharply defined by the drops condensed on the ions formed along the trajectories.

Sudden expansion is not the only method of producing the required supersaturation. Recently interest has been revived in continuously sensitive chambers of the type due to Langsdorf (L 2), in which conditions for condensation on ions are produced by the diffusion of a vapour (methyl alcohol) through a region in which a large temperature gradient is maintained. Chambers of this type may have some important applications in the future, but they have not yet been applied in any extensive investigation.

The following discussion refers to the normal cloud-chamber of the Wilson type in which supersaturation of limited duration is produced by the adiabatic expansion of a given volume of gas saturated with vapour

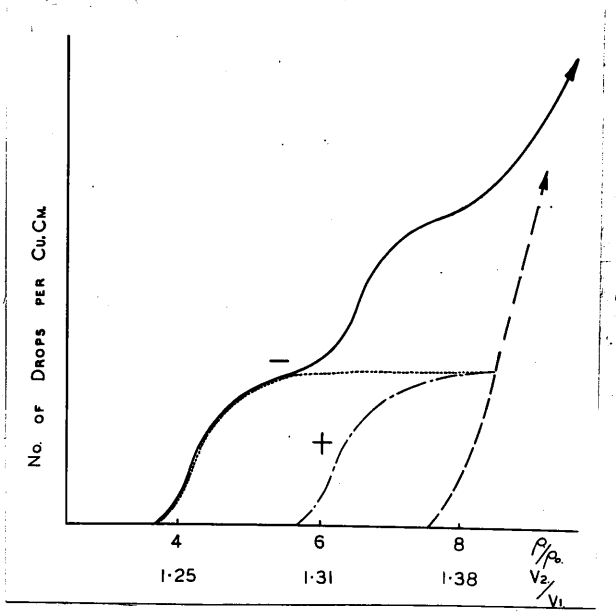

FIGURE 10

The full line in Figure 10 shows how the number of drops per unit volume varies as the saturation ratio is increased. The corresponding expansion ratios (for an air-water-vapour mixture) are also shown along the abscissa. The dotted lines indicate the contributions made at each value of supersaturation by the three types of condensation nuclei- negative ions, positive ions and neutral molecular aggregates. It is apparent from the figure that the most useful region, corresponding to condensation on all the ions without the formation of appreciable numbers of background drops, is of very limited extent. The corresponding values of expansion ratio are equally critical. It follows that a necessary feature of a good cloud-chamber design is provision for accurately adjusting the expansion ratio (to within one part in 200 or better).

The figure is drawn to represent ideal conditions in which complete condensation on ions occurs before the background drops are appreciable in number. The realisation of such conditions requires careful choice of the constructional materials of the chamber and the utmost attention to cleanliness in assembling the parts in contact with the sensitive volume. The introduction of even minute quantities of some substances advances the onset of background condensation and may easily lead to conditions in which the tracks are scarcely distinguishable against the background fog. The presence of small leaks must also be avoided because of the deleterious effect of the introduction of dust-laden air.

In Wilson's cloud-chamber the only substances which came into contact with the sensitive volume were glass and gelatine: this was ideal for the avoidance of contamination. In later chambers substances

such as perspex, stainless steel, brass and rubber have been introduced without any appreciable effect on the quality of the tracks, but aluminium, and base metals in general, appear to be sources of contamination. The action of ultraviolet light undoubtedly leads to heavy condensation but there is usually no difficulty in excluding such radiation from the chamber.

In a chamber assembled from clean materials and completely free from leaks it is necessary before operation to remove the dust nuclei which are always present in the gas. This is done by making repeated slow expansions during which drops are formed on the nuclei and allowed to settle on the floor of the chamber. The clearing process is considerably accelerated if the floor is covered with gelatine, which presumably acts by firmly retaining the nuclei which settle on it, thus preventing their redispersion during subsequent expansions. Indeed Wilson on occasion went so far as to coat the entire inner surface of the chamber with gelatine, but the optical properties of the glass were thereby destroyed. An alternative and frequently used background material is a black velvet sheet saturated with the condensing substance. This was found by the writer to be only slightly less efficient than a gelatine layer in its clearing action.

When a chamber has been thoroughly cleaned by repeated slow expansions it is interesting to observe the change in the appearance of the tracks as the expansion ratio is gradually increased. This is best done with a chamber containing air and water vapour, for which the critical supersaturation limits and the corresponding expansion ratios are accurately known. The expansion ratio control is first calibrated by

observing the pressure changes at various settings in the normal and expanded positions, time being allowed between each reading for the re-establishment of temperature equilibrium. Application of Boyle's Law then gives the corresponding volume changes.

A weak β-particle source, such as a small piece of an old radon tube placed near a window in the side of the chamber, forms a convenient source of electrons. A good source of illumination focussed into a flat beam is necessary for the visual observation of the tracks and drops, which are most clearly seen from an oblique angle (vide infra.). As the expansion ratio is gradually increased from a low value, a point is eventually reached (E.R. 1·25) at which condensation begins to take place on negative ions. The tracks at this stage appear diffuse as some of the ions move appreciably in the electric field before being fixed by condensation. As the expansion ratio is further increased, more and more ions act as condensation centres. Negative ions formed along tracks are fixed almost immediately so that the tracks are sharply defined. At this stage the density of background drops in a 'clean' chamber is negligible. As the expansion ratio rises beyond the limit for condensation on positive ions (1·31), a diffuseness or trailing appearance occurs on one side of the tracks. This is due to movement of the positive ions in the electric field from the region of the track where the supersaturation is reduced by condensation on the negative ions to a region where the supersaturation is sufficient for the positive ions to act as condensation centres. Further increase in expansion ratio removes the diffuseness and results in appreciable improvement in the quality and sharpness of the tracks. The practical limit in very clean chambers occurs at about

an expansion ratio of 1·35, at which value condensation takes place on all ions of each sign. The increase in the number of background drops, which is slow during the stages described, then becomes much more rapid, and if the expansion ratio is further raised, the tracks soon become indistinguishable against the heavy drop background. The onset of background condensation occurs at lower expansion ratios in the presence of small traces of contamination, and tracks of the highest quality are not then obtainable. It is usually found that the performance of an initially clean chamber deteriorates slowly with time, presumably owing to the accumulation of contamination by chemical action. After some weeks of use the background conditions become unacceptable and the chamber has to be dismantled and cleaned. This may involve immersing metal parts in weak acid solution followed by scrubbing in water containing a detergent such as 'teepol' and then by prolonged and thorough rinsing in clean running water. The glass parts, particularly the upper plate through which the photographs are taken, must also be thoroughly cleaned and polished. The opportunity is usually taken to wash or replace with fresh material, parts such as rubber diaphragm, background velvet, etc. which come into contact with the sensitive volume.

The values of supersaturation and expansion ratio shown in Figure 10 refer to a chamber containing air and water vapour. In all cases the critical region in which condensation takes place on ions but not on other nuclei is of very limited extent. It may happen of course that no such region exists, general cloud formation occurring before condensation on ions, in which case the vapour is useless for cloud-chamber work. Water vapour is exceptional in condensing more easily on negative than on positive ions. For nearly all other vapours or combinations of vapours

the reverse is found to be the case.

A combination of vapours frequently used is that of water and ethyl alcohol in the proportion by (liquid) volume of 1:3. This mixture has the advantage of requiring a lower expansion ratio than either of the vapours alone. This in turn reduces the mechanical movement and temperature drop during the expansion, which helps in the avoidance of turbulence. One disadvantage is that the alcohol diffuses through rubber more rapidly than water vapour, so that in chambers with rubber diaphragms the proportion of the vapours, and consequently the expansion ratio, alters slowly with time. The behaviour of the chamber at a given expansion ratio cannot then be taken as a definite indication of its performance.

The fall in temperature during an expansion is large- an easily remembered mnemonic for the combination air plus water vapour is the following :- an expansion ratio of 1·xy corresponds to a drop in temperature of xy°C. e.g. if the expansion ratio is 1·30, the fall in temperature is 30°C.

In Figure 11 the line AB represents the variation with temperature, θ, of the saturation vapour density ρ. Representing the initial state of the vapour by the point C, and assuming that the gas mixture obeys the perfect gas laws, the relation between θ and ρ during an adiabatic expansion is $\theta/\rho^{\gamma-1}$=const., indicated by the curve CD.

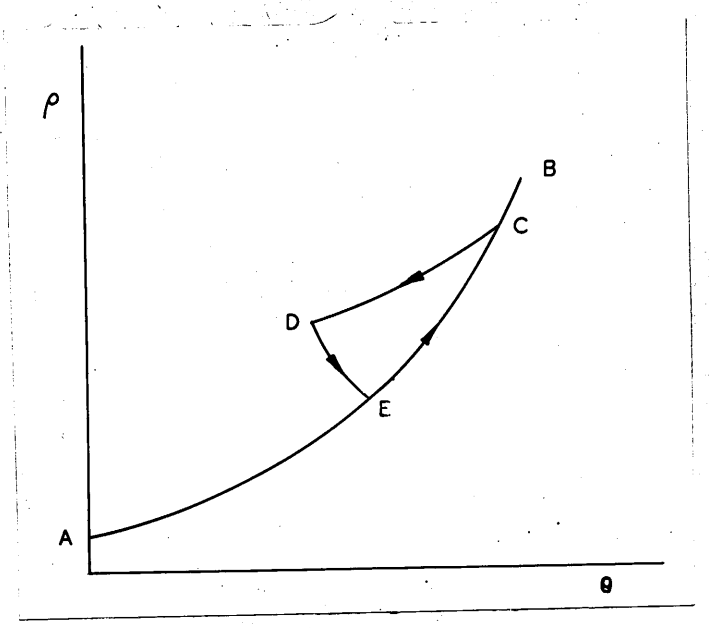

FIGURE 11.

The point D represents a supersaturated state of the vapour, which, however, persists for a short time only, the vapour returning to its original state via a path such as DEC. This is due partly to the heat liberated by condensation into drops and partly to heat absorbed from the walls of the containing vessel, which do not share appreciably in the fall in temperature. The latter effect is the more important in limiting the sensitive time (time during which the supersaturation is sufficient for condensation on ions) in normally operated chambers. Williams (W 4) analysed the effect, and distinguished two regions of the chamber - a thin layer near the walls heated directly by conduction from the walls: this expands and heats by compression the second region, the main volume of gas in the chamber. The rise in temperature which destroys the supersaturated condition and sensitivity of the chamber thus occurs almost simultaneously throughout the whole volume. Williams deduced for

T_o, the sensitive time of a chamber of volume V and surface area S, the expression

$$T_o = 0{\cdot}77 \frac{\rho S}{K(\gamma-1)^2}\left(\frac{V}{S}\right)^2\left(\frac{\delta r}{r}\right)^2 \qquad \text{(III.1)}$$

where $(1 + r)$ is the minimum expansion ratio for condensation on ions and $(1 + r + \delta r)$ is the actual expansion ratio. The sensitive time is greater in large chambers where the volume to surface ratio is large.

If the condensation is heavy, the heat liberated in the process is not negligible, but since the liberation of heat is localised, the magnitude of the effect is less easily calculated. Hazen (H 1), however, deduced a formula corresponding to (III.1) for the limitation of sensitive time due to condensation, viz.

$$T_1^{3/2} = \frac{1}{4\pi}\frac{\rho S}{K(\gamma-1)}\frac{1}{2/3\, n\left(\frac{da_o^2}{dt}\right)^{\frac{1}{2}}}\frac{\delta r}{r}, \qquad \text{(III.2)}$$

where n is the number of drops condensed per cc. and $\frac{da_o^2}{dt}$ is proportional to the rate of drop growth. Hazen also showed that the resultant sensitive time $\bar{T}$ is related to T_o and T_1 by the expression

$$\left(\frac{\bar{T}}{T_1}\right)^{3/2} + \left(\frac{\bar{T}}{T_o}\right)^{\frac{1}{2}} = 1$$

Measurements of the sensitive times of a number of chambers have shown fairly good agreement with the theory.

Prolongation of the sensitive time of a chamber, though worth pursuing in some applications such as searching for rare cosmic ray events, is of little advantage where accurate measurements are required. The useful sensitive time is limited by the onset of turbulent motion of the gas, which produces distortion of the tracks. This becomes appreciable within less than a second after the completion of an expansion, and may limit not only the useful sensitive time but also the period available for drop growth before the tracks are photographed. The turbulent motion is caused

largely by inequalities of temperature in the gas but may be accentuated if (1) the gas is not in thermal equilibrium before expansion, (2) the movement of the piston or rubber diaphragm is not uniform during expansion and free from oscillation at the end, or (3) pockets of gas are present in recesses in the sensitive volume.

It is of great help in setting up stable thermal equilibrium before expansion if the temperature of the floor of the chamber is kept slightly below that of its surroundings. This may be done by regulating the flow of cooling water round the base of the sensitive volume (see next chapter). Points (2) and (3) are taken care of in a well designed expansion chamber, and are also discussed in the next chapter.

Illumination of Tracks.

Two types of illumination are required - a steady source for the visual observation of chamber conditions and an intense short-duration flash for photographic recording. For the former a tungsten lamp of the motor-car headlamp type with a straight horizontal filament was found very suitable, the beam being focussed into a flat sheet by means of a cylindrical lens. Care has to be taken to avoid local heating of the chamber near the lamp. This can be prevented by interposing a sheet of heat-absorbing glass.

For photographic illumination a number of different sources have been used, including filament lamps momentarily over-run, mercury vapour capillary lamps subjected to a high tension discharge (Wilson) or to a pulse from a high voltage transformer (Blackett): but in recent years these sources have been entirely superseded by the development of rare-gas discharge lamps which are now commercially available. These lamps

produce a good approximation to a line source of intense illumination of very short duration, and are therefore ideal for cloud-chamber illumination. Nevertheless, the collimation of the beam from such a source requires great care if the highest standards of track photography are to be attained.

The light-scattering efficiency of a drop falls off very rapidly as the angle between the direction of the illuminating beam and the line of view is increased. Measurements on the relative intensity of light scattered at various angles from water and water-alcohol drops of the size encountered in cloud-chambers (about 20 microns diameter) have been made by Webb (W 5). The results, illustrated in Figure 12, indicate a scattering intensity at right angles to the illuminating beam less than 1% of that at 20°.

Angle of scattering (°)	Relative scattered intensity	
	Water	Alcohol-water
20	100	63
40	12	13
60	2·5	4·7
80	0·8	2·0
100	—	1·0

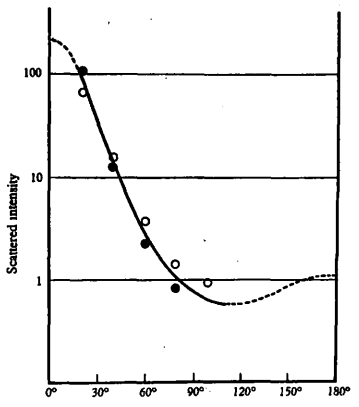

Scattering of light by cloud-chamber droplets. The full line covers the region investigated by Webb (1935) (● water, ○ alcohol-water), the broken curve is conjectural.

FIGURE 12.

In cloud-chamber work the experimental arrangement usually necessitates photography by light scattered through about 90°, at which angle, as noted above, the scattering efficiency of the drops is low. Even a small amount of stray light scattered from the background seriously reduces the visibility of the tracks. The amount of background scatter can be reduced by good collimation of the illuminating beam. The arrangement used is described in the following chapter. Figure 13 shows electron tracks taken under optimum conditions of illumination. In Figures 14 and 15 which are typical routine photographs taken with the apparatus described in the next chapter, light scattered by the velvet background is visible over a small area, but the intensity is not sufficient to interfere seriously with the visibility of the electron tracks and individual drops.

Photographic Requirements.

In applications where accurate information is required, it is always desirable and sometimes essential (as when drop counts are made) to be able to record on the photograph every separate drop in the illuminated part of the chamber. Even under optimum conditions of illumination, careful consideration must be given to the photographic system if single-drop recording is the aim.

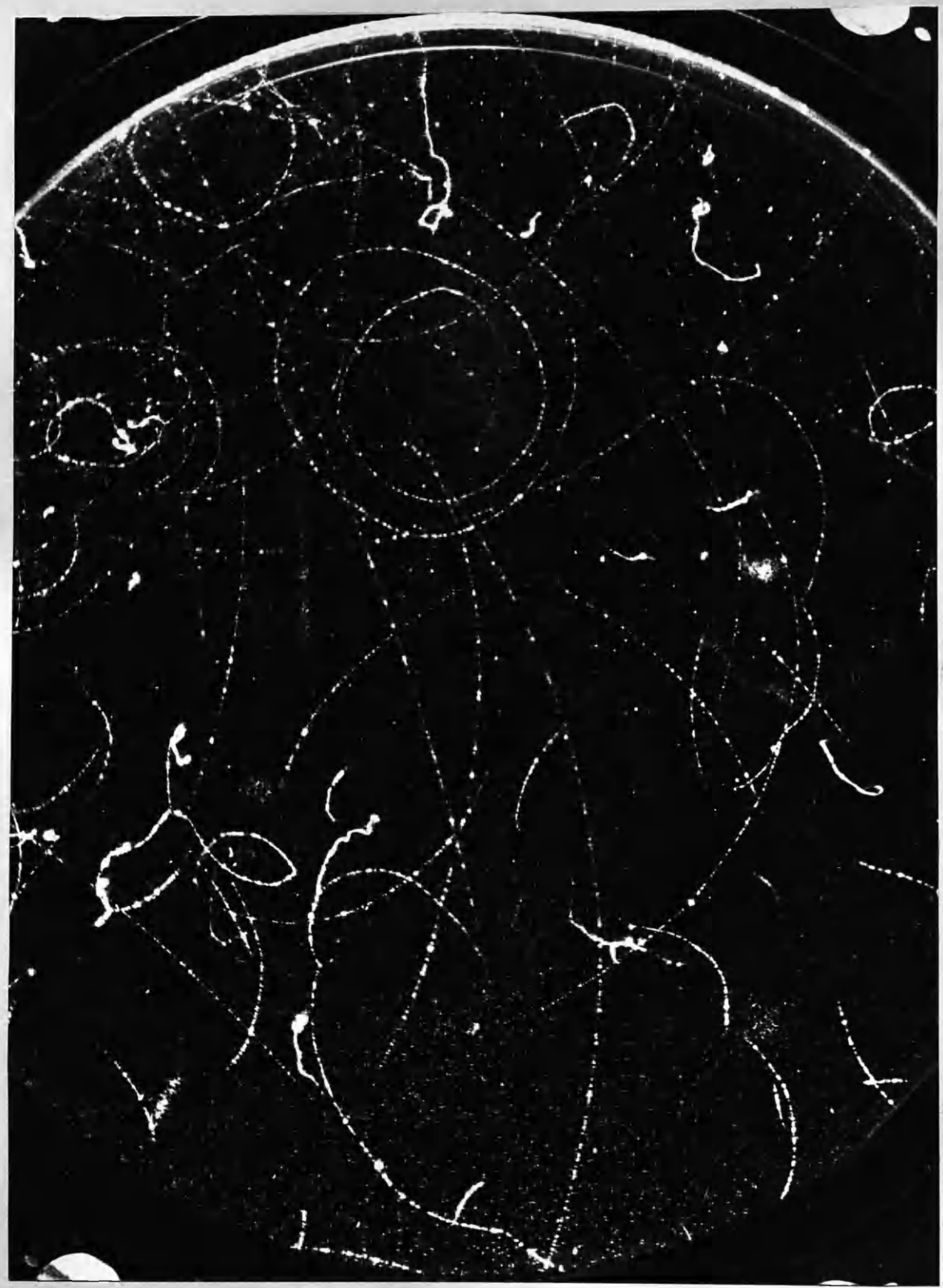

FIGURE 13:- Electron tracks of various energies; optimum conditions of illumination.

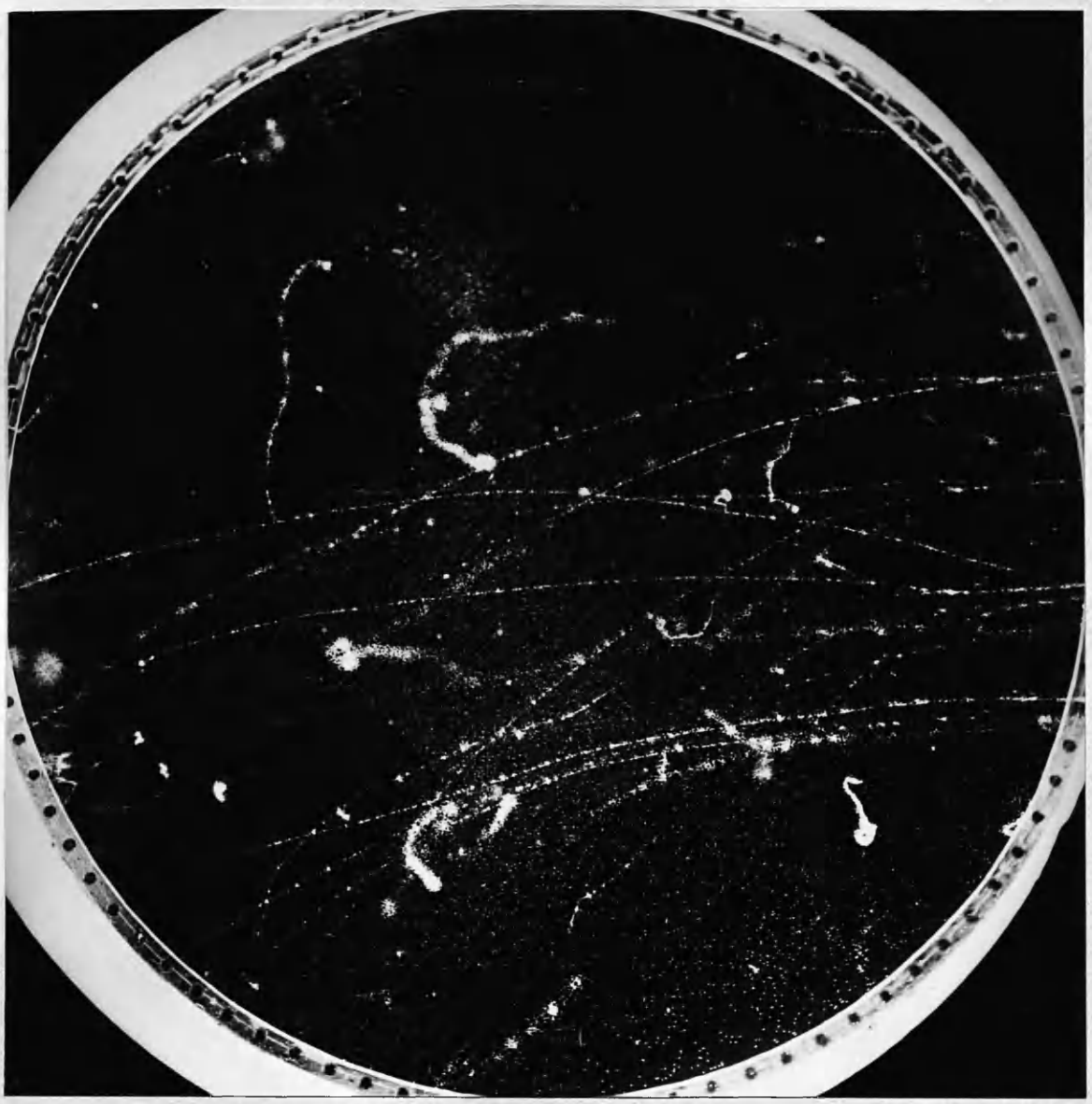

FIGURE 14:- Typical routine photograph showing electron tracks as analysed.

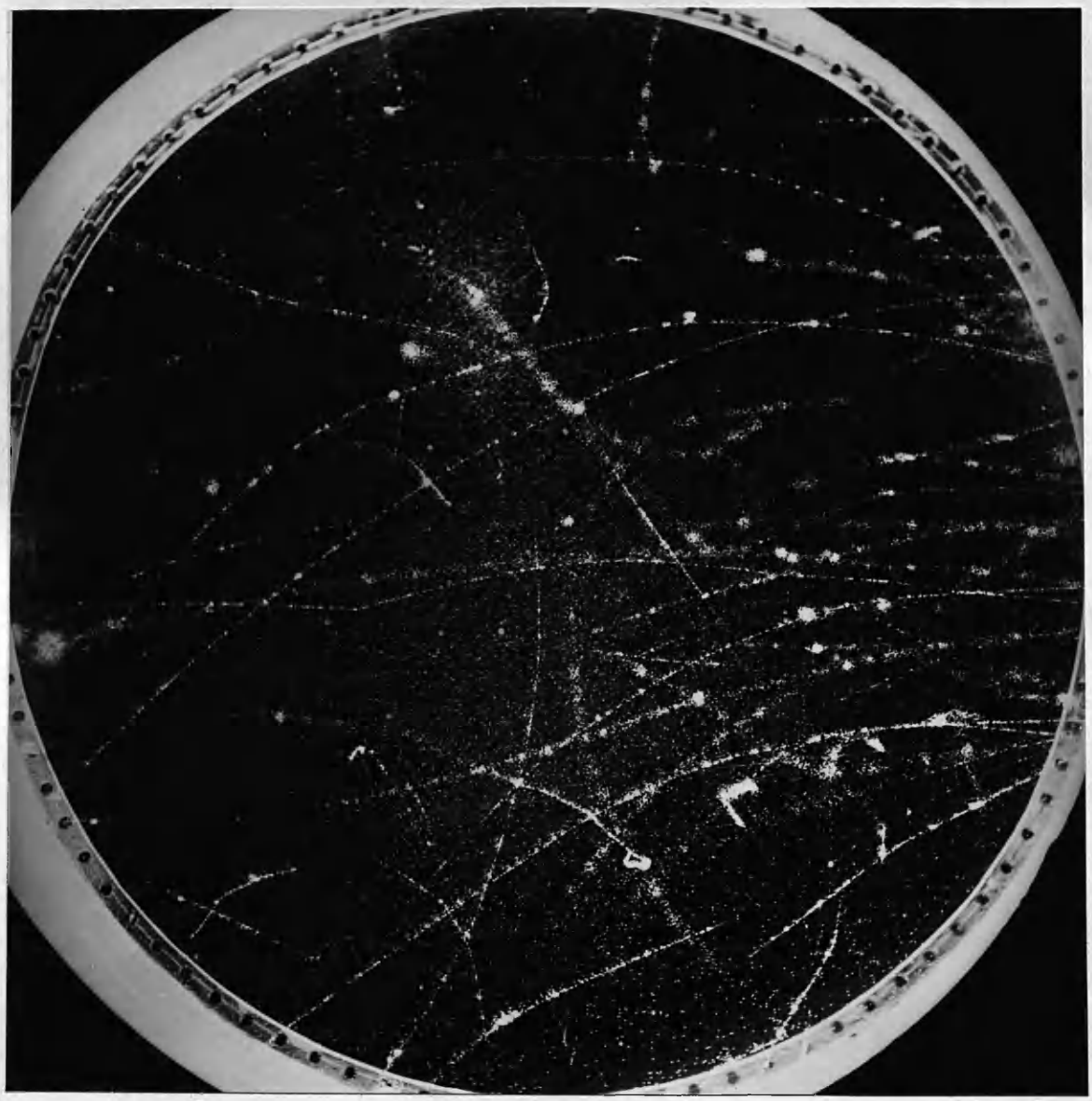

FIGURE 15:- Same as Figure 14; an electron-nuclear collision is visible to the left of the centre of the picture.

In recent years it has been customary, when large numbers of photographs are required, to record on 35mm film. In view of the small amount of light scattered and the necessity for stopping down to obtain sufficient depth of focus, it is always necessary to use a fast emulsion-high speed recording film is suitable. Preliminary work by the writer on 35mm film using a Leica camera with a 5cm focal length Ross-Resolux lens indicated that the aim of recording drops over the whole area of a 12-inch diameter chamber could not be completely realised even with a powerful light source dissipating several hundred joules per flash. It was found that even under conditions such that sufficient light was collected from each drop to produce an image, the spread in the fast emulsion was such that drops close together were not resolved. Since the size of the drop-image was found to be approximately independent of the magnification, a distinct improvement in drop resolution was obtained at higher magnifications. If, as is usually desirable, the whole chamber is to be covered by the photograph, the magnification is determined by the frame-width of the film used. For the present investigation 60mm film with standard perforations was employed. The frame width of this film is 50mm - more than twice that of standard 35mm film. To cover the entire 12" chamber the reduction factor required was 6, compared with 12 for 35mm film. As expected, the drop resolution showed considerable improvement over that obtained with 35mm film.

The size of the image sets a minimum value on the focal length of a suitable lens. Since the lens has to cover a field of 50mm diameter, a focal length somewhat greater than this is desirable. Other requirements are an adequate aperture to record drop-images, and minimum image distortion under the conditions of use. A lens designed for enlarging and thus

corrected for close working is the most suitable type.

A stereoscopic pair of cameras designed to meet the special requirements discussed above were constructed for use in the present investigation. The cameras are described in detail in Chapter IV.

Stereoscopic Arrangements.

To obtain information on the three-dimensional orientation and disposition of tracks, two photographs from different angles are required. A number of different arrangements have been used. Shimizu (S 8) employed the system shown in Figure 16(a) in which a single lens is used, but by means of a system of mirrors two images of the chamber as it appears from directions at right angles are produced alongside each other on the photographic plate. A serious disadvantage of this method is the small portion of the chamber volume which is in focus in both views. An alternative method used by Blackett (B 11) in which the image planes are at right angles is illustrated in Figure 16(b)

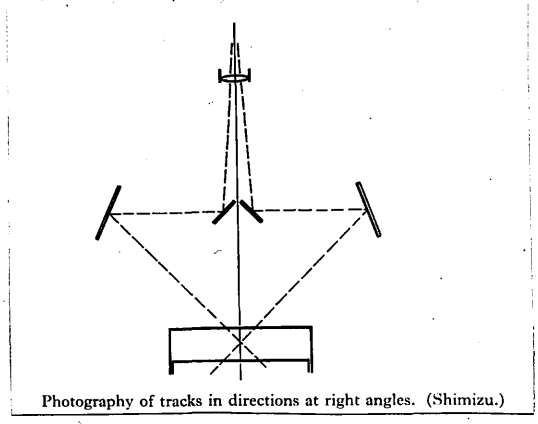

Photography of tracks in directions at right angles. (Shimizu.)

(a)

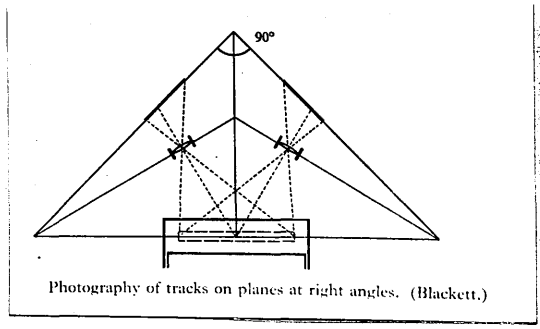

Photography of tracks on planes at right angles. (Blackett.)

(b)

FIGURE 16.

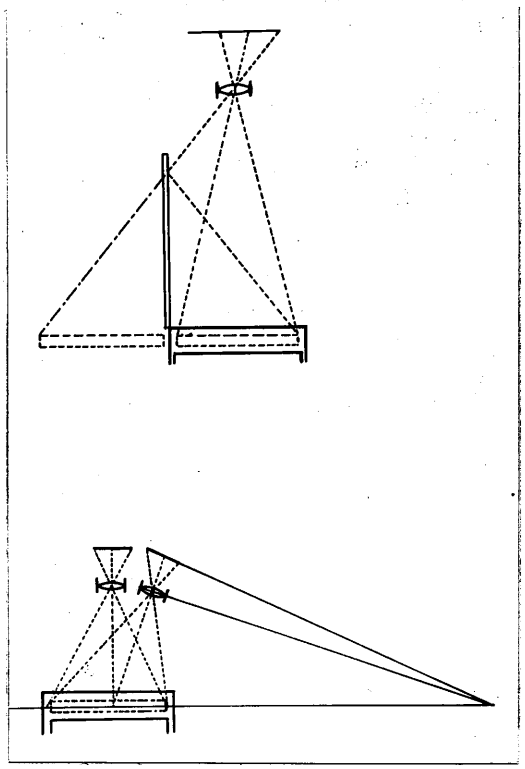

(a)

(b)

FIGURE 17.

The difficulty of keeping the whole of the chamber in focus is overcome by tilting the lens plane with respect to the image plane. It can be shown(Dict. of Applied Physics: Vol. 4. p.400) that if the object, image and lens planes are arranged to have a common line of intersection, as in the diagram, the whole of the object plane is in focus. The magnification, however, varies from point to point in the image. This is not a serious objection if the track analysis is carried out by reprojecting an image of the developed photograph through the same lens system, as all distortion is thereby automatically corrected.

In another arrangement shown in Figure 17(a) the axis of the lens is vertical. A direct image, and an oblique one obtained by reflection in a vertical mirror are formed alongside each other. The arrangement used in the present investigation is shown in Figure 17(b). Two separate cameras, one with its axis vertical, the other with axis inclined at 20° to the vertical were mounted on a rigid support. In the oblique camera, as in the Blackett arrangement, the lens was tilted so that the plane of the chamber was conjugate with the image plane.

CHAPTER IV.

APPARATUS AND MATERIALS.

The basic requirements of an expansion chamber may be summarised as follows:

(1) A perfectly sealed-off volume into which can be introduced the gas together with the condensing vapour at a suitable pressure.

(2) A mechanism for suddenly increasing this volume by an amount which can be accurately controlled.

(3) Provision of windows for illumination and observation or photography of tracks.

In addition, for normal cloud-chamber operation where successive expansions occur at intervals of, at most, a few minutes, it is necessary to make provision for slow clearing expansions in order to remove re-evaporation nuclei. It is also, in practice, essential to apply an electric field to the sensitive volume to remove rapidly from the field of view, ions produced by radioactive contamination, cosmic rays, or other sources. The operation of the cloud chamber is easily upset by fluctuations in temperature: for accurate work some form of temperature control such as water cooling of the chamber, or air conditioning of the room, is necessary. The expansion should be made in such a way as to avoid, as

far as possible, turbulent motion in the gas during and immediately after an expansion. Constructional materials have to be chosen carefully, as some substances such as aluminium and other base metals have been found to produce contamination when introduced into the sensitive part of the chamber.

The original cloud-chamber of C.T.R. Wilson (W6) has served as a model for subsequent designs which, with few exceptions, have followed the same general principles. Its construction is illustrated in Figure 18. The chamber proper consisted of a glass cylinder with a glass cover-plate, the expansion being effected by the movement of the floor which consisted of a piston ground to slide accurately into the outer cylinder. The expansion took place on opening a valve connecting the lower side of the floor to a vacuum reservoir. The pressure of the gas in the chamber caused the piston to drop suddenly until its motion was arrested by a wooden block. A pool of water at the base of the cylinder acted as a reservoir of vapour and also as a seal for the chamber. The floor was covered with a layer of blackened gelatine which served as a good photographic background, and also probably aided the removal from the gas of dust or other contaminants. The tracks were illuminated through the cylinder wall and photographed through the upper glass plate.

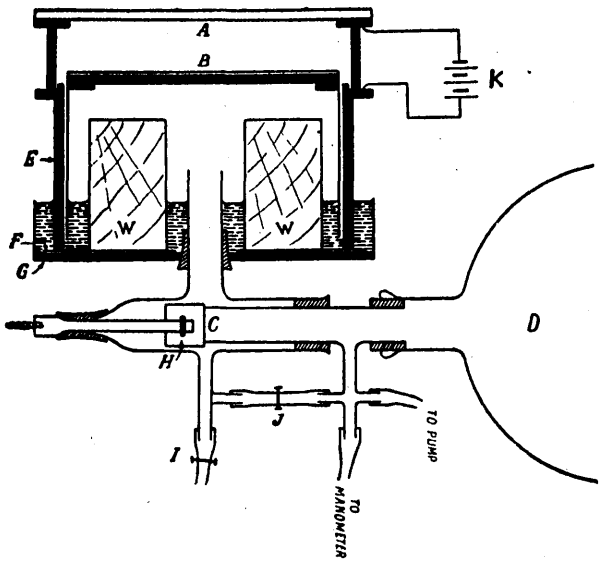

Wilson's original cloud chamber.

AB = expansion chamber, cylindrical in shape and completely closed,
B = movable base which slides inside cylinder E and serves as piston,
F = rubber sheet resting on a brass disk G to arrest downward motion of B,
D = highly evacuated vessel which may be put in communication with the space below B by opening the valve C,
WW = wooden blocks reducing the air space within the chamber,
I = stopcock on opening which space below B is connected with the atmosphere and the piston brought back to the original position,
J = pinch cock for adjusting the initial position of the piston and hence the expansion ratio,
K = battery providing the electric field to remove stray ions just before a fresh expansion.

FIGURE 18

This design of chamber has the advantage of using 'clean' materials throughout the sensitive volume. In the hands of Wilson it produced tracks of a quality which has probably not yet been improved upon. It was not, however, suitable

for rapid or long-continued operation, as the closely-fitting piston and cylinder were easily jammed by small particles of grit, and the valve release mechanism was cumbersome.

In the chamber described above the volume before and after expansion was defined. In a later design also due to C.T.R.Wilson (W7), the expansion was produced by the movement of a rubber diaphragm. The pressure below the diaphragm was suddenly altered between definite limits, one of which was usually atmospheric pressure, and the resulting changes, communicated to the sensitive volume, produced the required supersaturation. This method has not been much used as it requires more frequent adjustment of expansion conditions but the essential features of the design have been incorporated in many recent volume-defined cloud-chambers.

In subsequent work the general tendency has been to design the cloud-chamber for a specific purpose, and also to increase the rate of track recording by automatic control of the various operations. For example, Blackett (B13) designed an entirely automatic chamber for use in cosmic-ray work. The dimensions were such that the chamber could be placed in the restricted space between the poles of a large electromagnet. Descriptions of numerous other

expansion chamber designs have been published (cf. G2). A section of a chamber and associated equipment used in recent measurements on electron scattering is shown in Figure 19.

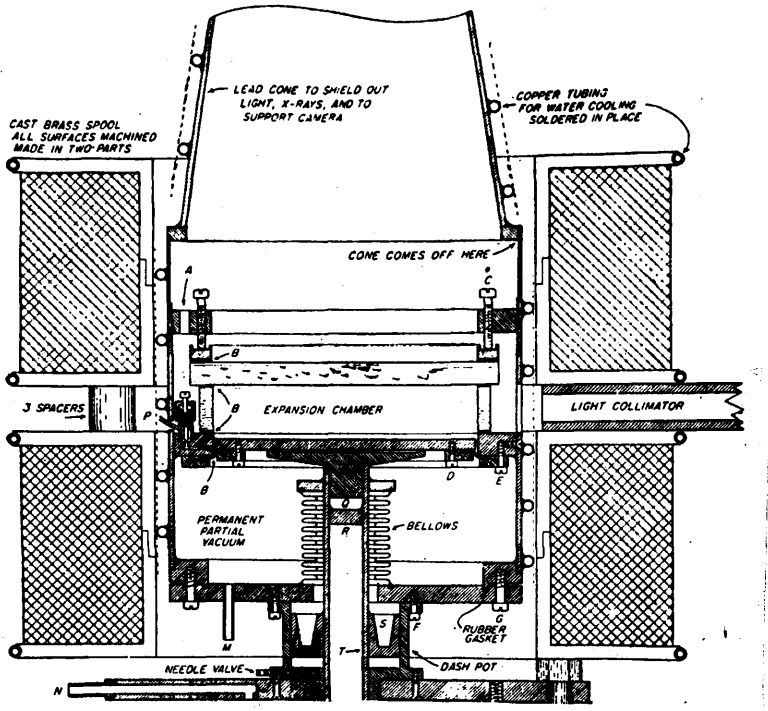

Detail of a Wilson cloud chamber (Crane).

FIGURE 19

The cloud-chamber and control equipment used in the present investigation were designed on the basis of the experience gained in the operation of two earlier models, designated types "A" and "B". These will now be briefly described.

Cloud-chamber, Type "A".

The sensitive volume of this chamber was bounded by a glass cylinder of diameter 10" and depth 2½", an upper plate of ½" thick, high quality plate glass, and a lower movable brass plate. The latter separated the chamber proper from the lower compartment which consisted of a similar glass cylinder sealed to a solid brass base-plate. The movable plate was suspended by means of an annular rubber support which was sealed between the two brass rings which separated the upper and lower cylinders. The essential features of the chamber are shown in a schematic diagram (Figure 20). The upper position of the movable plate, determined by the cone and disc arrangement shown in the figure, was adjustable by means of the screw (7). The plate was held in this position by a slight excess of pressure in the lower compartment. The expansion was produced by the opening of a magnetic valve (5) which connected the lower chamber to a vacuum reservoir. This valve could be reset by the lever (6). When the main valve was opened the pressure on the upper surface of the movable plate caused it to drop rapidly until its motion was arrested by the wooden block (4). The seal between the upper and lower compartments was maintained by the rubber annulus which stretched during the expansion. Slow expansions

CLOUD CHAMBER TYPE "A"

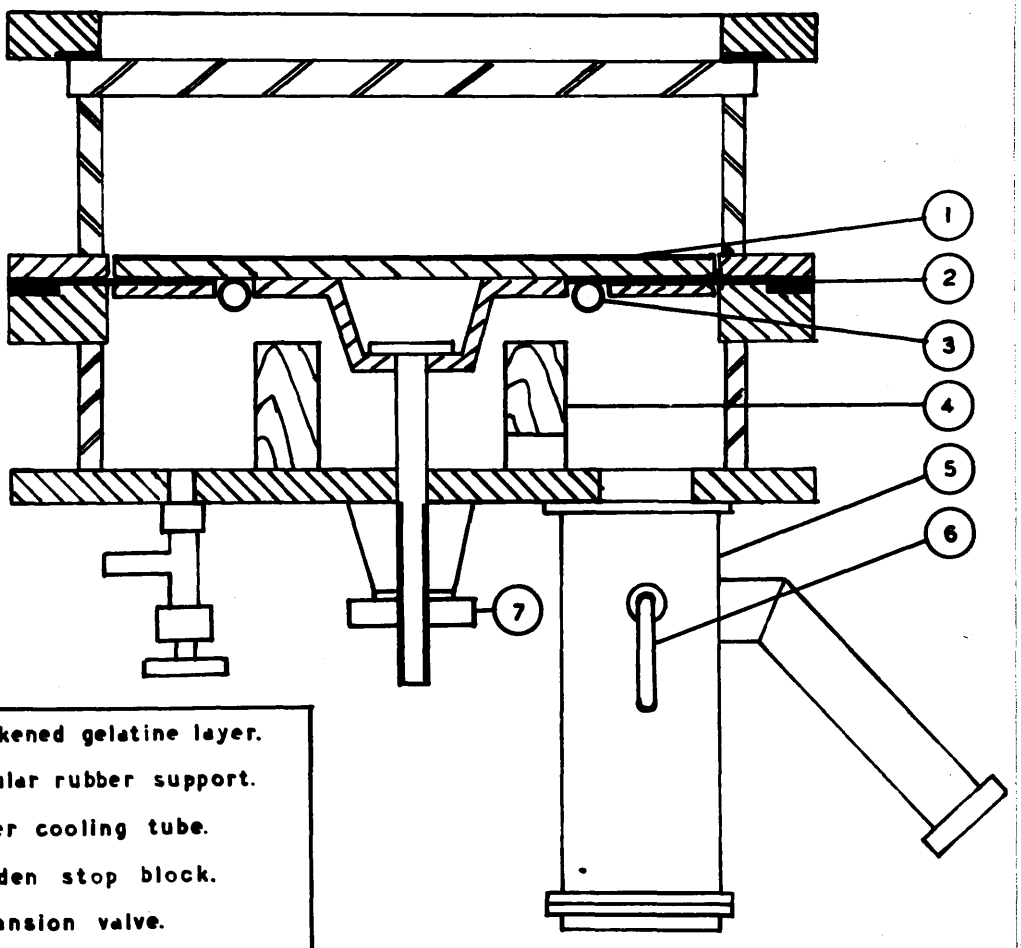

1	Blackened gelatine layer.
2	Annular rubber support.
3	Water cooling tube.
4	Wooden stop block.
5	Expansion valve.
6	Manual valve reset.
7	Expansion ratio control.

FIGURE 20.

were produced by alternately extracting air from and admitting air to the lower compartment *via* a needle valve.

With this chamber considerable difficulty was at first experienced in maintaining good thermal conditions. The movable plate was insulated from the rest of the chamber by the rubber ring and tended to respond more slowly to temperature changes. Overnight, this was responsible for a gradual movement of liquid from the base-plate to the top and sides of the chamber. This difficulty was largely overcome, and more stable thermal conditions during operation obtained, by attaching a water cooling tube (3) to the lower surface of the plate. By controlling the water flow, the base of the chamber could be maintained at a slightly lower temperature than its surroundings. Connections to the outside were made *via* flexible rubber tubes which did not affect the movement of the plate during expansions. During the night when the water flow was discontinued an electrically heated pad was placed above the glass plate to prevent migration of the liquid.

The upper surface of the movable plate has to be blackened since it is normally the background against which the tracks are photographed. It also acts conveniently as a reservoir for the condensing vapour. Surfaces of various kinds were tried, including black X-ray film soaked

in water, aquadag, filter paper soaked in dilute Indian ink, and blackened gelatine. The last was found most suitable provided a small quantity of copper sulphate or aspirin was added to prevent bacterial growth. With such a background and with this type of chamber the problem of light scatter is minimal since the smooth black surface scatters very little light and the plate is in any case well below the illuminating beam in the expanded position.

The chamber was designed with particular attention to the avoidance as far as possible of turbulent motion in the gas during and immediately after an expansion. For this reason the movable plate was made a close fit to the outer brass ring, the gap being about one tenth of an inch. This has the additional advantage of exposing very little rubber to the sensitive volume. The stretch in the rubber during an expansion, however, is correspondingly large, and difficulty was sometimes experienced in avoiding small leaks into the chamber during rapid expansions. The rapid change in tension of the rubber itself may be responsible for background condensation (cf. W8, p.51) but it seems more probable that the isolated puffs of condensation not infrequently observed were due to minute leaks.

When very carefully cleaned and assembled this chamber was very free from background condensation but difficulty

was experienced in maintaining it at its optimum working condition over long periods of time.

Cloud-chamber, Type "B".

This type of chamber, a diagrammatic section of which is shown in Figure 21, is a development of the rubber diaphragm chamber of C.T.R. Wilson, but the expansion is defined in terms of volume rather than pressure changes. The upper compartment was similar to that of type "A", but the floor consisted of a fixed brass plate perforated with a large number of holes (2). Clamped between the ring of this plate and a similar ring attached to the base plate was a rubber diaphragm dividing the chamber into two sealed compartments. In the lower compartment there was a second perforated plate (5), the vertical height of which relative to the fixed plate could be accurately adjusted by the screw (8). The position of the lower plate determined the expansion ratio. Attached to the base plate was the main expansion valve (6) with manual reset (7).

The pressure in the lower compartment was normally held slightly in excess of that in the upper, the rubber diaphragm then lying in contact with the lower surface of the upper perforated plate. When the valve plunger was released the rubber was forced on to the lower perforated plate, thus producing the required sudden expansion of the

CLOUD CHAMBER TYPE "B"

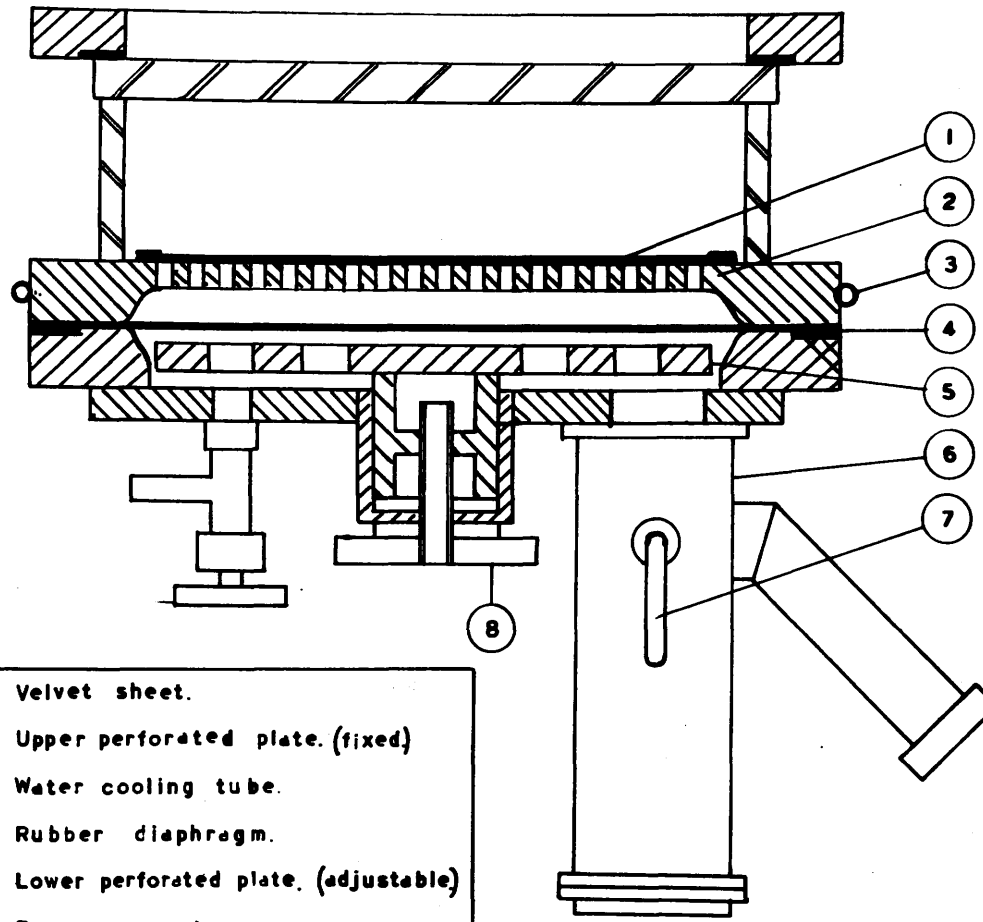

1	Velvet sheet.
2	Upper perforated plate. (fixed)
3	Water cooling tube.
4	Rubber diaphragm.
5	Lower perforated plate. (adjustable)
6	Expansion valve.
7	Manual valve reset
8	Expansion ratio control.

FIGURE 21.

gas in the chamber. Turbulence was minimised by distributing the flow of air over a large number of holes in the fixed plate. To increase further the uniformity of the flow and to provide a suitable background against which to photograph the tracks, the upper surface was covered with a sheet of black velvet (1). This also retained the excess condensed vapour. Temperature control was maintained by running water through a tube (3) attached to the lower plate.

One disadvantage of this type was the appreciable amount of light scattered by the velvet base. This could be minimised only by severely collimating the illuminating beam. The velvet was not as efficient as gelatine in retaining dust or other small particles, but provided the velvet was kept damp, no difficulty was experienced in 'cleaning' the chamber. The drop background in this type was not appreciably greater than in Type "A" and it retained a good performance for a much longer period. Owing to the absence of heavy moving parts it was faster and much quieter in operation than the first type. Light gases, however, such as hydrogen and helium, and even alcohol vapour, diffuse fairly rapidly through the rubber, so that, if such are present, the composition of the chamber gases cannot be considered constant over long periods, and the

optimum expansion ratio changes slowly with time.

Despite the disadvantages mentioned, the relative simplicity in construction and especially the reliability in operation over long periods of type "B" was such that it was decided to construct a similar but larger version for use in the main scattering investigation.

Twelve-inch Cloud-chamber.

A diagram showing in detail and to scale a section of this chamber is presented in Figure 22.

In general construction and mode of operation it was similar to type "B" described above, but it incorporated a number of new features and improvements, some of which resulted from the author's experience with the smaller chambers. The upper plate through which the tracks were photographed was of the highest quality plate glass, free from bubbles and other defects. Its optical properties were further improved by having the surfaces polished and freed from small scratches by an optical firm. For the best photographic results a high optical quality and strict cleanliness of the upper plate is essential.

The seal between the upper plate and cylinder (3) and between the cylinder and the perforated plate (6) was of lead wire. This, when compressed by tightening the nuts round the upper ring, made an excellent air-tight seal:

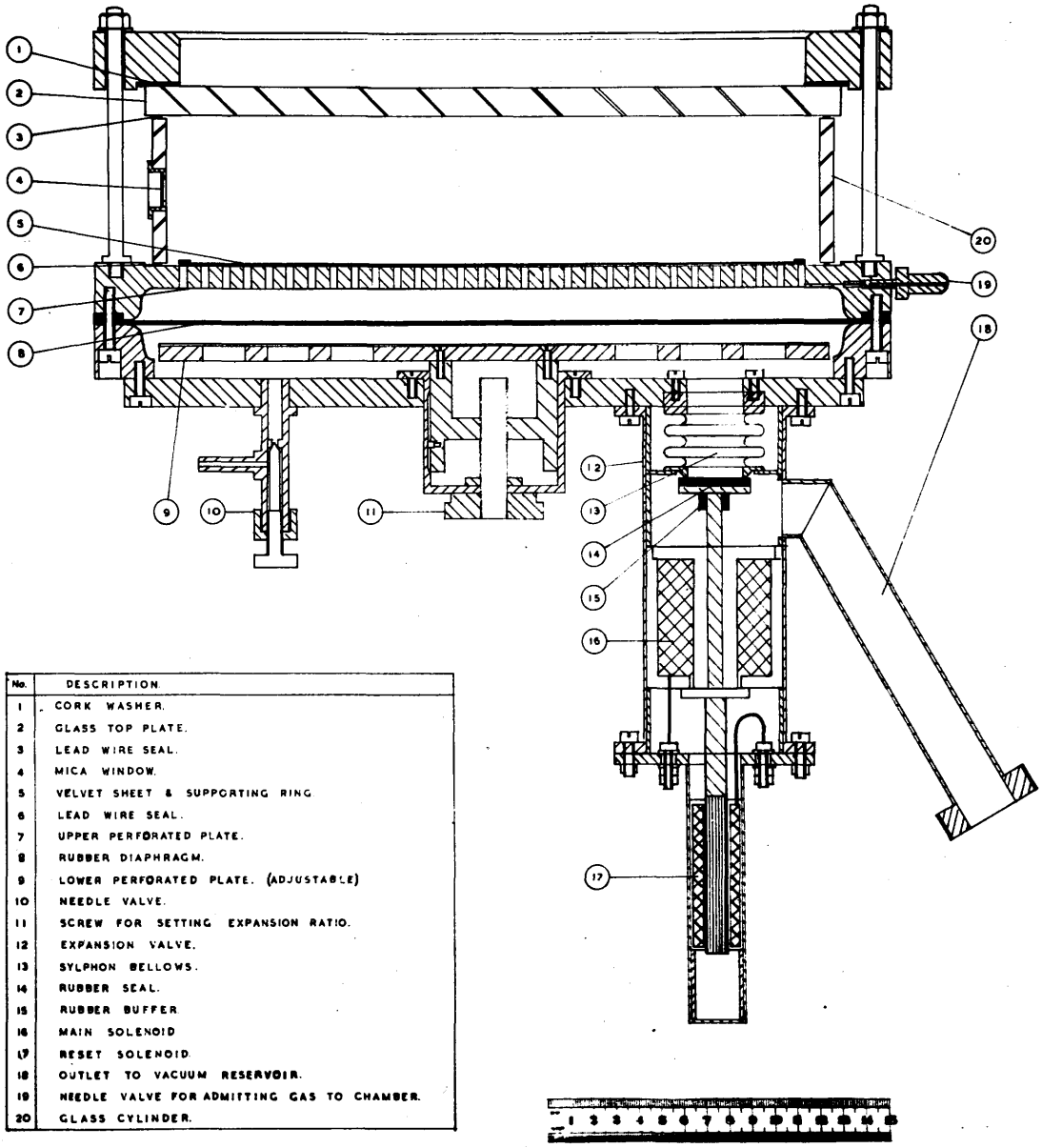

No.	DESCRIPTION.
1	CORK WASHER.
2	GLASS TOP PLATE.
3	LEAD WIRE SEAL.
4	MICA WINDOW.
5	VELVET SHEET & SUPPORTING RING.
6	LEAD WIRE SEAL.
7	UPPER PERFORATED PLATE.
8	RUBBER DIAPHRAGM.
9	LOWER PERFORATED PLATE. (ADJUSTABLE)
10	NEEDLE VALVE.
11	SCREW FOR SETTING EXPANSION RATIO.
12	EXPANSION VALVE.
13	SYLPHON BELLOWS.
14	RUBBER SEAL.
15	RUBBER BUFFER.
16	MAIN SOLENOID.
17	RESET SOLENOID.
18	OUTLET TO VACUUM RESERVOIR.
19	NEEDLE VALVE FOR ADMITTING GAS TO CHAMBER.
20	GLASS CYLINDER.

FIGURE 22:- A section of the twelve-inch expansion chamber used in the investigation.

the upper wire also formed a convenient electrode for the electrostatic clearing field.

The five windows (4) through which the particles were introduced into the chamber consisted of thin mica discs attached to brass rings which were waxed into holes drilled in the glass cylinder. Care was taken in the design of the ring supports to ensure that the mica windows, when in place, were flush with the inner surface of the cylinder.

The velvet sheet (5) was stretched tightly across a metal ring to give as flat a background surface as possible. The sheet was saturated with the water-alcohol mixture by spraying from an atomiser.

Various types of rubber sheet were tried for the main diaphragm (8). These were examined carefully for flaws and minute pin-holes and only specially selected areas were used. Suitable portions were treated with dilute caustic soda solution, scrubbed in soapy water and finally thoroughly rinsed and allowed to dry. Good results were obtained with sheets composed of equal proportions of natural rubber and neoprene of thickness 1/32" or 1/64". The rubber sheet was clamped between the fixed perforated plate and the ring of the base plate round which there was a double ridge of raised metal. To ensure a perfect seal

the thin rubber sheet was reinforced by an annulus of thicker rubber.

The upper plate (7) was perforated with a very large number of small holes (about 25 per square inch) to ensure uniformity of air flow during expansion. The lower plate was drilled with larger holes but was covered with a thin perforated metal sheet to provide a more uniform support for the rubber in the expanded position. The movement of the plate was controlled by a cylinder attached to the lower surface which slid smoothly into a second cylinder attached to the base plate. A pin on the outer cylinder running in a slot in the inner prevented the latter revolving when the screw (11) was turned. Movement of the screw was thus transferred into vertical movement of the lower plate. The position of this plate and hence the expansion ratio was in this way smoothly and accurately controllable.

The needle valve (10) shown in the Figure was one of two which gave access to the lower compartment, and enabled slow clearing expansions to be made. The main expansion valve (12) connected the lower compartment *via* the outlet (18) to a large steel tank kept continuously evacuated by a rotary vacuum pump. The valve was magnetically operated, its action being as follows. The small annular air gap is normally closed by a soft steel disc-shaped armature

which is attached to a brass rod and disc. To ensure proper seating of the armature a non-rigid connection is made between it and the brass rod. The upper surface of the disc is rubber covered (14) and in the closed position effects a seal against a brass ring attached to a short length of sylphon bellows (13). The magnet current is adjusted until the force on the armature is just sufficient to maintain the seal (14) against the pressure above it. When the current is suddenly reduced, the plunger is thrust rapidly downwards, thus leaving a large gap for the rapid flow of air from the lower chamber compartment. This movement was so rapid that it was found necessary to insert a rubber buffer (15) to avoid fracture of the metal at the point where the plunger hit the upper surface of the magnet.

To reset the valve it is not of course sufficient to restore the current: the armature has to be raised until it again makes contact with the poles of the magnet. This was accomplished by means of the reset solenoid and plunger (17). On applying a large momentary current the steel plunger,which normally rests against the bottom of the cylindrical extension to the main valve casing, is pulled sharply upwards and conveys the movement, via a brass rod, to the armature which is then held firmly by the action of the main solenoid. This type of valve and reset

mechanism worked very satisfactorily for long periods without trouble.

Valve (19) is one of the two used for admitting gas to, or flushing out the chamber. The hole leading to the inside of the chamber is made of very small diameter (1/64") to minimise movement of trapped gas during expansions.

Cloud-chamber Control Circuit.

The function of the control circuit was to carry out automatically the numerous operations involved in taking a cloud-chamber photograph. These may be listed as follows:

(1) Opening of main expansion valve
(2) Opening of camera shutter.
(3) Opening of particle shutter.
(4) Triggering of flash discharge lamp.
(5) Resetting main valve.
(6) Closing camera shutter.
(7) Closing particle shutter.
(8) Performance of slow clearing expansions.
(9) Transport of film.

The timing of these operations has to be controlled to varying degrees of accuracy.

The whole of the above sequence of events was initiated by pressing a button on the control panel. The series of operations was controlled partly by mechanical

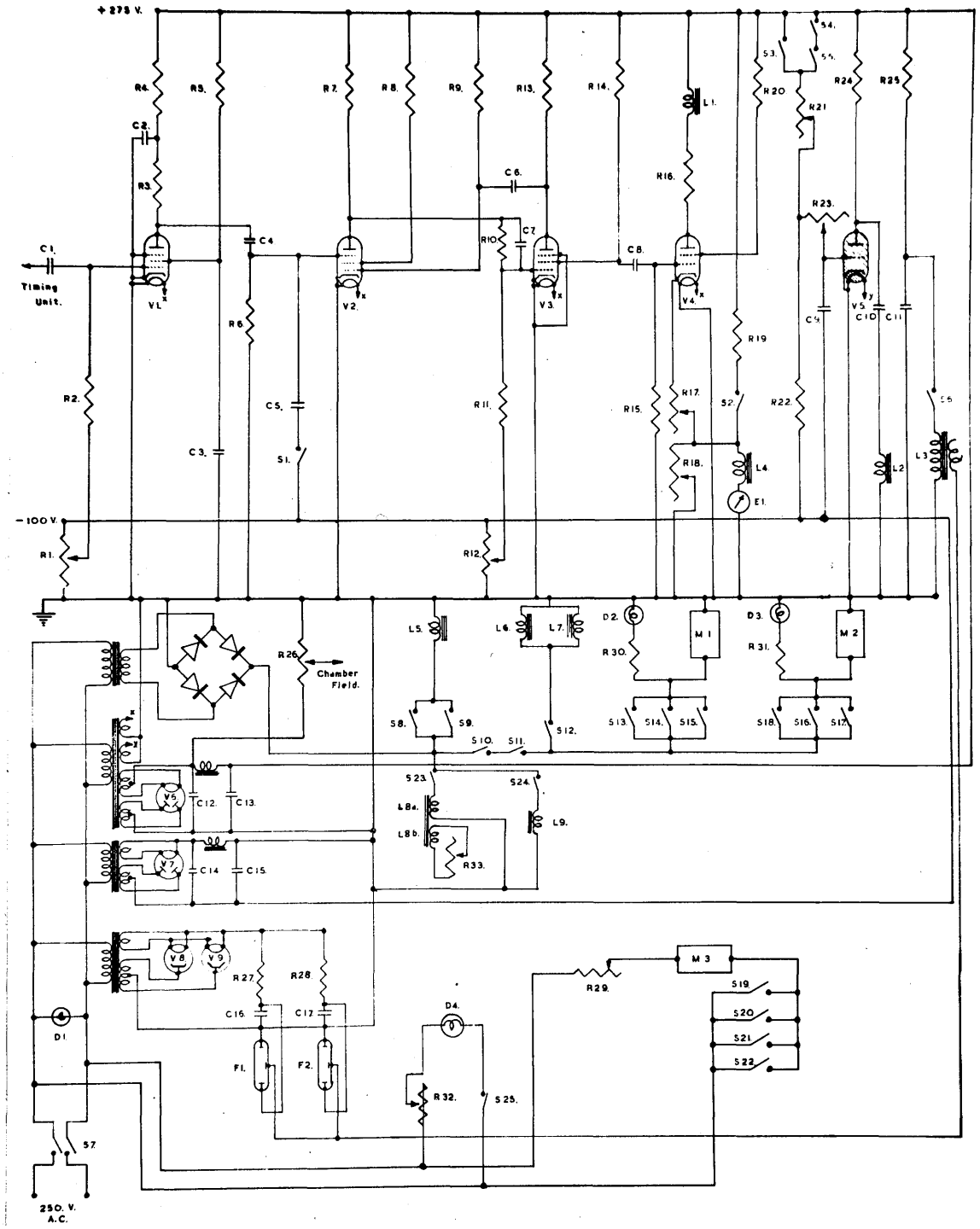

FIGURE 23:- The cloud chamber control circuit.

and partly by electronic means. The essential elements in the control circuit, together with the associated electrical power supplies are shown in Figure 23.

Conventional rectifier units supply +275 volts (smoothed), - 100 volts (smoothed), 2500 volts (for discharge lamps) and 24 volts (for motors, relays, etc).

V.1 is an amplifying valve for use in conjunction with a timing unit designed to synchronise cloud-chamber expansions with pulses from a synchrotron. It is not required in the type of investigation described here.

S.1 is the main operating button. When this switch is closed a large negative pulse is applied to the grid of V.2 which stops conducting. The resulting positive pulse on the anode of V.2 is applied via condenser C.7 to the grid of V.3 which is normally biased to cut-off. The negative pulse on the anode of V.3 acting across C.6 prevents the grid of V.2 attaining its normal potential for about one second, until it is restored via R.9. V.2 then becomes conducting again. The long negative pulse on the screen of V.3 is fed to the control grid of V.4 which stops conducting for about a second. The main valve solenoid L.4 and the main relay L.1 which are in series with V.4 are thus given ample time to operate. The current through L.4, which is indicated on the meter E.1, is adjusted by

resistors R.17 and R.18 till it is just sufficient to hold the main expansion valve closed. Thus, immediately the negative pulse reaches the grid of V.4 the expansion is initiated. When switch S.2 is closed, sufficient current passes through L.4 to hold the expansion valve closed, and pressing the main button does not produce an expansion. This is useful in testing the operation of other parts of the circuit.

V.5 is a thyratron valve. Switch S.5 is normally closed. S.4 is a contact switch on the relay L.1. When S.4 closes, the grid potential of V.5 rises at a rate depending on the setting of the variable resistors R.21 and R.23, until V.5 fires, discharging condenser C.18 through the relay L.2. The operation of this relay closes the contact switch S.6 which discharges condenser C.11 through the primary circuit of the induction coil (motor ignition coil) L.3. The resulting high voltage pulse in the secondary is conveyed to the triggering electrodes in the discharge lamps F.1 and F.2. The spark breaks down the electrical resistance of the gas, and the condenser banks C.16 and C.17, each of capacity 100μF and charged to 2500 volts, then discharge through the lamps producing an intense flash of short duration. The duration of the flash may be increased and the energy dissipation of the lamps

improved by inserting in series with each lamp an inductance consisting of a few turns of low resistance wire. The switch S.3 allows the lamps to be discharged independently of the main button S.1.

Another contact S.12 on relay L.1 energises the solenoids L.6 and L.7 which open the camera shutters. The shutters open almost as soon as the main button is pressed and remain open for about a second. This amply covers the time during which the expansion is completed and the drops grow to a size suitable for photography.

The relay L.1 further closes the contacts S.23 which by connecting the 24 volt supply to the winding L.8a operates the relay L.8. The switch contact S.24 on L.8 closes after a short interval which is controlled by the setting of R.33, a "slugging" resistance across a second winding L.8b on the relay. The closing of S.24 sends a current through the solenoid L.9 which operates the source shutter. The opening of the shutter can thus be delayed to coincide with the beginning of the sensitive time of the chamber.

A further series of operations involving longer time delays is controlled by electrical contacts operated by adjustable cams on a shaft driven by reduction gearing at about 1 r.p.m. by an electric motor M.3. The speed of the motor M.3 can be adjusted by means of a series resistor R.29.

The motor is started by the closing for about a second of the contacts S.22 on the relay L.1 and the driving current is maintained for a complete revolution of the shaft by one of the cam contacts S.21. The shaft also operates a valve which connects the lower compartment of the chamber via the opening (10) alternately to the vacuum reservoir and to the atmosphere. Thus, after the main valve closes following a rapid expansion, two complete clearing expansions are automatically performed. After a further interval of about 40 seconds to allow the re-establishment of temperature equilibrium, the chamber is ready for another rapid expansion. The button switch S.20 enables the motor M.3 to be started independently of the relay L.1. S.19 operates in conjunction with S.11: when S.19 closes S.11 opens. The motor can then be set to run continuously, and any required number of clearing expansions made, without actuating the cameras during each revolution of the shaft.

The reset solenoid L.5 is also normally operated by a cam switch S.9 on the motor-driven shaft. The valve can alternatively be reset by the button switch S.8.

Two further switches S.15 and S.17 on the cam shaft activate the motors M.1 and M.2 which transport the film in the cameras. The motors are stopped after the film

has moved on exactly one frame by micro switches (S.14, S.16) inside the cameras (vide infra). The films can also be set in motion by the button switches S.13 and S.18.

The lamps D.2 and D.3 indicate that motors M.1 and M.2 are running. D.4, a lamp for continuous illumination and visual observation of events in the chamber, is controlled by switch S.25. The lamp D.1 indicates whether the mains "on-off" switch S.7 is closed.

A list of the various elements of the control circuit with short descriptions and component values where appropriate is given in Appendix I.

Cameras.

The cameras were designed to meet the following requirements.

(1) Automatic shutter action and transport of film.

(2) Large capacity for film and accurate location in position of exposure.

(3) Provision for reprojection of developed film for purposes of analysis.

The cameras were supported on a brass framework, one with its lens axis vertical, the other with its axis inclined at 20° to the vertical. The latter was fitted with a wedge-shaped collar between the body and the lens mount,

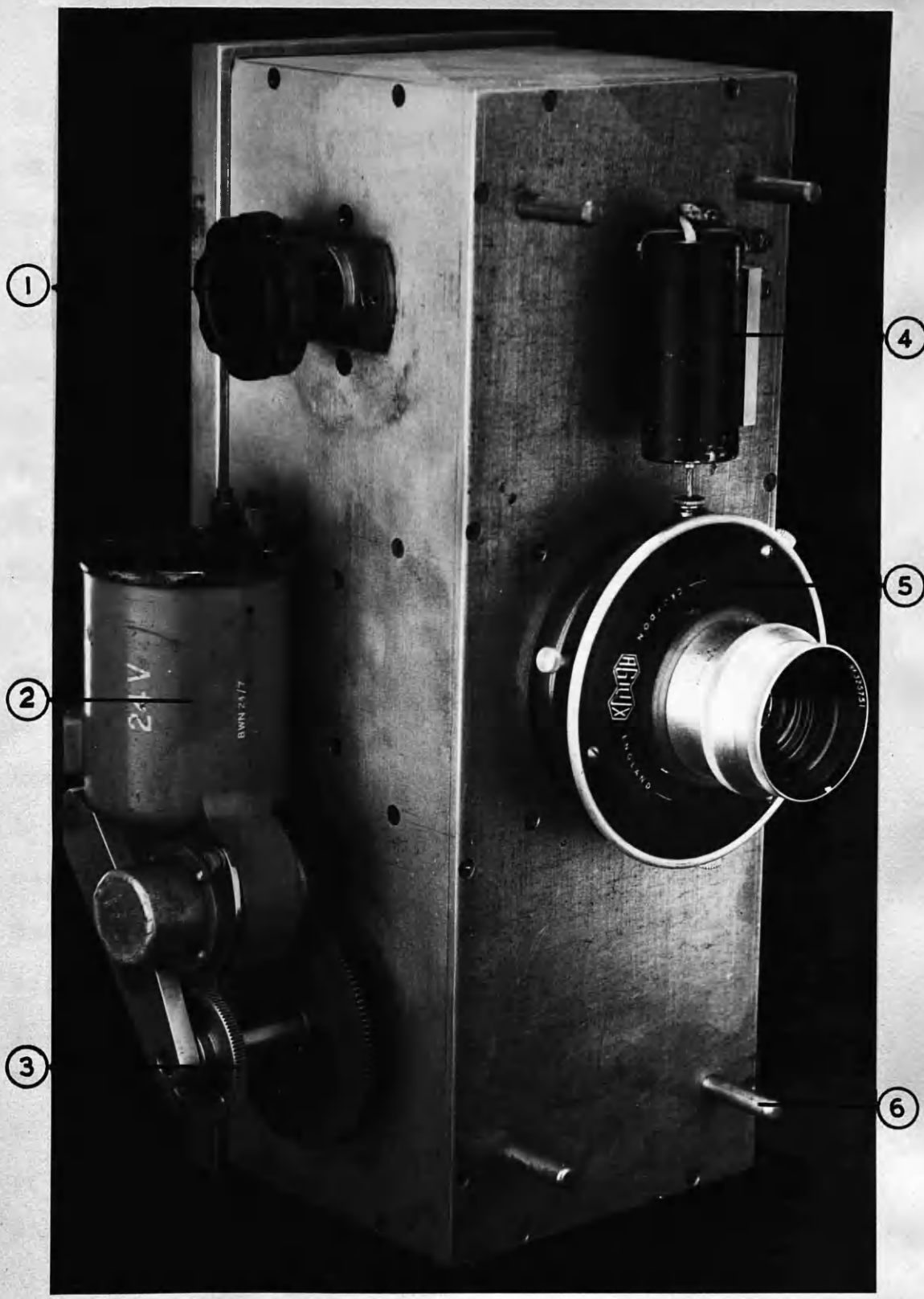

FIGURE 24:- View of exterior of camera.

the angle of the wedge being such that the whole plane of the cloud-chamber was in focus in the image plane. Apart from this feature the cameras were identical.

An external view of one of the cameras is shown in Figure 24. The body, essentially a rectangular box of dimensions approximately 12" x 4½" x 4", was constructed of ¼" thick duralumin sheet. The sections were carefully machined and assembled to ensure light-tightness. The removable back was likewise accurately machined and recessed to take the rim of the camera body (Figure 25).

In Figure 24 is shown at (4) the solenoid which opens the shutter (5) by forcing a plunger against the cable-release pin. The shutter closes by spring action when the current in the solenoid is cut off and the pressure is released. A 24 volt D.C. motor (2) geared down to about 10 r.p.m. drives the take-up spool. Manual advancement of the film is possible by turning knob (3) after depressing to disengage the gear wheel. Movement of the film in the opposite direction is controlled by knob (1). The pins (6) are used in locating the camera on the supporting framework. The lens is one of a matched pair of 80 mm. focal length f/4.5 Taylor-Taylor-Hobson "Ental" enlarging lenses.

Figure 25 shows the interior of the camera and lid.

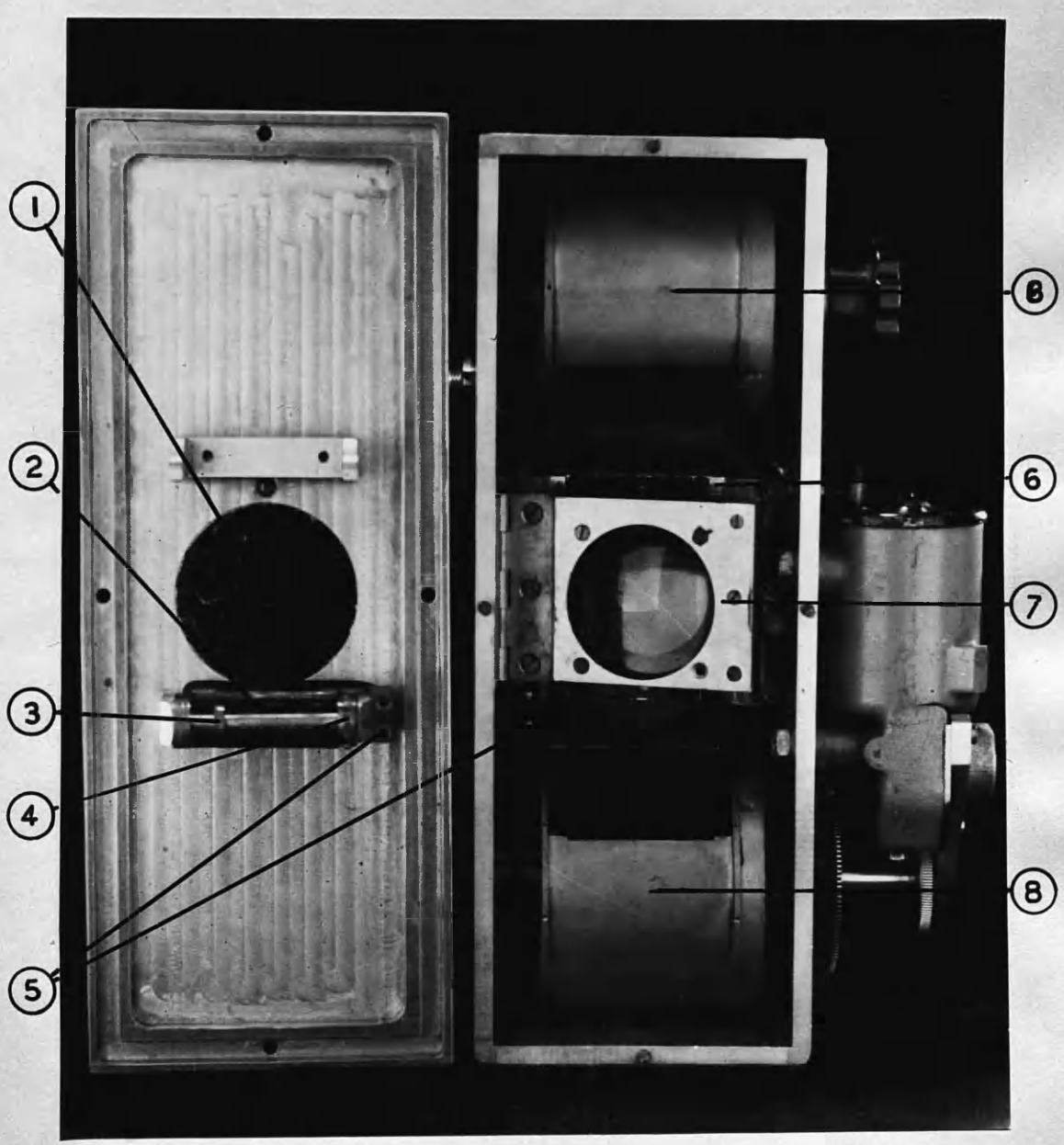

FIGURE 25:- View of interior of camera.

The cassettes (8) hold 100 feet of 60 mm. perforated film which is pulled through an accurately machined gate (6) by the motor-driven take-up spool. The film is held flat in the position of exposure by a spring-loaded glass pressure plate (7). By means of the sprocket wheel (4) the film drives the cam (3) which opens the microswitch (2) once in each revolution. The electrical connections to the switch are made by the plug and socket (5) which are mated on closing the lid. The light-tight cover (1) in the lid can be removed to allow the insertion of a condensing lens system for use in the reprojection of tracks.

The electrical connections to the motor, shutter and microswitch were taken to a seven-pin socket fitted to the side of the camera and thence *via* a plug and cable to the electronic control chassis immediately below the cloud-chamber. The action of the control circuit in the operation of the cameras has already been described.

The cameras could be loaded with 100 feet of film, but for a normal run of the apparatus 25 feet, giving about 150 exposures, was found convenient. Ilford 5G91 or Kodak R55, fast recording films of high contrast, were used. The films were tank developed in 25 feet lengths. A developing spool and winding guide designed for 35 mm. film was adapted to take the wider film.

The vertical camera was normally operated at full aperture (f/4.5) at whichvalue the depth of focus was approximately equal to the depth of the illuminated part of the cloud-chamber (2.5 cm). For the oblique camera a smaller aperture (f/5.6) was sufficient, since even over 20°, the increase in light-scatter is appreciable.

Illumination.

As part of the preliminary work with the smaller cloud-chambers the conditions for optimum illumination and the most satisfactory types of lamps were studied. The first lamps constructed were similar to those used by Wilson, in which the discharge takes place in a short column of mercury vapour produced by heating the central portion of a quartz capillary tube filled with mercury. Shortly afterwards commercially produced lamps filled with one of the rare gases - argon, krypton or xenon - became available. As the design of these lamps improved it became obvious that in convenience of operation and in light output they were superior to the mercury vapour type.

A description of the types investigated with comments on their performance is given below.

(1) B.T.H. - argon and mercury filled. This was an early type of lamp dissipating about 10 joules, not superior in light output to the mercury capillary type, but

more convenient in operation as it did not require heating.

(2) Siemens - krypton filled. This lamp consisted of a tube of $\frac{3}{4}$" diameter with an electrode at each end, the discharge being guided down the centre by an inner tube of diameter about $\frac{1}{4}$". The discharge was initiated by applying a high voltage pulse to a wire wrapped round the central portion of the tube. These lamps, rated at 100 joules, survived many hundreds of flashes. The only obvious change was a crazing of the inner tube and some increase in the breakdown voltage. Disadvantages were a rather short and, more serious, wide discharge arc, which increased the difficulty of focussing the beam into a flat sheet of light.

(3) G.E.C. - argon filled. A distinguishing feature of this design was the bulb (about one inch in diameter) blown in the quartz tubing between the central capillary and each electrode. During the discharge the pressure in the capillary rises to a very high value and this in conjunction with the crazing of the inner surface may be sufficient to disrupt the tube. The bulbs presumably are designed to relieve the pressure built up during the discharge. Despite this feature the life of this type was not satisfactory when they were used at their rated capacity, 150 joules.

(4) Philips - xenon filled. This lamp consisted of a long quartz tube with slight protuberances at the ends where

the main electrodes entered, the whole being enclosed in a glass protective casing. A third electrode conveyed the triggering pulse. It proved to be the most satisfactory type and was used throughout the main investigation. A single lamp of this type dissipating 500 joules at each flash was found to give adequate illumination for single-drop photography over the whole of the 12" cloud-chamber.

Collimation of Beam.

The lamp was mounted in a cylindrical casing which was entirely closed except for a long rectangular opening in front of which was mounted a cylindrical lens. The position of the lamp relative to the lens could be adjusted to give as parallel a beam as possible. The rear surface of the discharge tube was covered with polished aluminium foil which acted as a reflector. The lamp housing was supported about 9" from the cloud-chamber cylinder by rods attached to the clamping pillars of the chamber. The beam was limited to a depth of 2.5 cm. by masks, one near the lens, the other round the chamber wall. Careful adjustment of the vertical height and tilt of the lamp was necessary to prevent stray light reaching the velvet background.

The Magnets.

The cloud-chamber magnetic field was produced by a pair of large Helmholtz coils each of which consisted of six flat

coils of about 160 turns of $\frac{1}{8}$" wide copper strip insulated by "Armite" impregnated paper strip. The individual coils could be connected in series or in parallel. For the present investigation, where comparatively low magnetic fields of 150 - 200 oersted were employed, the coils were connected in series with a variable resistor across the D.C. mains.

The resolving magnet was constructed from $\frac{1}{2}$" thick steel plates (kindly supplied and machined by Messrs Colvilles Ltd.) and was designed (by Dr. B. Touschek) primarily for use with high energy electrons and positrons from a synchrotron. The gap was rectangular, of dimensions 10" x 6" x $\frac{3}{8}$". The magnet served a useful purpose in collimating the particles and in eliminating the low energy electrons and X-rays emitted by the source. The cloud-chamber was further screened from stray electrons by suitably placed lead blocks. The particle shutter, operated by a solenoid and plunger, consisted of a brass strip across the exit corner of the resolving field.

Experimental Arrangement.

The general experimental arrangement is shown in a plan view (Figure 26) and in a photograph (Figure 27). The cloud-chamber, together with the magnet coils, cameras, and lamps, was supported on the top section of a trolley built

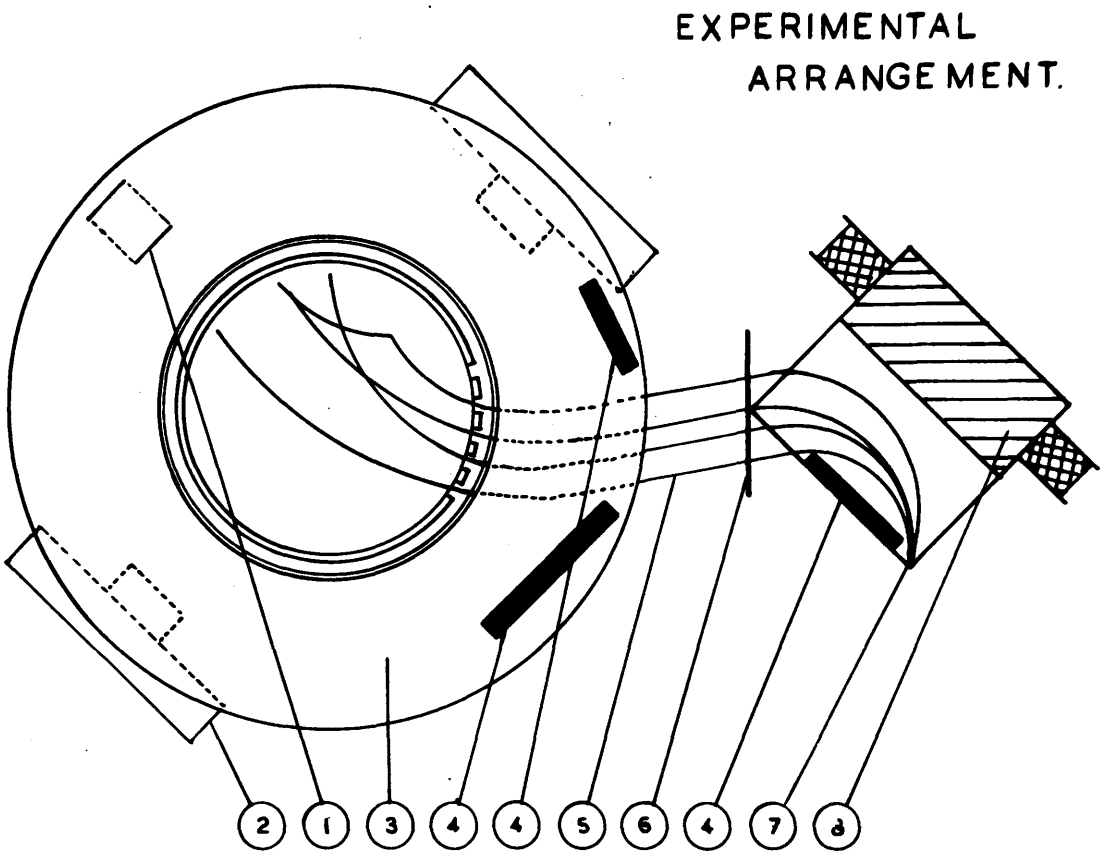

1	Visual observation lamp.	5	Particle paths.
2	Flash discharge lamps.	6	Particle shutter.
3	Helmholtz coils.	7	Source.
4	Lead blocks.	8	Resolving magnet.

FIGURE 26:- Schematic plan diagram of general experimental arrangement.

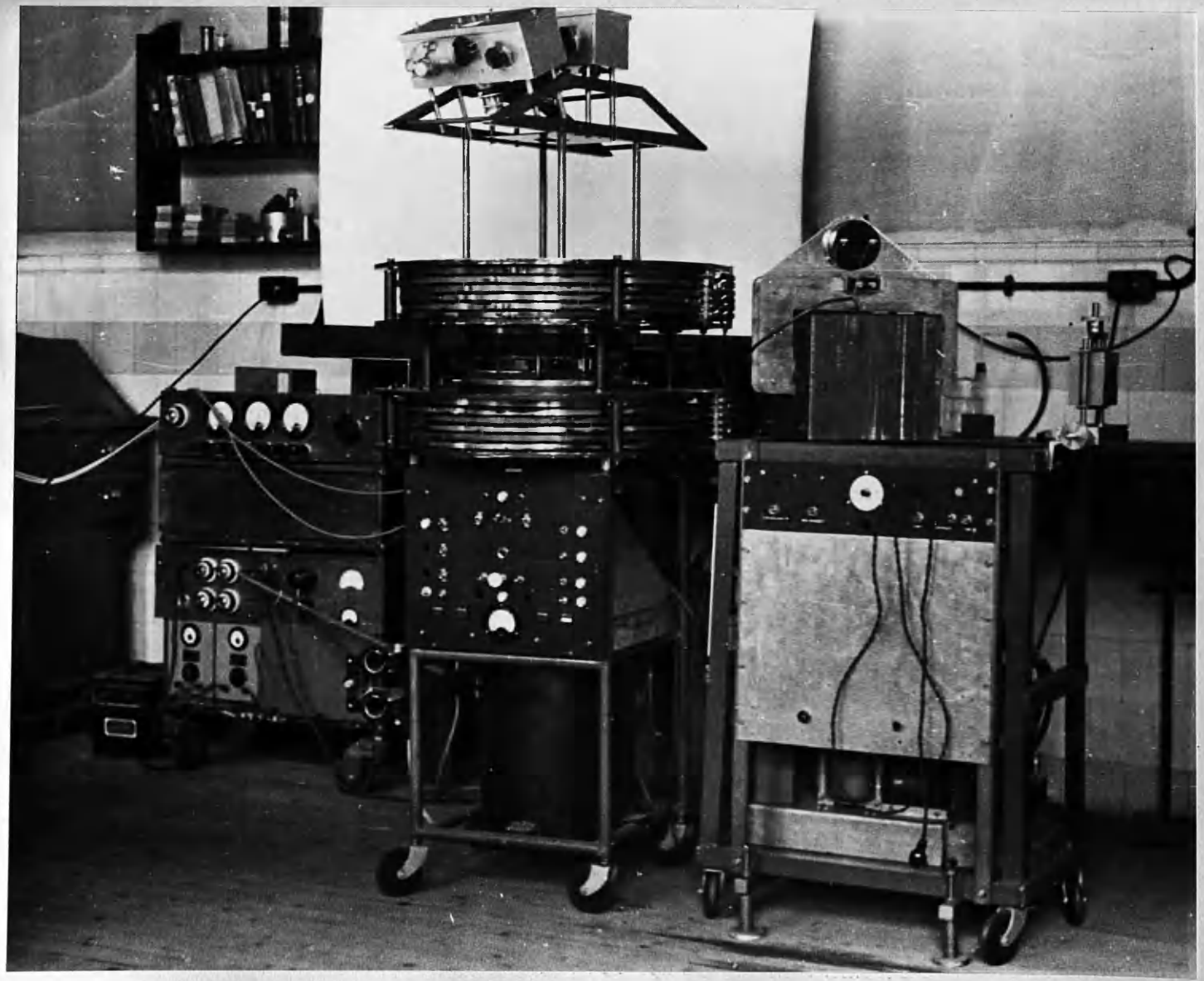

FIGURE 27:- General view of apparatus.

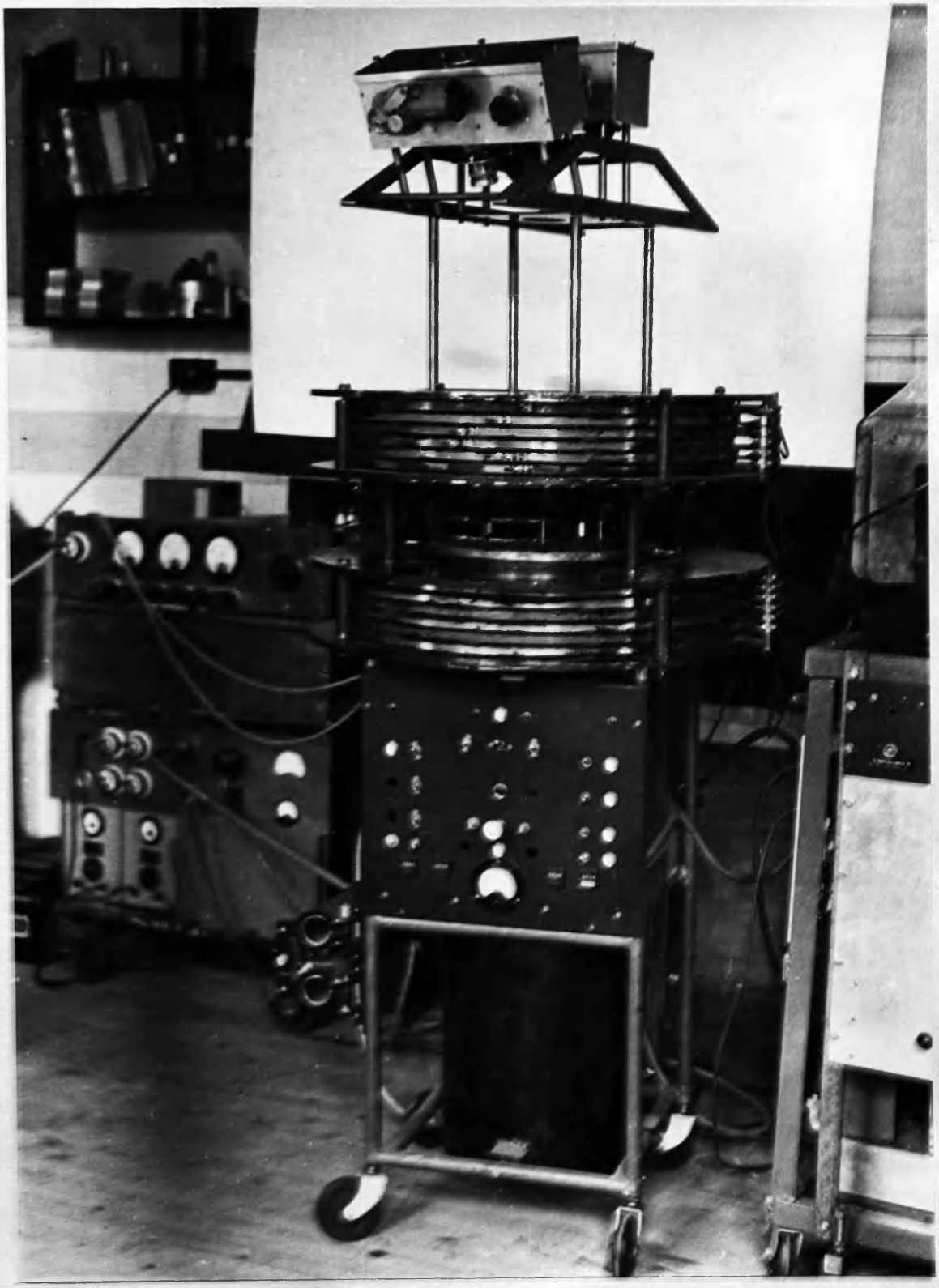

FIGURE 28:- A more detailed view of the main trolley showing the cloud chamber, field coils and stereoscopic cameras.

of welded steel tubing. The middle section housed the control-circuit gear. This was constructed as a complete unit which could be removed after disconnecting several plugs at the rear. The control panel with its numerous buttons and switches, and counters for registering the numbers of expansions, lamp flashes, photographs taken, etc., formed part of the unit. The bottom section was occupied by a large steel cylindrical vacuum reservoir, and a rheostat for controlling the magnet current. A more detailed view of this part of the equipment is shown in Figure 28. The arrangement of the cameras on the stand which fitted on to the upper ring of the cloud-chamber is also shown more clearly in this photograph.

Figure 27 shows on the left a second trolley which housed two large banks of condensers each totalling over 100μF and the rectifying unit which charged them, according to the setting of a Variac control to a potential of up to 3000 volts. The condensers were connected by low resistance, heavily insulated leads to the electrodes of the discharge lamps. On the lower part of this trolley was situated the rotary vacuum pump which during chamber operation kept the reservoir continuously evacuated. A third trolley, on the right in Figure 27, was used to support the resolving magnet. (The remaining equipment on this trolley was not

required in the investigation described). The electron source, a strip of indium metal activated by neutron bombardment in the Harwell pile, was mounted on a brass support and placed at one corner of the resolving magnet pole piece (Figure 25). The position of the magnet and lead blocks, and the magnet current, were adjusted until a suitable number of high energy electron tracks (about 5 to 10) were seen in the chamber during each expansion.

The positron source (vide infra) was too weak to be used with the resolving magnet but little trouble was experienced from low energy particles as these were mostly prevented from entering the chamber by the fringing field of the coils.

Projection Apparatus.

For the purpose of track analysis (described in Chapter V) the developed films were returned to the cameras, which together with the upper section of the supporting structure, were removed from the cloud-chamber and screwed to an iron framework above a table. In each camera a condensing lens system was inserted through the hole in the lid and a housing containing a 500 watt fan-cooled lamp fitted to the back. A full-size image of the tracks was projected on a suitable screen. The intensity of illumination was controlled by means of Variacs. The film could

FIGURE 29:- Reprojection equipment for analysis of tracks.

be moved either by hand or else automatically, as in taking the photographs, by connecting a 24 volts supply via press-button switches to the camera motors. The projection equipment is illustrated in Figure 29. The projection screen shown in the photograph, based on that described by Dee and Gilbert (D1), was designed for measurements in three dimensions. In the method of track-analysis adopted, measurements were made only in a horizontal plane so that a movable screen was not required.

Electron and Positron Sources.

The development of techniques for producing artificially radioactive elements, especially by bombardment with neutrons in atomic piles, has greatly increased the choice of suitable electron sources, and has made available sources for the study of positron scattering. The isotope Indium 114 was chosen as the source of electrons for the following reasons.

(1) It can easily be prepared by neutron bombardment of the stable isotope In.113.

(2) The source is in a convenient form for handling (metal strip).

(3) The electron energy is of suitable value (end point 1.98 Mev).

(4) The half-life is adequate. Indium 114 decays by an isomeric transition with an effective half-life of 48 days.

The selection of a suitable positron source presented much more difficulty. Numerous positron-emitting isotopes can be produced by slow-neutron bombardment but of those listed as available from the Harwell pile none combined a suitable positron energy with sufficiently long half-life (allowing for time of transport). It was decided therefore to use as a positron source copper 62 which may be obtained from the stable isotope copper 63 by a γ-n reaction, the threshold energy being about 10 Mev. The maximum energy of the positron is 2.6 Mev, but the half-life is only 10.5 minutes. The source was prepared by irradiating five $\frac{1}{2}$" side, one sixteenth inch thick copper squares in the beam of the Glasgow University synchrotron. After irradiation, the squares were attached to an aluminium support and placed one in front of each of the chamber portholes. As the activity weakened the squares were brought nearer the chamber, and in this way a useful working life of 30-40 minutes was obtained per radiation.

CHAPTER V.

ANALYSIS OF TRACKS AND ERRORS OF MEASUREMENT.

In the previous chapters the importance of maintaining a high standard of cloud-chamber performance and photographic technique has been stressed. Of equal importance is the necessity for adopting a method of analysis of the tracks which will enable an accurate comparison to be made with the theoretical predictions. The analysis is unavoidably laborious and unless the method is carefully chosen, the amount of work required to obtain results of statistical significance may easily become prohibitive.

The methods of analysis used by the earlier workers on electron scattering were seldom described in detail. Champion initially made measurements directly on negatives obtained from two cameras with their image planes at right angles (Blackett method, Figure 16(a)), but later apparently (C7) changed to a method of three-dimensional projection of the images. The author investigated a method of this type. The developed films are returned to their respective cameras and full sized images of the tracks, formed by illuminating the films from behind, are thrown on a screen (similar to that in Figure 29) which can be moved in all directions about a point near its centre. The screen is placed at the correct distance from the cameras, and by suitably tilting

it the two images of a particular track can be made to coincide for a distance over which the tracks are approximately planar. If, as during a collision, the direction of a track suddenly changes, the orientation in space of the deflected track can be similarly determined and a measurement of the angle of deflection made. The energy of the particle before and after collision can be determined by measuring the curvature of the track and the angle between its plane and the direction of the magnetic field.

The method is very suitable for analysing tracks of heavy particles such as protons or α-particles, or for obtaining maximum information about rare cosmic-ray events, but for extensive measurements on electron tracks it is both difficult and extremely laborious. For accurate work a high degree of precision in the location of the films in the cameras is essential and the track photographs must be of a very high standard. Even with good quality tracks, the method is subject to difficulties as, for example, when an electron is deflected sharply out of the illuminated part of the chamber leaving a branch track too short for measurement.

It follows that, for accurate measurement of scattering angles and curvature of deflected particles, a minimum length must be placed on acceptable scattered tracks. For

tracks which pass near the walls of the chamber it is satisfactory to omit scattering events occurring within, say, 2 cm. of the walls (track-length in this region not being recorded). It is not possible, however, to apply this method at the two surfaces defining the upper and lower limits of the illuminated region, as this would involve the loss of too many scattering events. It is therefore necessary, in comparing experimental and theoretical results, to allow for the fact that some scattering events cannot be recorded. The adjustment of the scattering formula can be accurately made if the geometrical conditions are specified. The scattering probability $P(\theta)$ is reduced by a factor $R(\theta)$ which is independent of $F(\theta)$, the function giving the angular distribution. Bosshard and Scherrer (B6) obtained $R(\theta)$ by a geometrical method, under the condition that the actual length of the scattered track should be greater than a prescribed value. Barker (B10) derived values of $R(\theta)$ for the case where only tracks of projected length greater than a certain critical length are measured. The function $R(\theta)$ will be discussed further in dealing with the effect of projection on the measured number of scattering events.

An alternative to the three-dimensional reprojection method described above is to measure the projected lengths,

curvatures and scattering angles in a single horizontal plane and to compare the experimental values with a suitably modified form of the scattering law. This method was first described in detail by Randels et al. (R1) who, however, did not apply a minimum track-length condition. The theory of the method was further developed by O'Ceallaigh and MacCarthaigh (O1) and by Barker (B10). The projected form of the general scattering law is derived in the form of a double integral. This involves a parameter $\rho = \lambda_c/2a$ where 2a is the depth of the illuminated layer of the chamber and λ_c is the critical length. Deflected tracks shorter than λ_c are rejected since such tracks would not allow accurate measurement of scattering angles and curvatures.

Barker (B10) and O'Ceallaigh (O2) have drawn up tables for various values of ρ from which may be calculated the number of scattering events predicted by theory in successive intervals of scattering angle.

Advantages of Projection Method.

The chief advantage of the method of projected angles lies in the fact that all measurements are made in a single plane, and can therefore be carried out expeditiously and accurately. The reduction in the number of scattering events observed in the projected system is not serious,

and is more than offset by the greatly increased speed at which data is collected. Moreover, as has been pointed out by O'Ceallaigh and MacCarthaigh (O1) and by Barker (B10), if a minimum track length condition is applied, projection scarcely alters the number of scattering events at large angles ($\sim 90^{o}$), but considerably reduces the number observed at smaller angles. This is apparent from the values shown in Table 12 for $R(\theta)$, the function obtained by applying a minimum track length condition to scattering in three dimensions.

TABLE 12.

		10°	20°	30°	40°	50°	60°	70°	80°	90°
$R(\theta)$	$\rho=1$	0.889	0.773	0.651	0.515	0.388	0.330	0.299	0.284	0.279
	$\rho=2$	0.778	0.546	0.331	0.244	0.202	0.179	0.161	0.156	0.152

The reduction in the number of events observed increases rapidly with increasing scattering angle. Since the illuminated volume of the chamber consists of a very shallow cylinder, electrons deflected through a large angle will often pass out of the illuminated volume without leaving sufficient length of track for accurate measurement, but this will happen much less frequently if the scattering angle is small. Thus the observed number of large-angle scattering events is unavoidably reduced. Projection of the tracks scarcely alters the number of such large angle

events, but appreciably reduces the number observed at small scattering angles by transferring a considerable proportion from the observable class (20° or greater) to the unobservable class (less than 20°). As interest usually centres on large-angle scattering statistics, this is a distinct advantage as it effectively reduces the number of small-angle scattering events.

It is strongly emphasised, however, that the second oblique photograph is indispensable for accurate work, as it serves an important function in clarifying cases where the association of crossing tracks is in doubt, or where, for any other reason, the trajectory of a particle is not clearly defined.

During the present investigation the oblique photograph was examined in every case to ensure that the maximum possible information about the tracks was obtained.

Measurement of Tracks.

The procedure adopted in analysing the tracks was as follows.

The developed films were returned to the appropriate cameras and the lamp housings and condensing lens systems, described in the previous chapter, were fitted to the backs. The cameras, together with the supporting framework, were removed from the cloud-chamber and placed above

a table. A natural size image of the tracks was projected on to a square sheet of paper on which was drawn a circle of diameter 23 cm., the latter being adjusted to be concentric with the image of the chamber cylinder. Tracks which emerged from the windows and were of good quality were traced on the paper with a sharp pencil. The oblique image was also examined but the tracks were not traced, its function being, as previously mentioned, mainly to clear up doubtful cases where tracks crossed.

Each track was numbered and the following information entered in a table at the upper right-hand corner of the sheet.

(1) The length ℓ within the limits of the circle, determined by means of a map measurer.

(2) The radius of curvature, obtained by finding the best fit of a series of curves consisting of arcs of concentric circles engraved on a celluloid sheet.

(3) Nuclear deflections were noted and the angle of scattering measured where this exceeded a certain minimum value. The lowest value required was 15° but as a precaution against omitting borderline cases, deflections down to 10° - 12° were routinely checked. In looking for nuclear deflections it was found advantageous to view each track along its length from an almost grazing angle. Dev-

iations from uniform curvature were then easily observed.

The method of measuring the scattering angle is illustrated in Figure 30. When the circular arc which best fits the curve of the track is found, the radius at the point of deflection is drawn both for the incident and emergent track. The angle between the radii which is also the (projected) scattering angle, ϕ, is measured with a protractor.

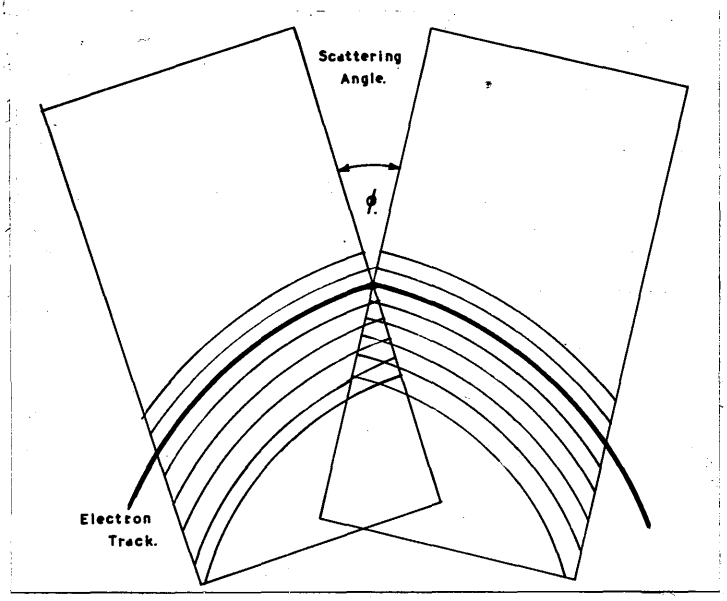

FIGURE 30

Deflections occurring outside the 23 cm. circle were ignored, though parts of tracks outside the circle were often used in measuring angles and curvatures relating to events occurring inside. The drawing of the circle serves the same purpose as the fixing of a minimum track length, viz., it ensures that no scattering events are recorded of which it is impossible by reason of the shortness of the scattered track to measure accurately the curvature and angle of scattering.

In addition to the above information, remarks were entered in a fourth column on any unusual features such as apparent large energy loss during collision.

Errors of Measurement.

One of the chief sources of error lies in the unavoidable presence of small-angle scattering. Inspection of a graph of scattering cross-section against scattering angle (Figure 31) shows how rapidly the number of scattering events increases as the scattering angle decreases.

The ideal form of track consists of two arcs of circles of equal curvature with a cusp at the point of deflection (as shown in Figure 26). Also satisfactory, but rather more difficult to observe, is the type of deflection shown in Figure 30, where the particle is deflected towards the centre of curvature of its path. Close

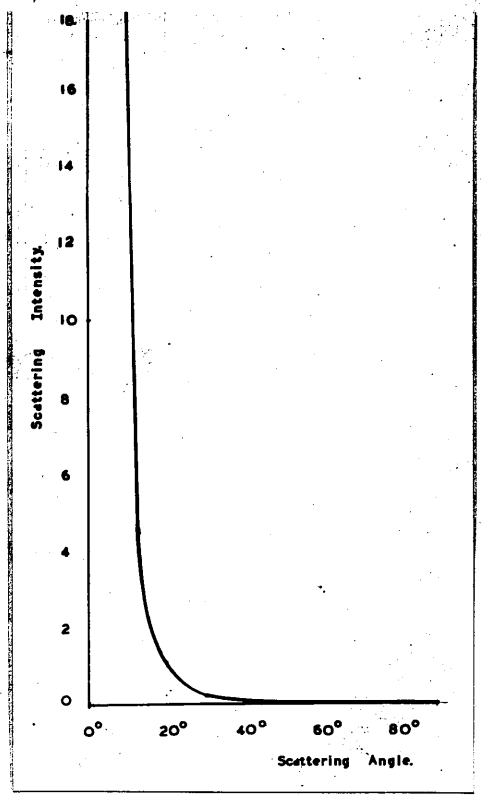

FIGURE 31

approximations to these forms are, in practice, frequently observed. However, owing to numerous small angle deflections, many tracks deviate to a greater or less extent from true arcs of circles.

Since the small deflections form a Gaussian distribution, the average curvature over the whole length of the track (usually 20 cm. or more) may be assumed to give

the best value, but where a small deflection large enough to be observed (i.e. of 5° or more) is present, the curvature is best determined from the approximately circular arcs on either side of the point of deflection.

The theory of the multiple scattering of fast charged particles has been discussed by Williams (W4,9), by Goudsmit and Saunderson (G4) and by Bethe (B14). The theory was developed with special reference to the effect of small-angle scattering on measurements on the very high energy particles encountered in cosmic-ray work, but the results have some bearing also on the present type of investigation.

Williams considered the scattering experienced by a fast particle of charge e, velocity βc and momentum 300 $H\rho$ ev/c, in traversing a layer of thickness t of a material of density σ, containing N atoms/cc. of atomic number Z and atomic weight A. He derived for the mean projected angle of scattering $\bar{\phi}$, the relation

$$\bar{\phi} = \frac{2Ze(Nt)^{\frac{1}{2}}}{\beta(H\rho)} \cdot \bar{\alpha},$$

where $$\bar{\alpha} = 1{\cdot}45 + 0{\cdot}80\left(7{\cdot}45 + 2{\cdot}3\log_{10}\frac{Z^{4/3}\sigma t}{A\beta^2}\right)^{\frac{1}{2}}$$

A succession of deflections smaller than those which can be individually detected may thus result in a spurious

deflection or curvature of the track which limits the accuracy with which the curvature due to the magnetic field can be measured. If $\bar{\rho}_s$ is the uniform radius of curvature which would give rise to the deflection $\bar{\phi}$ in distance t,

$$\bar{\rho}_s = \frac{t}{\bar{\phi}} = \frac{\beta (H\rho) t^{\frac{1}{2}}}{2 z e \bar{\alpha} N^{\frac{1}{2}}} ,$$

and thus $$\frac{\rho}{\rho_s} = \frac{2 z e \bar{\alpha} N^{\frac{1}{2}}}{\beta H t^{\frac{1}{2}}} .$$

Insertion of values appropriate to the present experiments ($t = 20$ cm., $z = 18$, $N = 1.8.10^{19}$, $H = 160$ oersted) gives

$$\frac{\rho}{\rho_s} \doteq \frac{1}{4}$$

If ρ_m is the measured value of ρ,

$$\frac{1}{\rho_m} = \frac{1}{\rho} \pm \frac{1}{\rho_s} = \frac{1}{\rho}\left(1 \pm \frac{1}{4}\right).$$

Thus according to Williams's theory, any individual measurement of curvature is subject to an uncertainty of $\pm 25\%$. The theory, however, refers the curvature only to the angles between tangents at the ends of a segment of track, whereas in the measuring procedure adopted here the whole length of the track was made use of in determining the curvature. In Bethe's treatment which gives curvature uncertainties rather greater than those esti-

mated by Williams, the lateral displacement of the centre of the track relative to the chord is taken as a measurement of the curvature. Here again the fact that more information is obtainable from the rest of the track is neglected. These criteria are, of course, more appropriate to cosmic-ray work where measurements on individual tracks are often of critical importance, and the smallness of the curvatures and scattering angles necessitates the use of different measuring techniques.

The experience of the writer in measuring curvatures by the method described earlier in this chapter suggests that the uncertainties are appreciably smaller than those predicted by the above theories. In general, when the curvature remained constant over at least 10 cm. of track, the value measured over this length was taken to be the correct value. When an obvious small-angle deflection took place, the curvature was determined from the segments on either side of the point of deflection. The accuracy of curvature measurement varied considerably from one track to another but many tracks were good approximations to arcs of circles over most or all of their length. In a fair proportion the radius of curvature was determinable to the nearest centimetre. Taking 25 cm. as an average value of radius of curvature, this gives an error of only

± 2%. For particles of higher energy (and smaller curvature) the radius was more frequently determined to the nearest multiple of five. For a radius of 50 cm. this corresponds to an error of ± 5%.

The number of curvature measurements made in the analysis of the electron and positron tracks was in each case well over 1000. Assuming that the errors of measurement due to small-angle scattering are symmetrically distributed, the resulting inaccuracy in the average curvature and hence the mean energy of the particles is of the order of $5/(1000)^{\frac{1}{2}}$%, i.e. less than 0.2%.

Small-angle scattering also affects the measurement of large scattering angles by rendering less certain the exact direction of the particle immediately before and after the collision. Clearly the distance of a small deflection from the point of collision is an important factor in the influence it exerts on the measurement of the scattering angle. The effect of such deflections is difficult to estimate. Randels et al. (R1) derived a correction based on somewhat arbitrary assumptions in an attempt to assess the importance of the factor. Fortunately the error due to this cause falls off very rapidly with increase in scattering angle, and is small or negligible in the angular range covered by the present investigation.

Such effects may, however, account at least in part for the discrepancy observed between the experimental results and theoretical predictions in the angular range 15° - 20°. A discussion of these results and of further experimental errors is included in the next chapter.

CHAPTER VI.

RESULTS AND CONCLUSIONS.

A total of 198 metres of electron track and 163 metres of positron track was analysed by the method described in the previous chapter. The scattering gas in the chamber was argon at a pressure of about 60 cm. Hg., together with small quantities of air, and water and alcohol vapour. For purposes of comparison with theory, the numbers of scattering events observed were grouped in angular intervals of 10° in the range 20°-90°. Scattering angles of 20°, 30°, 40°, etc. were assigned half to the lower and half to the upper interval. Measurements made in the interval 15°-20° are not included in the main table of results; they will be discussed separately.

Calculation of Theoretical Values.

The experimental results were compared with theoretical values based on (1) the Rutherford formula with relativistic mass, and (2) the formula deduced from Mott's theory by McKinley and Feshbach.

The Rutherford differential scattering cross-section (modified for the variation of mass with energy) may be written

$$\sigma(\theta) = \left(\frac{Ze^2}{2m_0c^2}\right)^2 \cdot \frac{1-\beta^2}{\beta^4} \cdot \operatorname{cosec}^4\theta/2 \qquad \text{——————} (\text{VI}.1)$$

or, since $$H\rho = \frac{m_0 c^2 \beta}{e(1-\beta^2)^{\frac{1}{2}}},$$

$$\sigma(\theta) = \left(\frac{Ze^2}{2H\rho}\right)^2 \cdot \frac{1}{\beta^2} \operatorname{cosec}^4 \theta/2$$

The number of deflections in the angular range θ to $\theta + d\theta$, suffered in a track length of t cm. in a medium containing N scattering centres per unit volume, is -

$$n(\theta)\, d\theta = \frac{Kt}{\beta^2} \operatorname{cosec}^4 \theta/2 \cdot 2\pi \sin\theta\, d\theta ,$$

where $K = N\left(\frac{Ze^2}{2H\rho}\right)^2$ is a constant depending on the pressure and atomic number of the scattering substance, and the energy of the particle.

The corresponding cross-section deduced by McKinley and Feshbach is -

$$\sigma(\theta) = \left(\frac{Ze^2}{2m_0c^2}\right)^2 \frac{1-\beta^2}{\beta^4} \left\{ \operatorname{cosec}^4 \theta/2 - \beta^2 \operatorname{cosec}^2 \theta/2 \pm \frac{\pi Z \beta}{137}\left(\operatorname{cosec}^3 \theta/2 - \operatorname{cosec}^2 \theta/2\right)\right\} \qquad \text{(VI.2)}$$

the sign of the third term being positive for electrons and negative for positrons. The number of deflections in the range θ to $\theta + d\theta$ is given by -

$$n(\theta)\, d\theta = \frac{Kt}{\beta^2}\left\{ \operatorname{cosec}^4 \theta/2 - \beta^2 \operatorname{cosec}^2 \theta/2 \pm \frac{\pi Z \beta}{137}\left(\operatorname{cosec}^3 \theta/2 - \operatorname{cosec}^2 \theta/2\right)\right\} 2\pi \sin\theta\, d\theta$$

The number of deflections $n(\theta_1, \theta_2)$ over any finite angular

range θ_1 to θ_2 can be obtained by integration. O'Ceallaigh (02) has compiled Tables from which the number of deflections in the angular ranges 20°-30°, 30°-40°, etc., can be calculated on evaluating the constants **K**, **t**, etc. If the projected angles on a plane perpendicular to the camera axis are considered, the number in each of the above angular ranges is reduced by about 50%. If, in addition, a lower limit is set to the length of acceptable scattered tracks, the number of deflections calculated to fall within the angular ranges is reduced still further. The numbers depend on the value of the parameter $\rho = \lambda_c/2a$, where λ_c is the minimum acceptable track length, and $2a$ is the depth of the illuminated layer of the chamber. O'Ceallaigh's Tables include integrated values over angular intervals of 10° corresponding to $\rho = 0$ (no minimum track length) and $\rho =$ 1.0, 2.0, 2.5, 3.0, 4.0, 5.0 and 10.0. These are given for each of the functions $\mathbf{cosec}^n \theta/2$ where n = 1, 2, 3 and 4.

By inserting the appropriate constants and summing over such terms, the number of deflections predicted by any of the usual theories can be calculated. In the present experiments the depth of the illuminated volume of the chamber was 2.5 cm. The minimum acceptable track length was taken to be 2.5 cm. also, so that the value of ρ was 1. Relevant parts of the tables compiled by O'Ceallaigh are reproduced,

with a short explanatory note, in Appendix II.

Evaluation of Experimental Constants.

In calculating the absolute scattering intensity the mean energy of the particles is an important quantity, since the scattering cross-section is approximately inversely proportional to the square of the energy. The energy of each particle is determined by measuring the magnetic rigidity $H\rho$, where H is the intensity of the magnetic field and ρ is the radius of curvature of the track. The method of measuring ρ and the errors associated therewith have already been discussed (Chapter V). The value of the magnetic field was calibrated in terms of the exciting current by means of an accurate flux-meter checked against a standard magnetic field. The field strength varied by not more than 2-3% over the volume of the chamber. The possible error in the mean field strength is estimated to be not greater than ± 2%.

To evaluate t, the total track length, the length of each accepted track (determined by means of a map measurer) was entered in a column under the appropriate value of ρ. If ℓ is the total track length with radius of curvature ρ, (the limits of which were normally 12 to 70 cm.) $\sum \ell$ gives the total track length t. To determine the effective energy (i.e. the energy which would give the same theoretical scattering as the measured values) the sum $\sum \ell/(H\rho)^2$ was

evaluated and equated to $\Sigma \ell/(H\rho_m)^2 = t/(H\rho_m)^2$. The energy corresponding to the effective curvature, ρ_m , can then be determined.

In evaluating N, the number of atoms per cc., the value corresponding to the expanded positron of the chamber was calculated. The mobilities of ions in the electric field (about 80 volts/cm.) are such that no sharp tracks could be formed by particles which entered the chamber before the expansion was complete. A small correction was made for the scattering in the residual air in the chamber (about 2.5 cm. Hg pressure) and in the alcohol and water vapour.

Experimental Errors.

A number of experimental errors have already been discussed, but the most important is probably associated with the selection and measurement of suitable tracks. This particular error is difficult to evaluate since the observer's judgment is necessarily involved to some extent. It has already been emphasised that to avoid serious errors in the interpretation of tracks, a high standard of cloud-chamber and photographic technique is required. Figures 14 and 15 illustrate groups of tracks which are typical of those from which the present data were obtained. If, in addition, strict rules for the selection and measurement of suitable tracks are adhered to (Chapter V) errors of this nature are

minimised. It is estimated that over the range of angles covered by this investigation (200-90°) the combined experimental errors are less than ±10%.

Scattering at Low Angles.

Measurements were made of scattering at angles down to 15° but, contrary to the results at larger angles, the number of deflections, both for electrons and for positrons, in the range 15°-20°, was found to be considerably lower than that theoretically predicted. For electrons a calculated value of 82.1 corresponded to the observed number of 49; for positrons the figures were 97.8 and 55. Attempts were made to determine the reason for this discrepancy. Tracks were grouped into those deflected (1) towards, and (2) away from the initial centre of curvature, as it was thought that some deflections in group (1) might have been overlooked. No significant difference in the numbers so deflected was, however, found. Tracks were also grouped into upper and lower ranges of energy but again no significant difference was detected. The conclusion reached was that the criterion adopted in the selection of clear-cut scattering events was probably too severe in the case of deflections as low as 15°, where the effects due to small-angle deflections became appreciable. Deflections of 20° and more, however, are easily distinguished from a succession

of small-angle deflections, and the results in the range 20^{o}-90^{o} are not considered to be appreciably affected by small-angle scattering.

Results for Electron Scattering.

The number of deflections observed in 198 metres of electron track in 10^{o} intervals over the angular range 20^{o}-90^{o} is shown in Table 13. Corresponding values from calculations based on formulae (1) and (2) are shown alongside.

TABLE 13.

SCATTERING OF ELECTRONS IN ARGON.

Ang.Range	Expt.	Theory (1)	Theory (2)
20^{o}-30^{o}	49.5	43.9	44.9
30^{o}-40^{o}	13.5	13.6	13.6
40^{o}-50^{o}	3.0	5.8	5.6
50^{o}-60^{o}	2.5	2.9	2.6
60^{o}-70^{o}	1.0	1.7	1.4
70^{o}-80^{o}	1.0	1.1	0.8
80^{o}-90^{o}	0.	0.7	0.5
20^{o}-90^{o}	70.5	69.7	69.4

The energy range of the electrons was 0.2 - 2.0 Mev., and the effective energy 0.83 Mev. The agreement between the experimental and theoretical results is excellent over the

range 20^{o}-90^{o}. The total number of scattering events predicted by theories (1) and (2) is 69.7 and 69.4 respectively, the observed number 70.5, giving ratios expt:theory of 1.02 and 1.01. Both of these values are well within the range of statistical fluctuations and experimental errors associated with the measurements. The distribution of number of events with scattering angle also agrees very well with theory. In particular, there is no indication of the excessive scattering between 25^{o} and 55^{o} of which Randels *et al.* claimed to have obtained strong, though not conclusive, evidence from their observations over several gases. The results obtained by Randels *et al.* for scattering in argon are shown for comparison in Table 14. The largest discrepancy occurs in the higher energy group in the lowest angular range (15^{o}-25^{o}). The opinion of the present writer is that measurements below about 20^{o} are subject to appreciable error mainly because of small-angle scattering. This may account at least in part for the discrepancy.

Earlier results of measurements of scattering in argon due to Zuber (1938), Stepanowa (1937, 1939) and Bleuler (1942) are collected in Table 15.

TABLE 14.

Scattering of electrons in argon ; Randels, Chao and Crane (1945).

Angular Range	Energy Range 0·8—3·3 MeV. Effective Energy 2·4 MeV.		Energy Range 3·3—9·3 MeV. Effective Energy 4·6 MeV.	
	Expt.	Theory	Expt.	Theory
15°–25°	30·0	30·3	52·0	32·2
25°–35°	10·5	7·2	10·5	7·6
35°–45°	5·0	2·7	4·5	2·8
45°–55°	2·5	1·3	5·0	1·4
55°–65°	1·0	0·7	1·0	0·7
65°–75°	0	0·4	0	0·4
75°–85°	1·0	0·2	0	0·2
85°–90°	0	0·1	0	0·1
15°–90°	50·0	42·9	73·0	45·4

TABLE 15.

Scattering of electrons in argon ; summary of earlier measurements.

Energy Range (MeV.)	Angular Range	Track Length (metres)	Number of Deflections	*Expt.* Theory	Author	Date
1·7–2·4	30°–180°	350	48	0·75	Zuber	1938
0·2–1·1	20°–150°	103	308	1·0	Stepanowa	1939
1·5–3·0	20°–150°	130	84	2·5	Stepanowa	1939
0·2–3·0	20°–180°	708	153	1·5	Bleuler, Scherrer & Zunti.	1942

In Figure 2 the experimental results have been plotted in histogram form with the theoretical curve superimposed. The theories (1) and (2) agree so closely that it is not possible to show more than one curve.

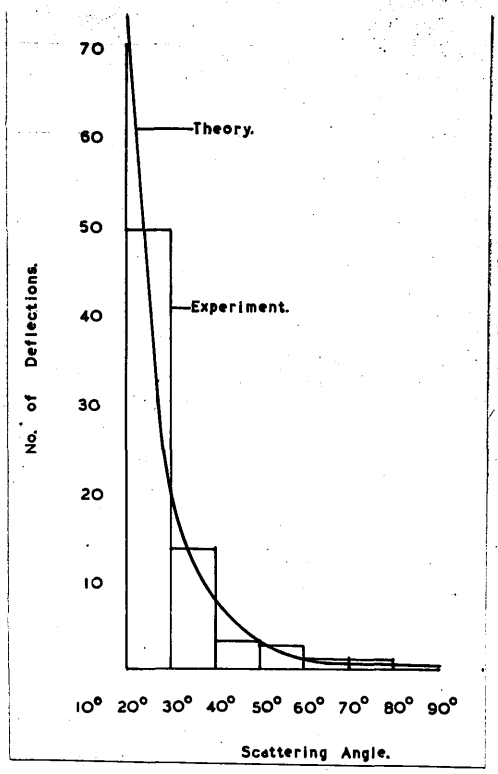

FIGURE 32.

The closeness of the values 69.7 and 69.4, obtained from theories (1) and (2) respectively, shows the great difficulty of distinguishing between the classical and relativistic theories by observations on electron scattering in a medium of atomic number such as argon. In formula (VI 2) the main contribution comes from the first term. The second and third terms, being of opposite sign and roughly equal in value when Z is not large, have but little effect on the cross-section. This can also be seen from the curve

for electrons in Fig. 9, in which the ratio of relativistic scattering to Rutherford scattering is plotted against the scattering angle.

Results for Positron Scattering.

The scattering statistics were compiled for positrons exactly as for electrons, the experimental conditions being essentially identical. The results were compared with calculated values based on theories (1) and (2) (the sign of the third term in formula (VI.2) being negative for positrons).

The results of the analysis of 163 metres of positron track in the energy range 0.2 - 2.4 Mev. and of effective energy 0.7 Mev. are shown in Table 16.

TABLE 16.

SCATTERING OF POSITRONS IN ARGON

Ang.Range	Expt.	Theory (1)	Theory (2)
20^{o}-30^{o}	41.5	52.8	47.1
30^{o}-40^{o}	15.5	16.4	13.8
40^{o}-50^{o}	3.5	6.7	5.3
50^{o}-60^{o}	3.0	3.4	2.5
60^{o}-70^{o}	1.0	2.0	1.3
70^{o}-80^{o}	1.0	1.3	0.8
80^{o}-90^{o}	0.	0.7	0.4
20^{o}-90^{o}	65.5	83.3	71.2

The number of deflections observed in each of the angular ranges is consistently lower than the number predicted by the Rutherford theory. Over the whole angular range 20^{o}-90^{o} the ratio expt:theory is 0.79. Comparison with theory (2) gives appreciably better agreement, though the total number of deflections observed is smaller than that predicted, the ratio expt : theory being in this case 0.92.

To test whether the difference observed between experiment and theory (1) is statistically significant the ψ^2 test was applied. This gives a probability of 0.2 that the observed differences are due merely to chance fluctuations. The statistical theory, however, takes no account of the sign of the difference which, as noted above, is the same in every angular interval. This is strong evidence that the differences are not entirely due to chance, but it is not possible to assess its value numerically.

On the other hand the probability is high that the differences between the experimental results and the values calculated from theory (2) can be ascribed to chance variations or to experimental errors which are of the same order of magnitude. In Figure 33 the experimental results are shown in histogram form for comparison with curves based on theories (1) and (2).

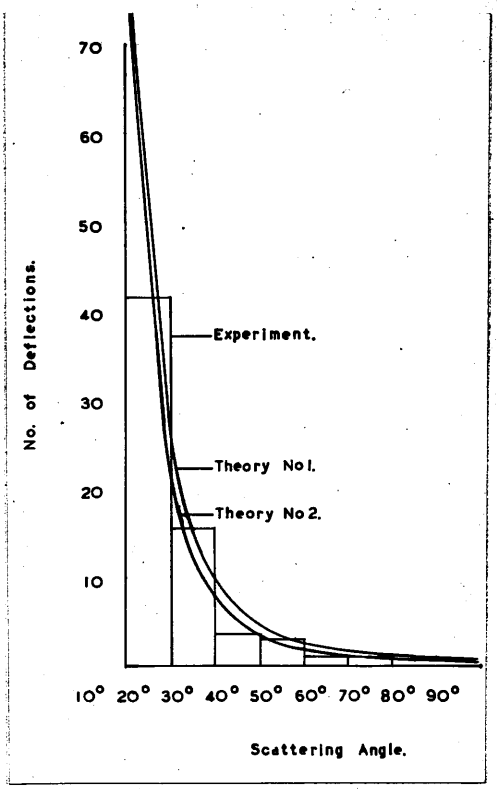

FIGURE. 33.

As already noted the agreement obtained in the case of electron scattering between the experimental and theoretical results (both classical and relativistic) is well within the range of statistical fluctuations and experimental errors. Such an agreement, obtained under experimental conditions identical to those prevailing during the positron measurements, provides further evidence that the discrepancies observed in the latter case between experimental results and theory (1) are real, and not due to experimental inaccuracies.

On the whole, the author considers that the evidence is strong that the scattering cross-section for positrons is lower than that predicted by the Rutherford theory. On the other hand the measured scattering is quite compatible with the values calculated from the formula derived on the assumption that the positron is a positively charged Dirac particle.

Comparison between Electron and Positron Scattering Intensities.

A direct comparison of the scattering cross-sections is not possible since the mean energy of the particles and the track lengths are different. The values were, however, normalised to 200 metres of track and an energy of 1 Mev. The theoretical ratio of electron to positron scattering was calculated to be 1.19. The corresponding value obtained from the experimental results was 1.22. For theories which neglect spin the ratio is, of course, unity, since the cross-sections for electron and positron scattering are the same. The experimental results thus appear to be strongly in favour of the Mott scattering theory.

Radiative Collisions.

Since track curvatures were measured on each side of a point of deflection, any large energy loss during collision could be detected. Several authors (S4, C3, L3) have re-

ported numbers of collisions involving large energy loss greatly in excess of theoretical values; others the reverse, or approximate agreement with theory. In the present experiments the theoretical number of collisions involving energy loss greater than 50% was very small (about two); none was observed. Numerous tracks which at first sight appeared to change direction and energy abruptly were found on closer inspection to be due to electron-electron collisions near the upper or lower boundary of the illuminated layer. The secondary electron track frequently appears to be a continuation of the track of the incident particle which passes out of the illuminating beam. The photograph obtained with the oblique viewing camera is very valuable in resolving doubts about such apparently anomalous collisions.

General Conclusions.

The conclusions drawn from the results of the experimental investigation may be summarised as follows.

(1) The cross-section for the nuclear scattering in argon of electrons of energy 0.2 - 2.0 Mev. over the whole of the angular range 20^{o}-90^{o} agrees with the predictions of either the semi-classical or the Mott relativistic theory. The experiments are not sufficiently sensitive to distinguish between the two theories.

(2) The scattering cross-section for positrons (energy

0.2 - 2.6 Mev.) is also of the predicted magnitude, but there is good evidence that it is significantly smaller than the value deduced from the semi-classical theory. Within the limits of experimental error and statistical fluctuations, the experimental results agree with the values obtained from the Mott relativistic theory. The ratio of electron to positron scattering is shown to be greater than unity in accordance with relativistic 'spin' theory.

(3) There is no evidence of anomalously large numbers of collisions involving large energy loss.

Summary.

A fully automatic Wilson cloud-chamber was constructed to obtain data on the nuclear scattering in argon of electrons from indium 114 and positrons from copper 62. The cameras were specially designed to take 60 mm. film and to allow the reprojection through the lens system of natural-size images of the tracks. 198 metres of electron track and 163 metres of positron track were analysed by the method of projected angles. The experimental angular scattering distributions were compared with calculated values based on the Rutherford semi-classical theory, and on Dirac's relativistic theory. Good agreement with the latter theory over the angular range 20° - 90° was obtained both for electrons

and for positrons, but the positron scattering intensity was lower than the value predicted by the semi-classical theory. No anomalies in the energy loss during scattering were detected.

APPENDIX I.

CLOUD CHAMBER CONTROL CIRCUIT. FUNCTION AND VALUE OF COMPONENTS.

SWITCHES.

S.1. Main operating button.

S.2. 'No expansion' switch.

S.3. 'Lamps only' button.

S.4. Contact on L.1.

S.5. 'No lamps'switch.

S.6. Contact on L.2.

S.7. Mains 'on-off' switch.

S.8. Main valve reset button.

S.9. Cam switch operated by M.3.

S.10. Cameras 'on-off' switch.

S.11. Switch to inactivate cameras when M.3. runs continuously

S.12. Contacts on L.1. for operating camera shutter.

S.13. Button for advancing film one frame, camera 1.

S.14. Cam-operated switch inside camera 1.

S.15. Cam-operated switch driven by M.3.

S.16. As S.14., camera 2.

S.17. As S.15.

S.18. As S.13., camera 2.

S.19. Switch for continuous running of M.3.; when S.19. closes S.11. opens.

S.20. Button switch to start M.3.

S.21. Cam-operated switch driven by M.3.

S.22. Relay contacts operated by L.1.

S.23. Contacts on L.1.

S.24. Contacts on L.8. activating L.9.

S.25. Steady lamp switch.

RELAYS AND SOLENOIDS.

L.1. Main relay.

L.2. Lamp flash relay.

L.3. Ignition coil for triggering lamp discharge.

L.4. Main valve solenoid.

L.5. Reset solenoid.

L.6. Shutter solenoid: camera 1.

L.7. Shutter solenoid: camera 2.

L.8a. Relay coil (activating).

L.8b. Relay coil (slugging).

L.9. Source shutter solenoid.

MOTORS.

M.1. Film transport motor: camera 1.

M.2. Film transport motor: camera 2.

M.3. Cam switch motor.

LAMPS AND METERS.

D.1. 'Mains on' indicator lamp.

D.2. 'M.1. running' indicator lamp.

D.3. 'M.2. running' indicator lamp.

D.4. Continuous illumination lamp.

E.1. Main solenoid current meter.

F.1. Flash discharge lamp.

F.2. Flash discharge lamp.

VALVES.

V.1. EF50.

V.2. EF50.

V.3. EF50.

V.4. KT66.

V.5. GT1C.

V.6. 5Z4G.

V.7. 5Z4G.

V.8. VU111.

V.9. VU111.

CONDENSERS.

C.1.	0.5	F.	C.10.	8	F
C.2.	1.0	"	C.11.	2	"
C.3.	2.0	"	C.12.	16	"
C.4.	0.1	"	C.13.	16	"
C.5.	0.001	"	C.14.	8	"
C.6.	0.2	"	C.15.	8	"
C.7.	20.0	F	C.16.	100	"
C.8.	2.o	F	C.17.	100	"
C.9.	1.0	"			

RESISTORS.

R.1.	100k.	ohms. (variable)	R.13.	50k.	ohms.
R.2.	1M.	"	R.14.	50k.	"
R.3.	30k.	"	R.15.	2M.	"
R.4.	10k.	"	R.16.	2k.	"
R.5.	25k.	"	R.17.	5k.	" (variable)
R.6.	500k.	"	R.18.	2k.	" (variable)
R.7.	50k,	"	R.19.	10k.	"
R.8.	50k.	"	R.20.	15k.	"
R.9.	5M.	"	R.21.	1M.	"
R.10.	200k.	"	R.22.	2M.	"
R.11.	100k.	"	R.23.	1M.	" (variable)
R.12.	100k.	" (variable)	R.24.	1M.	"

RESISTORS. (continued).

R.25.	1M.	ohms.	R.30.	75.	ohms.
R.26.	1M.	"	R.31.	75.	"
R.27.	500k.	"	R.32.	100.	" (variable)
R.28.	500k.	"	R.33.	5K.	" (variable)
R.29.	2.5k.	" (variable)			

APPENDIX II.

The following Tables consist of selected parts of a set of Tables compiled by O'Ceallaigh (Proc.Roy.Irish Acad. A 53, 133 (1950)).

For each of the functions $\mathrm{cosec}^{n}\theta/2$, n = 1, 2, 3 and 4, are listed in angular intervals of 10 degrees, the values of:-

$$(1) \quad \int_{\theta_1}^{\theta_2} \frac{P(\theta)\,d\theta}{N f(Z,\beta)} = \int_{\theta_1}^{\theta_2} \mathrm{cosec}^{n}\theta/2 \cdot 2\pi \sin\theta\, d\theta = n(\theta_1, \theta_2).$$

(unprojected angles : denoted by θ in table).

$$(2) \quad \int_{\phi_1}^{\phi_2} \frac{P(\phi)\,d\phi}{N f(Z,\beta)} = n(\phi_1, \phi_2), \quad \text{(projected angles)},$$

for various values of the parameter $\rho = \lambda_c/2a$. $\rho = 0$ corresponds to projection without any selection criterion

$\rho = 1$ corresponds to the conditions of measurement in the present experiments in which $\lambda_c = 2a$.

When the track-measuring conditions have been established and the experimental constants evaluated, the information obtainable from these tables enables the calculation to be made of the number of deflections predicted by various scattering formulae in the angular intervals 20°-30° 30°-40°, etc.

$F(\theta) = \operatorname{cosec} \frac{1}{2}\theta$ $\quad \left| N(\eta_1, \phi_2) \right| \begin{matrix} \lambda \geqslant \lambda_c \\ -a \leqslant y \leqslant +a \end{matrix}$

ρ	20°–30°	30°–40°	40°–50°	50°–60°	60°–70°	70°–80°
θ	2·1406	2·0911	2·0257	1·9448	1·8492	1·7395
0	2·1838	1·8014	1·5435	1·3574	1·2174	1·1091
1·0	1·1469	0·8822	0·7183	0·6079	0·5294	0·4714
2·0	0·7166	0·5314	0·4234	0·3536	0·3053	0·2702
2·5	0·5970	0·4385	0·3477	0·2896	0·2496	0·2207
3·0	0·5099	0·3721	0·2941	0·2446	0·2106	0·1861
4·0	0·3929	0·2845	0·2241	0·1840	0·1600	0·1412
5·0	0·3186	0·2297	0·1806	0·1498	0·1287	0·1136
10·0	0·1624	0·1164	0·0983	0·0756	0·0649	0·0573

ρ	80°–90°	90°–100°	100°–110°	110°–120°	120°–150°	150°–180°
θ	1·6165	1·4813	1·3347	1·1781	2·5108	0·8564
0	1·0238	0·9558	0·9013	0·8576	2·3926	2·2538
1·0	0·4274	0·3933	0·3667	0·3458	0·9530	0·8893
2·0	0·2440	0·2239	0·2083	0·1960	0·5392	0·5024
2·5	0·1991	0·1826	0·1698	0·1598	0·4394	0·4092
3·0	0·1678	0·1538	0·1430	0·1346	0·3700	0·3446
4·0	0·1273	0·1167	0·1085	0·1020	0·2804	0·2611
5·0	0·1024	0·0939	0·0872	0·0821	0·2255	0·2100
10·0	0·0516	0·0473	0·0439	0·0413	0·1135	0·1057

$F(\theta) = \operatorname{cosec}^2 \frac{1}{2}\theta$ $\quad \left| N(\phi_1, \phi_2) \right| \begin{matrix} \lambda \geqslant \lambda_c \\ -a \leqslant y \leqslant -a \end{matrix}$

ρ	20°–30°	30°–40°	40°–50°	50°–60°	60°–70°	70°–80°
θ	10·0304	7·0055	5·3181	4·2258	3·4503	2·8632
0	7·5767	4·8909	3·4998	2·6711	2·1339	1·7654
1·0	4·7045	2·7287	1·7956	1·2822	0·9710	0·7693
2·0	3·1675	1·7256	1·0952	0·7606	0·5664	0·4436
2·5	2·6891	1·4396	0·9078	0·6253	0·4640	0·3626
3·0	2·3261	1·2303	0·7656	0·5306	0·3920	0·3059
4·0	1·8181	0·9487	0·5866	0·4034	0·2982	0·2324
5·0	1·4982	0·7582	0·4738	0·3253	0·2402	0·1870
10·0	0·7603	0·3981	0·2401	0·1644	0·1212	0·0943

ρ	80°–90°	90°–100°	100°–110°	110°–120°	120°–150°	150°–180°
θ	2·3968	2·0121	1·6846	1·3985	2·7438	0·8713
0	1·5024	1·3092	1·1647	1·0552	2·7438	2·4374
1·0	0·6321	0·5353	0·4652	0·4136	1·0481	0·9118
2·0	0·3615	0·3043	0·2633	0·2333	0·5887	0·5106
2·5	0·2951	0·2481	0·2145	0·1900	0·4791	0·4153
3·0	0·2487	0·2090	0·1806	0·1599	0·4031	0·3493
4·0	0·1888	0·1585	0·1369	0·1212	0·3054	0·2645
5·0	0·1518	0·1275	0·1101	0·0974	0·2454	0·2126
10·0	0·0765	0·0642	0·0554	0·0490	0·1235	0·1070

$F(\theta) = \operatorname{cosec}^3 \frac{1}{2}\theta$ $\quad N(\phi_1, \phi_2) \mid \lambda \geqslant \lambda_c$ $\quad -a \leqslant y \leqslant +$

ρ	20°–30°	30°–40°	40°–50°	50°–60°	60°–70°	70°–80°
θ	47·628	23·622	14·014	9·2037	6·4479	4·7180
0	28·608	13·870	8·1163	5·3150	3·7590	2·8153
1·0	19·901	8·5512	4·5165	2·7128	1·7839	1·2568
2·0	14·232	5·6462	2·8288	1·6399	1·0525	0·7289
2·5	12·286	4·7580	2·3522	1·3530	0·8641	0·5965
3·0	10·755	4·0924	2·0055	1·1478	0·7309	0·5036
4·0	8·5323	3·1769	1·5410	0·8570	0·5567	0·3828
5·0	7·1292	2·5855	1·2474	0·7080	0·4487	0·3082
10·0	3·6710	1·3245	0·6340	0·3594	0·2266	0·1554

ρ	80°–90°	90°–100°	100°–110°	110°–120°	120°–150°	150°–180°
θ	3·5565	2·7346	2·1271	1·6606	3·0015	0·8866
0	2·2059	1·7941	1·5063	1·3005	3·1591	2·6503
1·0	0·9355	0·7289	0·5904	0·4949	1·1538	0·9353
2·0	0·5359	0·4138	0·3329	0·2776	0·6433	0·5189
2·5	0·4376	0·3373	0·2711	0·2259	0·5228	0·4215
3·0	0·3689	0·2841	0·2282	0·1900	0·4396	0·3542
4·0	0·2800	0·2155	0·1729	0·1493	0·3327	0·2680
5·0	0·2253	0·1733	0·1390	0·1157	0·2674	0·2153
10·0	0·1135	0·0873	0·0700	0·0582	0·1345	0·1082

$F(\theta) = \operatorname{cosec}^4 \frac{1}{2}\theta$ $\quad N(\phi_1, \phi_2) \mid \lambda \geqslant \lambda_c$ $\quad -a \leqslant y \leqslant +$

ρ	20°–30°	30°–40°	40°–50°	50°–60°	60°–70°	70°–80°
θ	229·151	80·168	37·067	20·093	12·069	7·7827
0	115·326	40·787	19·200	10·685	6·6537	4·4980
1·0	86·619	27·134	11·430	5·7578	3·2834	2·0553
2·0	65·020	18·599	7·3613	3·5439	1·9587	1·1990
2·5	56·968	15·830	6·1521	2·9346	1·6115	0·9822
3·0	50·390	13·703	5·2650	2·4952	1·3648	0·8297
4·0	40·486	10·756	4·0627	1·9114	1·0496	0·6311
5·0	33·689	8·7555	3·2958	1·5449	0·8394	0·5083
10·0	17·793	4·5114	1·6802	0·7834	0·4244	0·2565

ρ	80°–90°	90°–100°	100°–110°	110°–120°	120°–150°	150°–180°
θ	5·2814	3·7185	2·6867	1·9724	3·2866	0·9022
0	3·2410	2·4596	1·9499	1·6056	3·6526	2·8988
1·0	1·3855	0·9929	0·7496	0·5923	1·2718	0·9598
2·0	0·7952	0·5630	0·4212	0·3305	0·7037	0·5275
2·5	0·6495	0·4589	0·3428	0·2687	0·5713	0·4278
3·0	0·5477	0·3865	0·2884	0·2259	0·4800	0·3592
4·0	0·4158	0·2930	0·2185	0·1710	0·3634	0·2712
5·0	0·3346	0·2356	0·1756	0·1374	0·2916	0·2180
10·0	0·1686	0·1186	0·0884	0·0691	0·1467	0·1095

REFERENCES.

A.1. ALICHANOV, ALICHANIAN & KOZODAEV. C. R. Acad. Sci. U.S.S.R. 6, 527, (1939).

2. ALICHANOV, ALICHANIAN & WEISENBERG. Report on Nuclear Physics Conf. Moscow (1940).

3. ALICHANOV, ALICHANIAN & WEISENBERG. J. Phys. U.S.S.R. 9, 280 (1945).

4. AITKEN. Collected Papers p.34. (1880-81).

B.1. BARTLETT & WATSON. Phys. Rev. 56, 612 (1939).

2. BARTLETT & WATSON. Proc. Am. Acad. Arts & Sci. 74, 53 (1940).

3. BUECHNER, VAN DE GRAAFF, SPERDUTO, BURRHILL & FESHBACH. Phys. Rev. 72, 678 (1947).

4. BLACKETT. Proc. Roy. Soc. A. 123, 613 (1929).

5. BLACKETT. Proc. Roy. Soc. A. 102, 294 (1922) ; Ibid. 103, 62 (1923). ; Lbid. 107, 349 (1925).

6. BOSSHARD & SCHERRER. Helv. Physica Acta 14, 2, 85, (1941).

7. BORISOV, BRAILOVSKY & LEIPUNSKY. C. R. Acad. Sci. U.S.S.R. 26, 142 (1940).

8. BLEULER. Helv. Phys. Acta. 15, 613 (1942).

9. BLEULER SCHERRER & ZUNTI. Phys. Rev. 61, 95 (1942).

10. BARKER. Jnl. Sci. Inst. 25, 165 (1948).

11. BLACKETT. Jnl. Sci. Inst. 6, 184 (1929).

12. BARBER & CHAMPION. Proc. Roy. Soc. A. 168, 159 (1938).

13. BLACKETT. Proc. Roy. Soc. A. 146, 281 (1934).

14. BETHE. Phys. Rev. 70, 821 (1946).

C. 1. CHADWICK & MERCIER. Phil. Mag. 50, 208 (1925).
2. CHASE & COX. Phys. Rev. 58, 243 (1940).
3. CHAMPION. Proc. Roy. Soc. A. 134, 672 (1932).
4. CHAMPION. Proc. Roy. Soc A. 153, 353 (1936).
5. CHAMPION & BARBER. Phys. Rev. 55, 111 (1939).
6. CHAMPION & RAY. Proc. Phys. Soc. 61, 532 (1948).
7. COULIER. J. Pharm Chim. 22, 165 (1875).
8. CHAMPION. Nature 148, 727 (1941).

D. 1. DARWIN, Phil. Mag. 25, 201 (1913).
2. DEE & GILBERT. Proc. Roy. Soc, A. 163, 265 (1937).

F. 1. FOWLER & OPPENHEIMER. Phys. Rev. 54, 320 (1938).

G. 1. GRAAFF, Van de, BUECHNER & FESHBACH. Phys. Rev. 69, 452 (1946) ; Ibid. 71, 142 A (1947).
2. GUPTA & GHOSH. Rev. Mod. Phys. 18, 225 (1946).
3. GUPTA. Proc. Phys. Soc. 51, 355 (1939).
4. GOUDSMIT & SAUNDERSON. Phys. Rev. 57, 24 (1940).

H. 1. HAZEN. Rev. Sci. Inst. 13, 247 (1942).

K. 1. KLARMANN & BOTHE. Zeits. f. Phys. 101, 489 (1936).

L. 1. LASICH. Aus. Jnl. Sci. Res. A. 1, 249 (1948).
2. LANGSDORF. Rev Sci. Inst. 10, 91 (1939).
3. LEPRINCE RINGUET. Comptes Rendus 207, 712 (1935).

M. 1. MOTT. Proc. Roy. Soc. A. 124, 426 (1929).

2. MOTT. Proc. Roy. Soc. A. 135, 429 (1932).

3. McKINLEY & FESHBACH. Phys. Rev. 74, 1759 (1948).

4. MASSEY. Proc. Roy. Soc. A. 181, 14 (1942).

N. 1. NEHER Phys. Rev. 38, 1321 (1931).

O. 1. O'CEALLAIGH & MacCARTHAIGH. Proc. Roy. Irish Acad.A. 50, 13 (1944).

2. O'CEALLAIGH. Proc. Roy. Irish Acad.A. 53, 133 (1950).

P.1. PETUKHOV & VYSHINSKI. J. Phys. U.S.S.R. 4,3, 235 (1941); Ibid 5, 2-3, 137 (1941).

R. 1. RANDELS,CHAO & CRANE. Phys. Rev. 58, 201 (1940); Ibid. 68, 64(1945).

2. RUTHERFORD,CHADWICK & ELLIS. "Radiations from Radioactive Substances."

3. RAY & CHAMPION. Nature 158, 753 (1946).

S. 1. SCHONLAND. Proc. Roy. Soc. A. 113, 87, (1926).

2. SCHONLAND. Proc. Roy. Soc. A. 119, 673 (1928).

3. SAUNDERSON & DUFFENDACH. Phys. Rev. 60, 190 (1941).

4. SKOBELTZYN & STEPANOWA. Nature 137, 234,456 (1936).

5. STEPANOWA. Phys. Z. Sowjet. 12, 550 (1937).

6. STEPANOWA. J. P. U.S.S.R. 1. 204 (1939).

7. SEGRIST. Helv. Phys. Acta 16, 471 (1943).

8. SHIMIZU. Proc. Roy. Soc. A. 99, 425 (1921).

W. 1. WENTZEL. Ann. d. Physik 69, 333 (1922).

2. WILLIAMS. Proc. Roy. Soc. A. 169, 531 (1938).

3. WILSON(C.T.R.). Phil. Trans. Roy. Soc. 189, 265 (1897); Ibid. 192, 403 (1899).

4. WILLIAMS. Proc. Camb. Phil.Soc. 35, 512 (1939).

5. WEBB. Phil. Mag. 19, 927 (1935).

6. WILSON(C.T.R.). Proc. Roy. Soc. A. 87, 277 (1912).

7. WILSON(C.T.R.). Proc. Roy. Soc. A. 142, 88 (1933).

8. WILSON(J.G.). "The Principles of Cloud Chamber Technique". C.U.P.

9. WILLIAMS. Phys. Rev. 58, 292 (1940).